$$O_{2(g)} + 2H^+ + 2e^- \xrightarrow{\text{Co catalyst}} H_2O_2$$

INVESTIGATIONS INTO THE ELECTROCHEMICAL SYNTHESIS OF HYDROGEN PEROXIDE

Maria Inês Q. R. Campos

Masters in Chemistry

Department of Chemistry

FCTUC

July 2010

· U   C ·

UNIVERSIDADE DE COIMBRA

"It takes about 50 years for a new idea to break through and become vogue; no one likes an intruder, particularly when he is upsetting the commonplace"

Kallen H, Mann A.
The one and the many
University Press of Chicago, 1979

INVESTIGATIONS INTO THE ELECTROCHEMICAL SYNTHESIS OF HYDROGEN PEROXIDE

Maria Inês Q. R. Campos

Dissertation presented for the Master in Chemistry, Specialisation in- Quality Control and Environment

Supervisor Prof. Christopher Brett

July 2010

Universidade de Coimbra

TABLE OF CONTENTS

TABLE OF SYMBOLS

		S.I. Units
A	Geometric area of electrode	m
c	Concentration	mol dm^{-3}
c_∞	Concentration at infinite, when $\alpha_a + \alpha_b = 1$	mol dm^{-3}
D	Diffusion coefficient	m^2 s^{-1}
E^θ	Standard potential	V
$E^{\theta'}$	Formal potential	V
E_{eq}	Equilibrium potential	V
ΔE_{act}	Voltage drop related to activation losses	V
ΔE_{Ohm}	Voltage drop related to Ohmic losses	V
ΔE_{con}	Voltage drop related to concentration losses	V
E_{cell}	Cell voltage	V
E_{OCV}	Open circuit voltage	V
E_c^θ	Standard potentials of the cathode	V
E_a^θ	Standard potentials of the anode	V
E_c	Nernst electrode potential for cathode	V
E_a	Nernst electrode potential for anode	V
E^t_{OCV}	Open circuit voltage theoretical	V
F	Faraday constant	J V^{-1} mol^{-1}
I_a	Anodic current	A
I_c	Cathodic current	A
I_0	Exchange current	A
I_L	Limiting current	A
I_K	Kinetic current	A
I_D	Disk current	A
I_R	Ring current	A
j	Current density	A m^{-2}
j_c	Cathodic current density	A m^{-2}
j_k	Kinetic current density	A m^{-2}
k_a	Anodic rate constant	m s^{-1}
k_c	Cathodic rate constant	m s^{-1}
k_0	Standard rate constant	m s^{-1}
L	Loading	g m^{-2}
L_{Pt}	Loading	g Pt m^{-2}

m_{water}	Mass of water	G
MW	Molar weight	$g\,mol^{-1}$
n	Number of electrons	-
N	Collection efficiency	-
n_{air}	Molar amount of dry air	mol
n_{water}	Molar amount of water	mol
n_{H2O2}	Molar amount of H_2O_2	mol
P_{O_2}	Partial pressure for O_2	Pa
P_{H_2}	Partial pressure for H_2	Pa
$P_{cathode}$, P_{ca}	Cathode pressure	Pa
P_{anode}, P_{an}	Anode pressure	Pa
P_{total}	Total pressure (gauge)	Pa
Q	Charge	C
Q_H	Hydrogen adsorption charge	C
Q_{Total}	Total charge	C
Q_{DL}	Charge related to capacitance (double layer)	C
R	Ideal gases constant	$J\,mol^{-1}\,K^{-1}$
R_{Ohm}	Internal electrical resistance	Ω
RH	Relative humidity	-
SVP	Saturated vapour pressure	-
T	Temperature	°C
T_{Hum}	Temperature of humidifier	°C
V_m	Volume molar	$m^3\,mol^{-1}$
$wt\,\%$	Weight percentage	-
W_{PP}	Water partial pressure	-
W_{inlet}	Fraction of water flowing into the FC	-
α_a	Anodic transfer coefficient	-
α_b	Cathodic transfer coefficient	-
δ	Thickness	m
ν	Kinematic viscosity	$m^2\,s^{-1}$
ω	Rotation speed/rate	$rad\,s^{-1}$
ΔH	Enthalpy	$J\,mol^{-1}$
$[O]_\infty$	O_2 concentration at infinite	$mol\,dm^{-3}$
$[O]_*$	O concentration close to the electrode surface	$mol\,dm^{-3}$
$[R]_\infty$	R concentration at infinite	$mol\,dm^{-3}$

ABBREVIATIONS

AFC	Alkaline fuel cell
AO	Anthraquinone process
AHQ	Anthrahydroquinone
CV	Cyclic voltammetry
Co-TMPP	Cobalt tetramethoxyphenylporphyrin
Co-TPP	Cobalt tetraohenylporphyrins
Co-TAA	Cobalt tetraazaannulene
CoPP	Cobalt-Porphyrin
Co-PPY	Cobalt polypyrrole
Co-TPTZ	Cobalt tripyridyl triazine
Co-TETA	Cobalt triethylenetetramine
EPSA	Electrochemical Pt surface area
ECA / ECSA	Electrochemical surface area
JM	Johnson Matthey plc.
MEA	Membrane electrode assembly
MCFC	Molten carbonate fuel cell
MBA	Methylbenzyl-alcohol
MSA	Membrane substrate assembly components
OCV	Open circuit voltage
ORR	Oxygen reduction reaction
OCV	Open circuit voltage
PAFC	Phosphoric acid fuel cell
PcTc	Phthalocyanines
PEFC	Polymer electrolyte fuel cells
PEM	Proton exchange membrane
PTFE	Politetrafluoretileno
RDE	Rotating disk electrode
RHE	Reversible Hydrogen Electrode
RRDE	Rotating ring disk electrode
RSD	Relative standard error
SOFC	Solid oxide fuel cell
TAA	Tetracarboxylic phthalocyanines
TMPP	Tetramethoxyphenyl porphyrin
TPP	Tetraphenyl porphyrin

ABSTRACT

This work concerns studies on a novel cobalt-based catalyst for the electrochemical generation of hydrogen peroxide, suitable for use in a proton exchange membrane (PEM) fuel cell device, discovered by Johnson Matthey.

Electrochemical characterization methods (in a three electrode cell) and existing PEM fuel cell technology and materials were adopted. A well-known platinum-based catalyst was analysed and used as a reference.

The electrochemical characterization methods were cyclic voltammetry (to characterize the metal surface), the rotating disk electrode (to calculate the activity of the catalyst, the limiting current associated with the kinetics of the reaction, the number of electrons involved, etc.) and the rotating ring disk electrode (to quantify the current efficiency of the catalyst to produce hydrogen peroxide).

PEM fuel cell technology was also used for electrochemical characterization. Factors directly influencing the concentration of the hydrogen peroxide produced were studied, for instance, the dependence on the humidifier temperature, pressure, and cathodic gas reactant (air or oxygen). Polarization curves were recorded to determine the current density obtained from the single cell, the resistance of the membrane, and other parameters. During this measurement, the hydrogen peroxide produced was collected. Afterwards it was quantified by volumetric analysis. The efficiency of the catalyst was calculated.

These studies revealed that the new catalyst represents a significant improvement for the production of hydrogen peroxide. Its production by using PEM technology was verified.

RESUMO

Este trabalho consiste no estudo de um catalisador novel para a síntese electroquímica de peróxido de hidrogénio, adequado para o uso de uma célula de combustível de membrana trocadora de protões (PEM).

Métodos de caracterização electroquímicos (numa célula de três eléctrodos) e a actual tecnologia PEM bem como os materiais necessários para as mesmas foram utilizados. O conhecido catalisador de platina foi analisado e usado como referência.

Os métodos de caracterização electroquímicos usados foram a voltametria cíclica (para caracterização da superfície do metal), o eléctrodo rotativo de disco - RDE (para calcular a actividade do catalisador, as correntes limite associadas à cinética da reacção, o número de electrões trocados, etc.) e o eléctrodo rotativo de disco e anel - RRDE (para quantificar a densidade de corrente relativa à produção de peróxido de hidrogénio).

A tecnologia PEM foi igualmente usada para a caracterização electroquímica. Alguns dos factores interferentes na concentração de peróxido de hidrogénio produzido foram estudados. Por exemplo, a dependência da temperatura dos humidificadores, da pressão e do gás reagente usado no cátodo (ar ou oxigénio). Curvas de polarização foram determinadas e usadas para determinar a densidade de corrente obtida na célula de combustível, a resistência da membrana e outros parâmetros relacionados. Durante a mesma, o peróxido de hidrogénio foi recolhido e analisado. A sua quantificação foi feita por análise volumétrica. A eficácia do catalisador foi calculada.

Estes estudos revelaram que o catalisador patenteado representa uma melhoria significativa para a produção de peróxido de hidrogénio. A produção do mesmo por via da tecnologia PEM verificou-se possível.

ACKNOWLEDGEMENTS

Since I started this Masters degree, years have passed. This stage of my life, more than professional skills, offered me a Life's lesson, and brought me up. The person who started it is no longer the same person finishing, even though physically it is. Therefore, it is extremely important to recognize and thank those I have come across in this period of my life.

I would like to thank Prof. Christopher Brett, my internal supervisor, for his availability and open-mindedness when he accepted this work. Furthermore, I would like to thank him for the honesty and help, principally in writing this thesis.

I would like to thank Prof. Sebastião Formosinho, Director of the Department of Chemistry of the Faculty of Science and Technology of UC, who gave me this opportunity to finish my Masters degree with work carried out during my job at Johnson Matthey plc.

Following this though, it is also important for me to thank Prof. Emília Azenha, who was the bridge between me and the Department of Chemistry, when I could not be present. Moreover, I would like to thank her for her friendship and for her words when I was in doubt about accepting this opportunity.

I would like to thank my external supervisors, Dr. Rob Potter and D. Sarah Ball, who believed in me and offered me this amazing opportunity to work for a multinational company - Johnson Matthey plc. I also think that it is important to mention that the time they spent with me, their patience and enthusiasm were true catalysts in my training and learning process.

I would like to thank my group manager in the Fuel Cells group – Dr. Jonathan Sharman, for the attention he gave to my work, and all my group colleagues, for their time, help, suggestions and support since I arrived.

Inside Johnson Matthey plc - Technology Centre at Reading, more than colleagues I have friends. Being the only Portuguese, I was never left out and have been treated as

another member of a 'family'. Help, support and care are something that I would like to write down, because that was what I received for free, since my interview day.

Finally, I would like to thank my family, my boyfriend and my friends. The ones that unconditionally love me, and that I love, without a reason. The decision to come to England and leave Portugal was hard, but the love in each travel back home makes me strong to always remember that no one is forgotten even if they are not always present.

AGRADECIMENTOS

Não foram meses que decorreram, mas sim anos, até ao presente. No fim de uma etapa é-me comum avaliá-la objectivamente. Em causa, este Mestrado, que mais do que competências profissionais me ofereceu uma lição de vida, me fez crescer. A pessoa que o começou não é a mesma que o acaba, ainda que fisicamente o seja.

É por isso de importância extrema reconhecer e agradecer àqueles que fizeram parte desta minha vivência.

Gostaria de agradecer ao Prof. Christopher Brett, na qualidade de supervisor interno, pela sua disponibilidade e abertura na aceitação deste trabalho. Mais do que isso, pela sua honestidade, e sua ajuda, principalmente na escrita desta tese científica.

Gostaria de agradecer ao Prof. Sebastião Formosinho, na qualidade de Director do Departamento de Química da FCTUC, por me conceder a oportunidade de terminar o meu Mestrado com o trabalho realizado no meu actual profissão na Johnson Matthey plc.

No seguimento, é-me igualmente importante agradecer à Prof. Emília Azenha, por ter sido a ponte entre mim e o Departamento de Química, quando a minha presença não foi possível. Mas acima de tudo, pela sua amizade e pelas suas palavras principalmente quando me vi indecisa na decisão de partir e agarrar esta oportunidade. As suas palavras continuam comigo.

Gostaria de agradecer aos meus supervisores externos, Dr. Rob Potter e Dr. Sarah Ball, por terem acreditado em mim e me terem concedido a fantástica oportunidade de trabalhar na empresa multinacional que é a Johnson Matthey plc., Acho importante referir que não apenas o tempo que despenderam comigo, mas a sua paciência e o seu entusiasmo, relativamente ao meu trabalho, foram verdadeiros catalisadores no meu treino e aprendizagem.

Queria agradecer ao chefe do meu grupo, Fuel Cells na Johnson Matthey plc. – Technology Centre, ao Dr. Jonathan Sharpman, pela atenção que dispensou ao meu

trabalho. E todos os meus colegas de grupo, pelo seu tempo, sua ajuda, suas sugestões, e apoio, desde o dia em que cheguei.

Dentro da Johnson Matthey plc. – Technology Centre, mais do que relações profissionais entre colegas, posso falar de amizade entre amigos. Ser a única portuguesa no centro nunca foi sinónimo de falta de compreensão, foi sim ser o que sou, mais um membro da família. Acolhimento, apoio e carinho é algo que quero que fique escrito, porque foi o que recebi de forma gratuita desde o dia da minha entrevista.

Queria por fim, agradecer à minha família, ao meu namorado e aos meus amigos. Àqueles que incondicionalmente me amam e amo, sem questionar. A decisão e a partida de Portugal foram difíceis para nós, mas o mimo redobrado a cada visita a casa, recordaram-me sempre que ninguém é esquecido mesmo não estando presente. Hoje, mais do que antes, sabemos e sentimos o que é a saudade.

CHAPTER 1

Introduction

The introduction chapter of this thesis is divided into context, state-of-the-art, fundamentals of techniques and objectives.

1.1. Context

Around 1.2 million tons of hydrogen peroxide are being manufactured every year. The principle of the current production process was introduced in the 1940s and remains the same. Disadvantages such as the fact that production cannot be implemented at the point of use, high energy consumption and waste generation have had a negative effect on the sustainability and on product costs. The necessity of a simple production process, which can be implemented at the point of use is nowadays the goal for the industries concerned[1].

1.1.1. Hydrogen peroxide

Hydrogen peroxide, H_2O_2, is a strong oxidising agent commercially available in aqueous solution over a wide range of concentrations. It is a weakly acidic, nearly colourless that is miscible with water in all proportions. Thenard discovered hydrogen peroxide in 1818, producing it by the reaction of dilute acids on barium peroxide BaO_2 [2,3].

Hydrogen peroxide (H_2O_2) is nowadays an important chemical, usually related to green and sustainable chemistry due to applications such as:

- paper industry, used as a bleaching agent and for the deinking in wastepaper recycling;
- textile industry used as a bleaching agent, oxidizer and desizing agent;
- environmental protection used for the detoxification and colour removal of wastewater;

- off-gas treatment and for bioremediation of contaminated soil;
- pharmaceutical and cosmetic industry used as a disinfectant and bleaching agent;
- detergent and cleanser industry;
- packaging and food industry used as a disinfectant for aseptic packaging and bacteria control;
- chemical industry used for epoxidation, hydroxylation and other oxidation reactions;
- electronics used for pickling of metal surfaces;
- electronics used for cleaning of silicon discs in the production of printed circuit boards;
- bleaching agent used for oils, waxes, fibbers and other natural products;
- used as a propellant – Figure 1.1 [2,3,4,5].
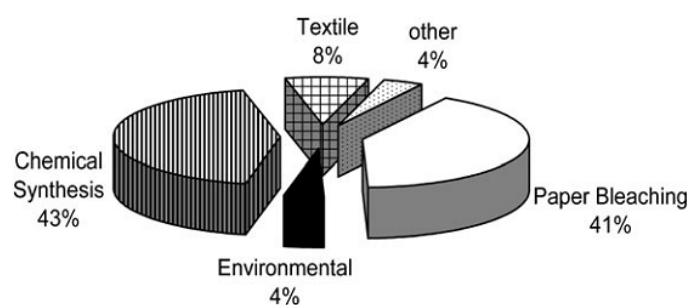
Figure 1.1 – Distribution of hydrogen peroxide consumption in Europe [5]

Hydrogen peroxide is also a versatile oxidant that is effective over the whole pH range with high oxidant potential ($E^{\theta} = 1.76$V vs RHE at pH 0, $E^{\theta} = 0.88$V vs RHE at pH 14) and water as the only co-product.

Equations 1.1 - 1.5 summarize the reactions that hydrogen peroxide may undergo, depending on the type of substrate: decomposition, oxidation, molecular addition, reduction, and substitution.

Decomposition	$2H_2O_2 \rightarrow 2H_2O + O_2$	(1.1)
Oxidation	$2H_2O_2 + M \rightarrow MO + H_2O$	(1.2)
Addition	$H_2O_2 + A \rightarrow AH_2O_2$	(1.3)
Reduction	$H_2O_2 + R \rightarrow RH_2O + O_2$	(1.4)

Substitution $$H_2O_2 + RX \rightarrow ROOH + HX$$ (1.5)
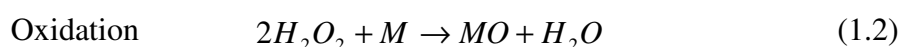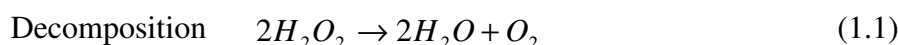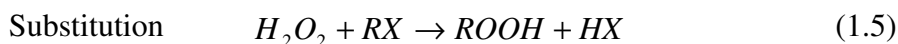
The decomposition of hydrogen peroxide (Eq. 1.1) must be controlled because the reaction produces gaseous oxygen and heat (100.4 kJ mol^{-1}) [3]. The rate of decomposition depends on the temperature and concentration of the peroxide, as well as the presence of impurities and stabilizers. Peroxide decomposes in the presence of many substances (for example transition metals and their compounds), this reaction is also catalyzed by the enzyme catalase, whose main function in the body is remove the toxic by-products of metabolism and to reduce oxidative stress. The rate of decomposition of a solution of H_2O_2 can be minimized by the removal of impurities and addition of stabilizers.

H_2O_2 is also a strong oxidizing agent in acidic solutions. In Equation 1.2, M can be for example lead sulphide (oxidized to lead sulphate), ferrous sulphate, potassium iodide, sodium arsenite, potassium ferrocyanide, or others.

H_2O_2 is capable of adding itself to double bonds: in Equation 1.3, A can be CH_2CH_2 (ethene).

As a strong reducing agent, hydrogen peroxide reduces other stronger oxidizing compounds such as $KMnO_4$, $Ce(SO_4)_2$, $NaOCl$ and Cl_2 (Eq. 1.4). Normally $KMnO_4$ and $Ce(SO_4)_2$ are used as standards for the volumetric determination of hydrogen peroxide [5].

Equation 1.5 shows the reaction of hydrogen peroxide with carboxylic acids producing the corresponding peroxy acid (for example, peracetic acid is a disinfectant prepared from acetic acid and H_2O_2).

1.1.2. Fuel cells

As early as 1839, William Grove discovered the basic operating principle of fuel cells by reversing water electrolysis in order to generate electricity from hydrogen and oxygen.

 "A fuel cell is an electrochemical "device" that continuously converts chemical energy into electric energy (and some heat) for as long as fuel and oxidant are supplied." 6

Used to convert the chemical energy of a fuel (hydrogen, natural gas, methanol, gasoline, etc.) and an oxidant (air or oxygen) into electricity, this device consists of an

electrolyte material that is sandwiched between two thin electrodes containing the catalysts. The fuel passes over the anode where it dissociates catalytically into protons and electrons. The electrons go through an external electrical circuit to provide power, while the ions move through the electrolyte toward the oppositely charged electrode. At the cathode, ions combine to create by-products, primarily water.

Fuel cell applications started with the beginning of space travel, followed by the functional generation of electric power (and drinking water). Fuel cell remains under extensive development and they may come into widespread commercial use through three main applications: transportation, stationary power generation, and portable applications.

However, in spite of the attractive system efficiencies and environmental benefits associated with fuel-cell technology, it has proved difficult to develop the early scientific experiments into commercially viable industrial products. These problems have often been associated with the lack of appropriate materials or manufacturing routes that would enable the cost of electricity per kWh to compete with the existing technology [7].

The key properties of a fuel cell, particularly the operating temperature, depend on the electrolyte used. For this reason, a whole family of fuel cells can be characterized by the electrolyte used – Table 1.1 [6, 8, 9].

Table 1.1 - Types of fuel cells, their characteristics and applications [6, 8, 9].

Fuel Cell type	Electrolyte	Charge carrier	Operating temperature	Fuel	Electric efficiency (system)	Applications
Alkaline FC (AFC)	KOH	-OH	60 – 120 °C	Pure H_2	35-55%	Space vehicles, possible uses in land vehicles and submarines
Proton exchange membrane FC (PEMFC)	Solid polimer (such as Nafion)	H^+	50 - 100°C	CH_3OH, Pure H_2 (tolerates CO_2)	35-45%	Best candidates for light-duty vehicles, for buildings and many other small applications.
Phosphoric acid FC (PAFC)	Phosphoric acid	H^+	~ 220°C	Pure H_2 (tolerates CO_2, approx. 1% CO)	40%	Mid-to-large statationary power generation applications.
Molten carbonate FC (MCFC)	Lithium and potassium carbonate	CO_3^{2-}	~ 650°C	H_2, CO, CH_4, other hydrocarbons (tolerates CO_2)	> 50%	Best suited for the provision of constante power in large utility applications.
Solid oxide FC (SOFC)	Solid oxide electrolyte (yttria, zirconia)	O^{2-}	~ 1000°C	H_2, CO, CH_4, other hydrocarbons (tolerates CO_2)	> 50%	Promising option for high-powered applications, such as industrial uses or central electricity generating station.

27

Proton Exchange Membrane FC (PEMFC) or Polymer Electrolyte FC (PEFC) are now attracting much attention due to their ability to generate highly efficient power at low temperatures of operation with minimal emission problems. The fast start-up mode, usually within a minute, enables applications in electric vehicles. A major drawback, however, is the cost compared to that of internal combustion engines or small-scale turbines. The polymer membranes represent the main cause of the high cost of this type of fuel cell [10]. However, the second biggest problem is related with the electrocatalyst.

1.1.3. Non-precious metal catalysts for fuel cells

Precious-metal catalysts, predominantly platinum (Pt) supported on carbon are used for both the oxidation of the fuel and reduction of the oxygen in a typical temperature range of 80 – 100 ºC. Although platinum catalyst has an almost ideal behaviour, two approaches are at present gaining momentum to replace Pt, which is scarce (only 37 ppb in the Earth's crust) and expensive (nowadays around 42 €/g) [11].

One approach uses non-Pt catalysts that, nonetheless, contain precious metals with limited abundance and/or limited world distribution. Such catalysts are typically based on palladium or ruthenium. Although Pt is thus avoided, the result is the replacement of one precious metal with another that is on the whole less active than Pt. An alternative approach is to replace Pt with abundant, non-precious materials that are not susceptible to price inflation under high-demand circumstances.

Potential electrocatalysts for O_2 reduction are N_4-chelates of Fe and Co such as tetraphenyl porphyrins (TPP), tetramethoxyphenyl porphyrins (TMPP), phthalocyanines (Pc), tetracarboxylic phthalocyanines (PcTc) and dibenzotetraazaanulenes (TAA), adsorbed on the high-area carbon and heat-treated at high temperatures under an inert atmosphere [12].

Cobalt's choice resides in its high ease of oxidation and reduction and excellent longevity in fuel cell applications [13, 14], and this reason is sufficient to sustain interest in research for more than four decades, since Jasinski et al. [15] (1964) found that Co-phthalocyanine exhibited catalytic activity.

Some of these studies are summarised in Table 1.2, in chronological order.

Table 1.2 – Some of the studies done with cobalt catalysts.

Type of Co		Conclusions	Ref.
Co-TMPP	Cobalt tetramethoxyphenylporphyrin	Heat treatment of 450 – 900 ºC gives long-term stability and activity.	16
		Catalyst supported on BP2000, Printex XE 2, Vulcan XC-72, heat treated from 300 – 1100ºC shows that the nº of electrons involved in the reaction starts in 2, increase to 4 and return to 2. Vulcan seems to be more sensitive to 2 electrons reaction.	17
CoTPP	Cobalt tetraohenylporphyrins	The most performing catalysts are obtained after pyrolysis of the precursor molecules between 500 and 700ºC. Fuel cells tests demonstrated lack of stability. More active and stable catalysts were obtained by pyrolyzing CoTPP/C at 900ºC or above.	18
CoTAA	Cobalt tetraazaannulene	"The effect of pyrolysis treatment turns out to be beneficial for the stability".	19
CoPP	Cobalt-Porphyrin	The cobalt structure heat-treated and impregnated in Nafion show good polarization performance and electrode stability (stable active sites) and established a process for cathodes preparation in PEFC.	20
CoTAA	Cobalt tetraazaannulene	Optimum value for the electrochemical activity has found to be in the range of 3.0 – 3.9 wt% Co.	21
Co aza complexes or Co with aminophenyl moieties, $Co-N_4$		After a heat treatment at 600ºC, the number of ligants to give good coordination site for O_2 was more than 3 and less than six. "The efficiency of oxygen reduction to water by monometallic ligands is in most cases less than 50%, and the major product is H_2O_2".	22

CoTPP	Cobalt tetraphenyl porphyrin	Cobalt complexes were found to be mores active to peroxide generation (around 30% current efficiency from RRDE analysis) than iron (around 2%).	23
CoTAA	Cobalt tetraazaannulene		
CoPP	Cobalt porphyrins	Specific interaction between the porphyrin and carbon black, which affects the onset potential for the electrocatalytic O_2 reduction by the Co porphyrins.	24
CoPP	Pyrolyzed cobalt-based catalysts	Studies with a rotating ring-disc electrode (RRDE) and gas diffusion electrodes found that catalyst performance depends on the cobalt loading, going through a maximum at 0.2 wt% Co. The percentage of produced H_2O_2 reached a maximum of 80% on RRDE and more than 90% on GDE. Oxygen is mainly reduced to H_2O_2 by catalytic sites formed on carbon support, (Vulcan XC72-R) during the heat treatment. When the cobalt loading is larger than 0.2% the oxygen reduction current still increases while the amount of produced H_2O_2 either decreases or remains constant. A hypothesis for that behaviour is that a fraction of the H_2O_2 produced on one Co-based catalytic site may be reduced on another catalytic site before leaving the catalytic layer.	25
Co-PPY	Cobalt polypyrrole	Polypyrrole introduced to mimic the atomic configuration in cobalt porphyrins. Co/C is far lower than Co-PPY. The cell performance increase during the conditionating step (30h) until reach a constant value. The catalyst generates ~ 0.2 $A.cm^{-2}$ at 0.50 V and a maximum power density of ~0.14 $W.cm^{-2}$. No drop during 100h operation, which is comparable to a 20 wt% Pt.	10

CoN$_x$		Imidazole was used to imitate porphyrin. A heat treatment from 600 – 900ºC has shown that at 600 ºC the number of electrons involved in the reaction is 2. However, at 700 ºC a highest activity was found. A cell performance for a loading of 2.0 mg cm^{-2} found 200 mA cm^{-2} at 80ºC (T_{cell}). Loading study including 1.0, 1.5 and 2.0 mg cm^{-2}, showed that 2.0 gives a better result.	26
Co-TPTZ	Cobalt tripyridyl triazine	Heat treatment from 600 to 900 ºC give stability. Co/N is more stable than Fe/N or even TPTZ/C. Different loadings were studied, from 0.6 to 7.2%, it was found that for 3.3% Co reaches the maximum. As hypothesis to justify this result the saturation of the sites was referred.	27
CoTETA	Cobalt triethylenetetramine	Heat treatment from 500 to 1000ºC shows that the number of electrons involved in the reaction starts as 2 at 500ºC, increases to 4 and returns to 2. A single cell test found a current density of 900 mA cm^{-2} for the catalyst treated at 800ºC. No drop during 30h operation.	28

In December 2007, Johnson Matthey plc published a patent about improvements in catalysts, disclosing an invention that provides a stable electrocatalyst comprising sub-nanometre sized particles of cobalt. The loading of cobalt, calculated as metal, on the active carbon is desirably less than 10 wt%, and is preferably approximately 2 wt%. This invention not only provides a method of preparing the electrocatalyst refereed but also a method for manufacturing hydrogen peroxide using the PEM fuel cell technology (described in Chapter 2 – Methods and Techniques) [29].

1.2. $\underline{H_2O_2}$ synthesis – History and State-of-the-art

The first record of commercial production of hydrogen peroxide appeared in the 1865 to 1875 period. Thenard's process was used essentially unchanged for the manufacture of hydrogen peroxide until nearly 1900. The formation of hydrogen peroxide in the electrolysis of sulphuric acid was first reported in 1853 and later developments made the manufacture of hydrogen peroxide by an electrolytic process possible in 1908. By 1939, only 10% of the world's production was by the barium peroxide process [2].

The manufacture of hydrogen peroxide involving the catalytic reduction of a substituted anthraquinone and subsequent oxidation back to the quinine structure with the production of H_2O_2 was introduced by IG Farben-industrie in Germany in the 1940s. All subsequent anthraquinone-based production plants built worldwide in the following five decades maintained the original concept [3].

Nowadays, hydrogen peroxide is produced almost exclusively by the anthraquinone oxidation (AO) process. However, the multi-step AO process has the disadvantages of high energy consumption and waste generation, which has a negative effect on its sustainability and production costs. Thus, novel, cleaner methods for the production of H_2O_2 are being explored. The large-scale processes (including the actual process) will be described. At the end, all the methods will be compared with the actual production process. Furthermore, emerging alternatives such as direct synthesis or fuel cells will also be mentioned.

1.2.1. Large-Scale Processes

Large-scale production processes are divided into auto-oxidation methods, alcohols oxidation and electrochemical synthesis.

A. *Autoxidation methods – Anthraquinone auto-oxidation*

The anthraquinone oxidation (AO) process has been improved in each of the four major steps: hydrogenation, oxidation, hydrogen peroxide extraction, and treatment of the working solution. A simplified flow diagram of the process steps is given in Figure 1.2.
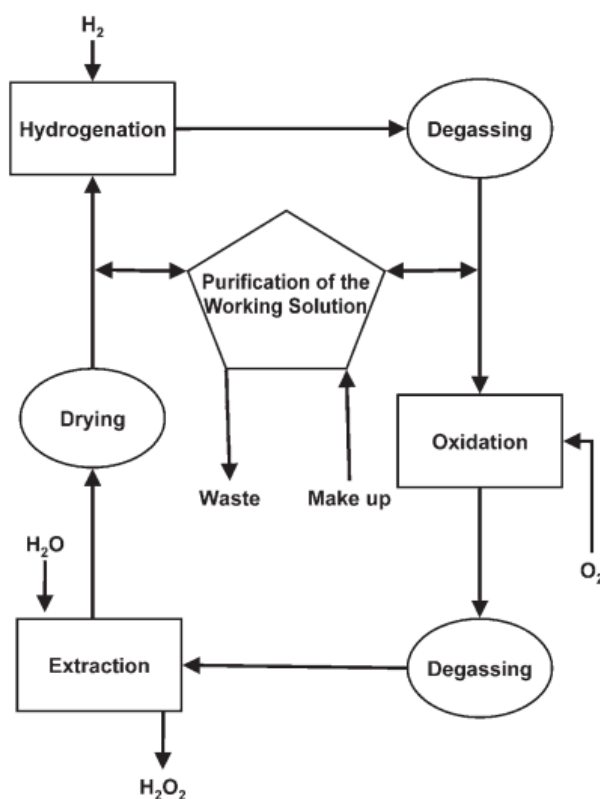
Figure 1.2 – The anthraquinone process for H_2O_2 manufacture [3].

The main reactions involved in the Riedl-Pfleiderer process will now be discussed. A 2-alkylanthraquinone (usually 2-ethylanthraquinone) is an appropriate solvent or mixture of solvents is hydrogenated catalytically to the corresponding anthraquinol or anthrahydroquinone (AHQ) – Figure 1.3.
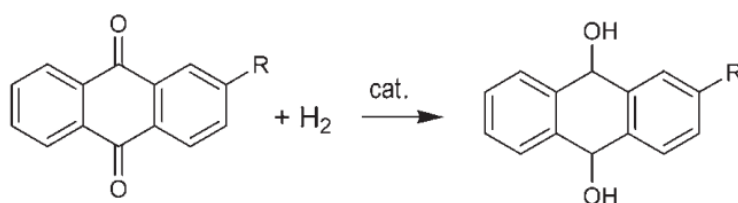

Figure 1.3 – Alkylanthraquinone hydrogenation [4].

A side reaction is the hydrogenation of the unsubstituted aromatic ring to yield 5,6,7,8-tetrahydroanthrahydroquinone – Figure 1.4.
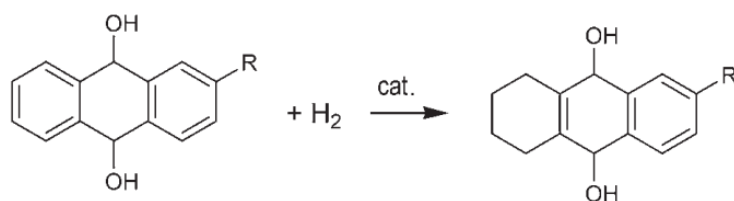
Figure 1.4 – Ring hydrogenation [3].

The solution containing the AHQ is separated from the hydrogenation catalyst and then oxidized with air to re-form the original anthraquinone while simultaneously produces H_2O_2 (Figure 1.5). The aqueous H_2O_2 (around 30% wt) is then distilled to remove impurities, this step increases the concentration to as high as 70%, the solvent/anthraquinone mixture is recycled.
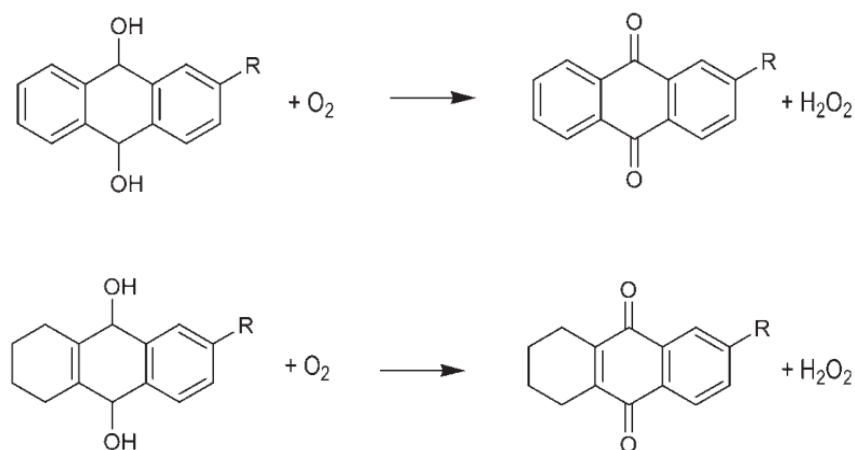

Figure 1.5 - Hydrogen peroxide formation [3].

This process can hardly be considered a "green" method. The AO process is a multistep method that requires significant energy input and generates waste (process not sustainable). The transport, storage, and handling of bulk H_2O_2 involve hazards and escalating expenses [5].

B. Alcohol Autoxidation

The partial oxidation of primary or secondary alcohols can be an alternative. From 2-propanol oxidation, an aldehyde or ketone will be produced as a co-product. This liquid-phase process is based on the auto-oxidation of 2-propanol – Figure 1.6. From this process, which was used by Shell Chemical from 1957 to 1980, the quality of the hydrogen peroxide produced is worst than that from the AO process.

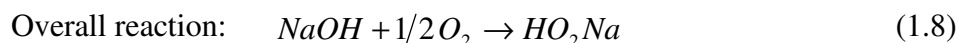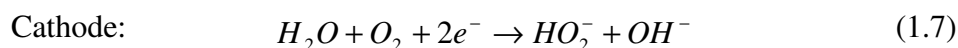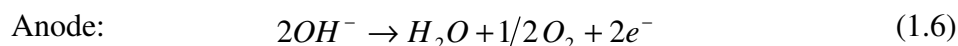**Figure 1.6 – H$_2$O$_2$ synthesis by the oxidation of a secondary alcohol [3].**

The oxidation of a methylbenzyl-alcohol (MBA) was used by Lyondell Chemical and Repsol Química. The patent claims a conversion of MBA of 32% and a selectivity for H$_2$O$_2$ of 97%. The hydrogen peroxide content attained in the liquid phase of about 7.5% is much higher than that achieved with the conventional anthraquinone-based process [5].

C. Electrolytic methods (The Huron-Dow Process)

In 1984, a patent was deposited by The Dow Chemical Company concerning the electrolytic production of peroxide solutions and specifically the production of alkaline peroxide solutions [30]. After ten years, the same company made a patent application about a "composite membrane for chemical synthesis, a method of using the composite membrane, and a chemical reactor into which the composite membrane is incorporated" [31]. Furthermore, in 1996, the same company reviewed and created another application, this time for a composite membrane for chemical synthesis of hydrogen peroxide from hydrogen and oxygen[32].

The Dow process consists in the synthesis of hydrogen peroxide by electrolysis of a dilute solution of NaOH in a electrochemical cell.

The anodic and cathodic reactions are given in Eqs. 1.6 - 1.8.

Anode: $2OH^- \rightarrow H_2O + 1/2\,O_2 + 2e^-$ (1.6)

Cathode: $H_2O + O_2 + 2e^- \rightarrow HO_2^- + OH^-$ (1.7)

Overall reaction: $NaOH + 1/2\,O_2 \rightarrow HO_2Na$ (1.8)

The alkaline peroxide is synthesized at an H_2O_2/NaOH weight ratio of 1:1:7 by cathodic reduction of oxygen on a trickle-bed cathode.

This alkali peroxide technology is best suited to applications for which it is not necessary to separate the peroxide from the caustic soda in the product, for example, pulp bleaching [5].

D. Comparison of Large-Scale production methods

The AO process has supplanted all its competitors (primary and secondary alcohol oxidation, electrochemical) and accounts for more than 95% of the world's production of H_2O_2. One reason for this is that H_2O_2 is produced continuously at mild temperatures and direct contact of O_2 and H_2 is avoided. However, the AO process suffers from inefficiencies caused by mass-transport limitations in the hydrogenation and oxidation reactors, as well as organic contamination of H_2O_2 during its recovery by liquid-liquid extraction. As a consequence, heavier equipment and higher temperatures than those for kinetically controlled reactions are required. The difficulty in controlling the H_2/AQ ratio and the AQ residence time during the hydrogenation step leads to the formation of by-products which must be continually removed. A further problem is cross-contamination of the phases as a result of contact between working solution and water within the stripping column. Furthermore, the partition coefficient of H_2O_2 between water and the organic phase is not optimal, and thus distillation of both the concentrated and purified H_2O_2 is required, which is associated with considerable consumption of energy.

1.2.2. Emerging alternatives

Emerging alternative processes are divided into direct synthesis and fuel cells. Photocatalysis, synthesis from $CO/O_2/H_2O$ mixtures, approaches related with living organisms (enzymatic synthesis), mixtures by plasma or oxygen reduction of

transition-metal complexes with catechol and semiquinone ligands are alternatives that are not referred to here [3].

A. *Direct Synthesis*

To avoid the use of AQ another alternative was suggested, the direct synthesis from hydrogen and oxygen in the presence of a catalyst. The reaction $H_2 + O_2 \rightarrow H_2O_2$ is, in principle, the simplest method to form hydrogen peroxide and should lead to a reduction in the capital investment and operating costs. However, the reaction scheme is more complex because of the occurrence of simultaneous or consecutive reactions, all of which are thermodynamically favoured and highly exothermic – Figure 1.7. Each of them are depending on the catalyst used, the promotors or additives in the reaction medium, and the reaction conditions.
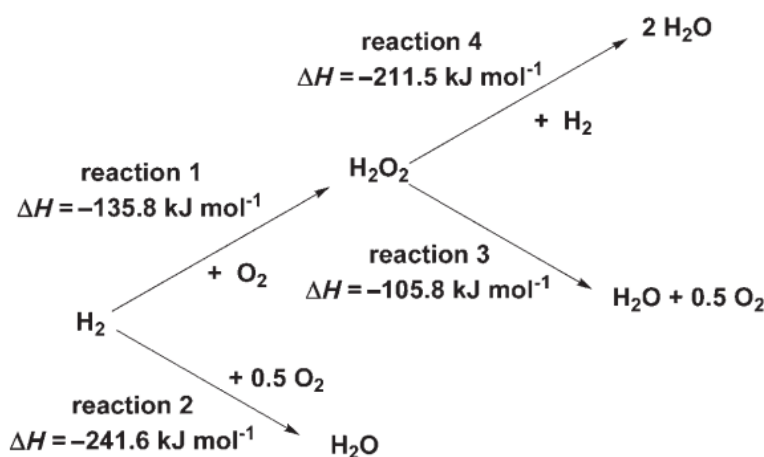

Figure 1.7 – Reactions envolved in the direct production of H_2O_2 [4].

There are two major drawbacks to the direct synthesis of hydrogen peroxide. First, hydrogen/oxygen mixtures are explosive over a wide range of concentrations, so either the ratio of hydrogen to oxygen needs to be carefully controlled or a diluent such as nitrogen, carbon dioxide, or argon must be added (which reduces productivity). The other problem in obtaining good selectivity for hydrogen peroxide over water is that catalysts for the production of hydrogen peroxide are also active for the combustion of hydrogen to water and the decomposition of hydrogen peroxide. These drawbacks appear to be controllable, as Degussa-Headwaters announced, in 2007, the construction of a new production plant for direct synthesis [2].

Yamanaka et al. [33], in the same year, studying the direct synthesis of H_2O_2 in a fuel cell system using a gas-diffusion cathode found a maximum H_2O_2 concentration under suitable reaction conditions (current density 12.7 mA cm^{-2}, reaction time 6h) of 1.2 wt%. His group also communicated the successful production of 7 wt% H_2O_2/NaOH solutions.

B. Fuel Cells

Hydrogen peroxide synthesis using fuel cell technology would provide many advantages over the current methods of manufacture, such as zero-emission process, no electricity required to power the cell, electricity produced can be used to reduce the energy costs, small modular unit and no transportation costs (H_2O_2 can be generated at the point of use) [6, 29]. However, the idea is not new and, so far, two distinct approaches have been adopted in the development of fuel cells for this purpose.

The production of H_2O_2 relies on the electrolysis of O_2 in alkaline solutions in an electrochemical cell containing a carbon cathode. On-site electrochemical production of H_2O_2 for industrial applications requires a production method with high reaction rates, high efficiency, and low costs.

Hydrogen peroxide can be electrosynthesized through the two-electron reduction of O_2 in acidic and alkaline media by using a large variety of three-dimensional electrodes, and gas-diffusion electrodes. As described in Eqs. 1.6 and 1.7, the hydroperoxide ion HO_2^- (the conjugate base of hydrogen peroxide) is produced in alkaline media through the anodic oxidation of OH^- as well as the cathodic reduction of O_2. The overall four-electron reaction for this electrolytic process is depicted in Eq. 1.9.

$$O_2 + 2OH^- \rightarrow 2HO_2^- \qquad\qquad (1.9)$$

The electrochemical production of HO_2^-, according to Equation 1.9, on an industrial scale in alkaline solution has been developed. For instance Oloman et al. [34], studied a trickle bed electrochemical reactor, which was shown to produce peroxide solutions of concentration 0.8 M with 60% efficiency using current densities of 0.12 A cm^{-2}.

A promising alternative is the production of hydrogen peroxide with inexpensive fuel cells which, unlike electrolytic devices, do not require electrical energy. Several methods have been proposed for the direct and continuous production of hydrogen peroxide in fuel cells. The simplest design consists of a fuel cell divided by an electrolyte membrane (Nafion 117) which, was presented by Otsuka et al [35]. The anodic face of this membrane (where H_2 is oxidized) is deposited with Pt, and the cathode face (where O_2 is reduced to hydrogen peroxide) is covered with graphite or an Au mesh. A current density of 10-30 mA cm^{-2} was obtained for a 0.1M HCl solution in contact with the cathode. The current efficiency sharply dropped from 100 to 70% during 3h of operation.

Another design of divided fuel cells comprises a membrane of polyfluorosulfonic acid ionomer sandwiched between an H_2-diffusion anode and an O_2^- diffusion cathode with different catalysts, and a water flow with O_2 is directly injected into the cathode. This system yields current efficiencies below 70% [3]. The limiting factor in these designs is the O_2 concentration in the cathode compartment.

Other designs are being studied, for instance alkaline fuel cells (AFC) containing an H_2-diffusion anode and a commercial O_2-diffusion electrode. Alcaide et al. [36] presented in 1998, this novel electrochemical method for the generation of HO_2^- using an alkaline fuel cell (AFC), with a 3% Pt catalyst. In which, H_2 gas is oxidized to water in a two-electron reaction at the anode Equation 1.10, and O_2 gas is reduced to HO_2^- at the cathode. The overall two-electron process of the AFC is given in Eq. 1.11.

$$H_2 + 2OH^- \rightarrow 2H_2O + 2e^- \qquad (1.10)$$

$$H_2 + O_2 + OH^- \rightarrow H_2O + HO_2^- \qquad (1.11)$$
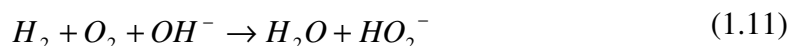
In this scheme, 1 mol of OH$^-$ is consumed per mol of HO_2^- generated. Quasi-steady-state behaviour is observed when a fresh KOH solution is continuously injected into the cell at rates of 20 mL min^{-1}, and current densities of about 100 mA.cm^{-2} and current efficiencies close to 100% are obtained for 1.0M KOH at 20ºC [37]. The application of AFC for production of hydrogen peroxide is a hypothesis that is still being studied [38].

In 2002, Gopal from The Electrosynthesis Company, Inc. presented a new method which "includes substantially simultaneously oxidizing water at the anode of an electrolytic cell to form hydrogen and proton, which in turn are transported to the cathode, preferably in a compartmentalized electrolytic cell to prevent destruction of peroxide at the counter electrode or anode" [39].

Other approaches are being investigated - probably one of the more important for this project (due to the similarities) is "an electrochemical cell that generates electricity, comprising gas diffusion electrodes and a bipolar membrane electrolyte", by Schiffrin et al. [40], in 2001, to be used for the synthesis of chemicals, particularly hydrogen peroxide. This electrochemical cell generates electricity, and comprises gas diffusion electrodes and a bipolar membrane electrolyte.

As mentioned in Section 1.1.3, in December 2007, Johnson Matthey plc., published a patent which not only provided a method for preparing the electrocatalyst but also a method for manufacturing hydrogen peroxide using Proton Exchange Membrane (PEM) fuel cell technology [29]. This methodology will be described in Chapter 2, Section 2.3.

1.3. <u>Fundamentals of the techniques used</u>

The goal of electrocatalysis is to provide alternative reaction pathways in electrochemical reactions which improve the electrode kinetics and permit the reaction to be carried out with a high current density close to the thermodynamically reversible potential, i.e. increase the exchange current density. The catalyst may be an adsorbed or a solution-free species [41].

Oxygen is the most abundant element in the Earth's crust, and the oxygen reduction reaction (ORR) is the most important reaction in life processes and in energy conversion systems such as fuel cells. Sabatier Analysis [42] was used to study the ORR reaction and establish a correlation between the metal catalysts and its maximal catalytic activity. The results were used to construct a volcano curve of the activity as a function of oxygen adsorption energies on a pure metal surface [43] – Figure 1.7.
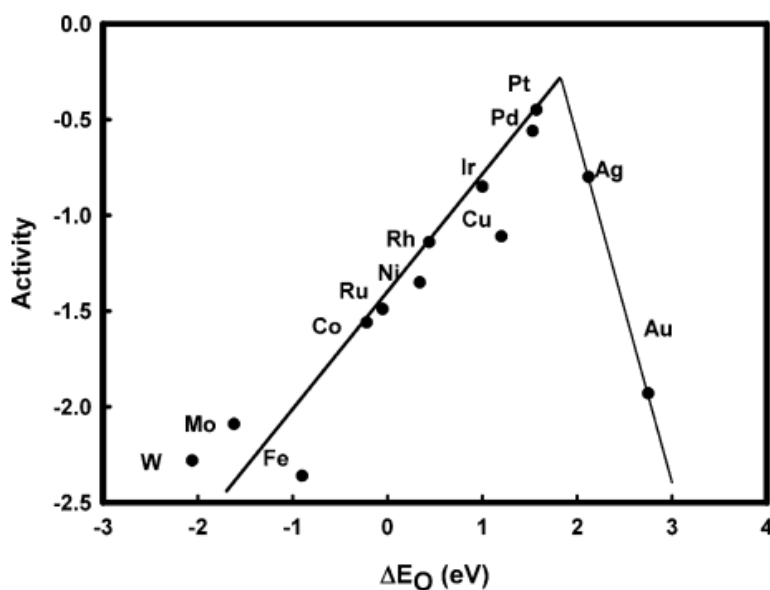
Figure 1.8 - Exchange currents for electrolytic hydrogen evolution vs strength of intermediate metal-hydrogen bond formed during electrochemical reaction [43].

Figure 1.8 shows the dependence of the rate of the ORR on the oxygen adsorption energy and "is a clear demonstration of electrocatalysis, i.e. an effect in electrochemistry due to the nature of metals similar to that observable in catalysis". Platinum is at the top, with the highest activity.

One of the biggest problems in fuel cell technology is related to the low rate of the cathode reaction where oxygen is reduced. Figure 1.7 shows clearly the reason why platinum is commonly used as electrode material [43].

This section will start by describing some of the essential thermodynamic concepts, concerning the oxygen reduction reaction (ORR), the reaction rate, current density Tafel analysis and mass transfer. Afterwards methods to evaluate the catalyst activity will be introduced: in 3-electrode cells, the cyclic voltammetry, the rotating disk electrode (RDE) and rotating ring-disk electrode (RRDE). In the single cell, the test station and recording of polarization curves will be introduced.

1.3.1. Thermodynamic concepts

A. Oxygen reduction reaction (ORR)

ORR in aqueous solutions occurs mainly by two pathways: the direct 4-electron reduction pathway from O_2 to H_2O, and the 2-electron reduction pathway from O_2 to hydrogen peroxide (H_2O_2). In non-aqueous aprotic solvents and/or in alkaline solutions, the 1-electron reduction pathway from O_2 to superoxide (O_2^-) can also occur – Table 1.3 [8].

Table 1.3 - Thermodynamic electrode potential of electrochemical O_2 reductions. Legend: A, B – the thermodynamic potentials for the 1-electron reduction reaction to form a superoxide, and its further reduction to O_2^{2-}, are not listed because their values are strongly dependent on the solvent used [8].

Electrolyte	ORR reactions	Thermodynamic electrode potential at standard conditions (V vs RHE)
Acidic aqueous solution	$O_2 + 4H^+ + 4e^- \rightarrow H_2O$	1.229
	$O_2 + 2H^+ + 2e^- \rightarrow H_2O_2$	0.70
	$H_2O_2 + 2H^+ + 2e^- \rightarrow 2H_2O_2$	1.76
Alkaline aqueous solution	$O_2 + H_2O + 4e^- \rightarrow 4OH^-$	0.401
	$O_2 + H_2O + 2e^- \rightarrow HO_2^- + OH^-$	-0.065
	$HO_2^- + H_2O + 2e^- \rightarrow 3OH^-$	0.867
Non-aqueous aprotic solvents	$O_2 + e^- \rightarrow O_2^-$	A
	$O_2^- + e^- \rightarrow O_2^{2-}$	B

The mechanism of electrochemical O_2 reduction is quite complicated and involves many intermediates, depending primarily on the nature of the electrode material, catalyst, and electrolyte.

In Table 1.3, the 1-, 2-, and 4-electron reduction pathways have unique importance, depending on the application. In fuel cell processes, normally, the 4-electron pathway is highly preferred. The 2-electron pathway is used in industry for H_2O_2 production. The 1-electron reduction pathway is important in the investigation of the ORR mechanism [8].

B. Electrode reactions in hydrogen fuel cells

A fuel cell is an electrochemical energy converter. Its operation is based on the following reactions occurring simultaneously on the anode and the cathode.

At the anode, hydrogen is stripped of its electrons and become protons and electrons.

$$H_2 \rightarrow 2H^+ + 2e^- \tag{1.12}$$

At the cathode, oxygen is reduced, meaning that it takes the electrons and forms water.

$$O_2 + 4H^+ + 4e^- \rightarrow 2H_2O \tag{1.13}$$

or is partially reduced, as in our case.

$$O_2 + 2e^- + 2H^+ \rightarrow 2H_2O_2 \tag{1.14}$$

C. Reaction rate, current density and Tafel analysis

Considering Equation 1.15, to represent the anode and the cathode reactions

$$O + ne^- \rightarrow R \tag{1.15}$$

for a simple electron transfer the Butler-Volmer formulation of electrode kinetics for anodic and cathodic rate constants can be applied [44, 45, 46]:

$$k_a = k_0 \exp\left[\alpha_a nF(E - E^{\theta'})/RT\right] \tag{1.16}$$

$$k_c = k_0 \exp\left[-\alpha_c nF(E - E^{\theta'})/RT\right] \tag{1.17}$$

where k_0 is the standard rate constant, α_a and α_b are the anodic and cathodic transfer coefficients and $E^{\theta'}$ is the formal potential for the system.

For metals, α is expected to be around 0.5, but this value can vary significantly for semiconductors.

In the rate determining step $\alpha_a + \alpha_c = 1$.

At equilibrium, the current is zero so $I_a = -I_c = I_0$, where I_0 is referred to as the exchange current. I_0 can be used to express the rate of an electrode reaction, for instance, for a reduction reaction:

$$I_0 = -I_c = nFAk_0[O]_\infty \exp\left[-\alpha_c nF(E_{eq} - E^{\theta'})/RT\right] \qquad (1.18)$$

assuming that $[O]_* = [O]_\infty$, when the subscript * refers to the reaction site very close to the electrode surface. This means that the production and consumption of O are equal. Considering $\alpha_a + \alpha_c = 1$, if $[O]_\infty = [R]_\infty = c_\infty$ then $E_{eq} = E^{\theta'}$ and

$$I_0 = nFAk_0 c_\infty \qquad (1.19)$$

Tafel found, from Eqs. 1.16 and 1.17, a region of potential close to the equilibrium potential where j depends exponentially on potential.

For a reduction, since $j_c / nF = -k_c[O]_*$,

$$\ln|j_c| = \ln|j_0| - \frac{\alpha_c nFE}{RT} \qquad (1.20)$$

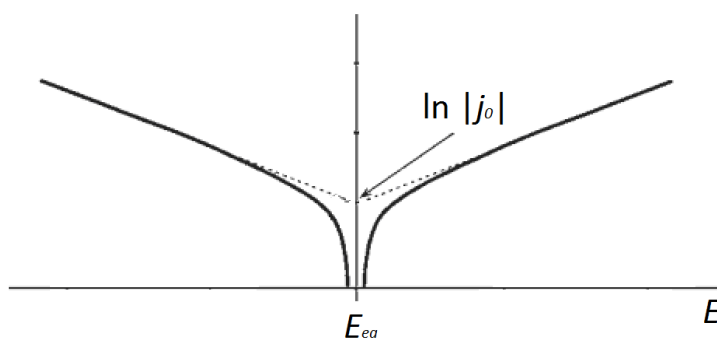Plots of $\ln|j_c|$ vs E (Figure 1.9) give $\alpha_c n$ (or $\alpha_a n$) from the slopes.

Figure 1.9 – Tafel plot [42].

The intercept at $E = E_{eq}$ is $\ln|j_0|$, where j_0 is the exchange current density, which can be related to the standard rate constant through eq. 1.19 [44, 45, 46].

D. Mass transfer

Transport processes are involved when a current is passed through a cell. Ions and neutral species that participate in the electrochemical reactions at the anode or cathode have to be transported to the respective electrode surfaces. There are three modes of mass transfer, which plays an important role in electrochemical dynamics:

Migration: movement of a charged body under the influence of an electric field (a gradient of electrical potential).

Diffusion: movement of a species under the influence of a gradient of chemical potential (i.e. concentration gradient).

Convection: stirring or hydrodynamic transport. Generally fluid flow occurs because of natural convection (convection caused by density gradients), and forced convection and may be characterized by stagnant regions, laminar flow, and turbulent flow.

1.3.2. Methods for catalyst activity evaluation

The characterization of an electrochemical reaction is carried out in various types of electrochemical cells.

A. Conventional 3-electrode cells

In these cells, the electrode (electrocatalyst) to be characterized forms the working electrode, the potential of which current passing through which is controlled. A counter electrode is added to form an electrical circuit - the current flowing through will cause a reaction on the surface, but is not of interest. In order to minimize electrolyte effects, a reference electrode is used to control the potential of the working electrode [47].

A.1 Cyclic voltammetry

Cyclic voltammetry (CV) is a very popular technique, particularly powerful for building up an understanding of new systems and is often the first experiment performed in an electrochemical study. In particular, it offers a rapid location of electrode potentials of the electroactive species, and convenient evaluation of the effect of media on the redox process [48, 49, 50].

CV refers to cycling the potential between chosen low and high values and recording the current as a function of potential. The resulting potential versus current plot is

called a voltammogram. The sweeping of the potential is carried out linearly, at a scan rate, *v*, and the sweep rate can be controlled over a wide range – Figure 1.10.
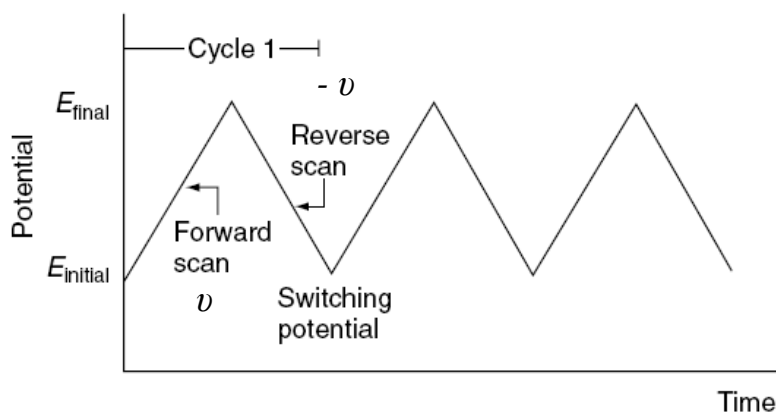

Figure 1.10 - Potential–time excitation signal in a cyclic voltammetric experiment [41].

Depending on the information sought, single or multiple cycles can be used. The working electrode is the electrode where oxidation and reduction processes are studied.

Characterisation of metal surfaces

As a surface sensitive technique, cyclic voltammetry is very useful for catalyst surface characterisation. When the potential is ramped to the upper limit, oxidation processes occur at the electrode. When the potential is reversed to the lower limit, reduction processes. In acidic aqueous electrolyte, noble metals adsorb hydrogen and oxygen by charge transfer. However, the shape and the potential of the corresponding features are characteristic of the metal [51].

CV can be used for the identification of features of a platinum electrode in acidic electrolyte, in which some interesting reactions occur at the surface of Pt electrode. Typical cyclic voltammogram of Pt in acidic media is shown in Figure 1.11.
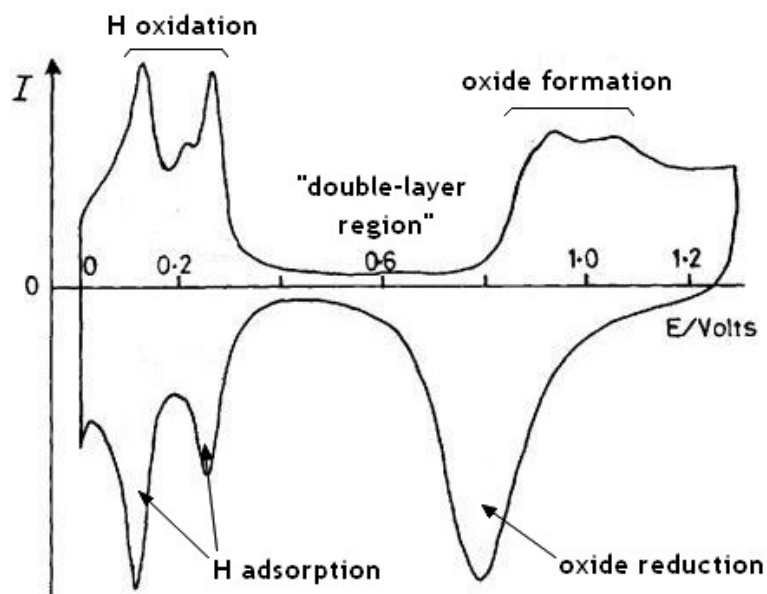
Figure 1.11 - Cyclic voltammogram of a Pt electrode in 0.5 M H_2SO_4 at 25 °C at 100 mV $^{s-1}$.

Three different regions can be distinguished. Between 0 and 0.4 V (vs RHE), hydrogen is adsorbed on the cathodic sweep and oxidised on the anodic sweep, giving rise to two pairs of peaks. These peaks have been assigned to weakly and strongly bound hydrogen [52, 53]. The adsorption-desorption of hydrogen occurs through the reaction:

$$M - H \leftrightarrow M + H^+ + e^+ \qquad\qquad (1.21)$$

In the double-layer region, between 0.4 and 0.8 V (vs RHE), no electrochemical reaction occurs and the current recorded is due to the accumulation of charges from the electrolyte at the polarised interface. Above 0.8 V (vs RHE), oxygen starts to be chemisorbed and oxides are formed. As the potential increases above 0.8 V (vs RHE), the oxygen adsorption becomes increasingly irreversible due to rearrangement of the oxygen species layer into two dimensional lattice of O species and metal atoms [54]. At the onset of oxide formation, the Pt surface interacts with the O-containing species present in the electrolyte (H_2O, OH^-) and as the process progresses a 3-dimensional oxide lattice develops.

Active surface of metals

In 1977, Bregoli [55] investigated the catalytic activity of platinum black and platinum supported on carbon for the electrochemical reduction of oxygen in 99 wt% phosphoric acid at 177ºC as a function of platinum surface area. The activity of platinum was found to be approximately double as the surface area of platinum was decrease from 80 to 10 m^2 g. He evaluated the "true platinum surface area" by the $H_{adsorption}$ area in the voltammogram (Figure 1.11).

The active surface are of a metal can be evaluated from cyclic voltammetry in acidic media. Assuming that each surface platinum atom has the ability to adsorb one hydrogen atom, the integration of the charge passed to form a hydrogen monolayer allows evaluation of the electrochemical Pt surface area (EPSA) in $cm^2_{Pt}\ cm^{-2}$, Equation 1.22 [51]:

$$EPSA = \frac{Q_H}{A \times 210 \times 10^{-6}} \tag{1.22}$$

where A is the geometric area of the electrode (cm^2) and 210×10^{-6} is Q_H, the charge it takes to oxidise one hydrogen monolayer on one square centimetre of Pt in C cm^{-2}_{Pt}.

The electrochemical surface area in $cm^2 mg^{-1}_{Pt}$ can be defined by Equation 1.23.

$$ECA = \frac{EPSA}{L_{Pt}} \tag{1.23}$$

where L_{Pt} is the loading of platinum in the electrode in g m^{-2}.

A.2 Rotating disk electrode

The transport of reactants to or from an electrode usually proceeds through diffusion and convection (charged species can also transport through migration under an electrical field) [50].

The mass transport rate can be significantly increased when forced convection is introduced, in this way reducing the diffusion layer thickness. Convection can be achieved by externally imposing movement of the electrode with respect to the

electrolyte for example by rotating the electrode, as in the rotating disc electrode (RDE).

The RDE consists of a disc (such as Pt or glassy carbon) set into an insulating (PTFE) sheath. The electrode is rotated about its vertical axis (Figure 1.12), typically between 400 and 10.000 rpm. Similar to cyclic voltammetry, in rotating disc voltammetry, the potential of the working electrode is normally swept back and forth between two potential limits.
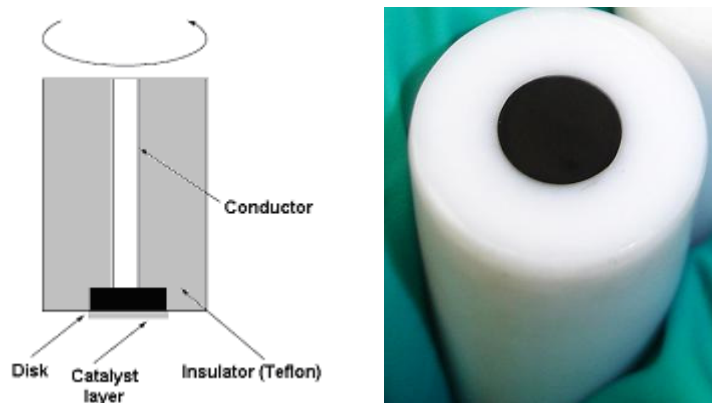

Figure 1.52 – Rotating disc electrode [56].

The working electrode rotation induces a well-defined flow pattern of the electrolyte – Figure 1.13, where it is pumped up from the bulk towards the electrode surface and then flung out centrifugally. The thin layer of liquid adjacent to the electrodes is essentially motionless with respect to the electrode and rotates at the same velocity. The theory of the hydrodynamics at the RDE shows that the electrode is uniformly accessible and affords a precise and reproducible control of the convection and diffusion of reactant to the electrode.

The concentration of the reactant is uniform in the electrolyte bulk and decreases linearly from the edge of the Nernst diffusion layer, to the electrode.
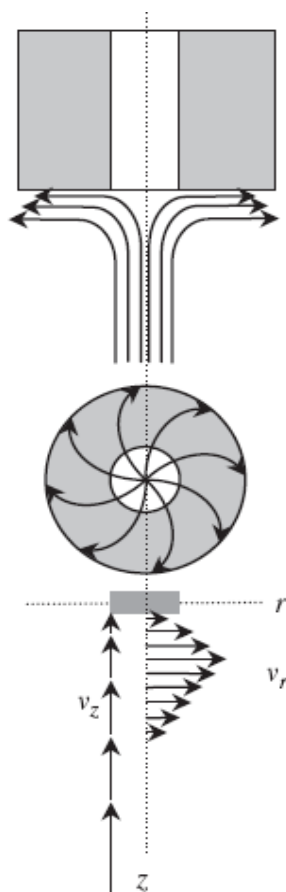
Figure 1.63 – **Streamlines for flow and vector representation of fluid velocities near a rotating disc electrode [47].**

The theoretical treatment yields the concentration profile of reactant towards the RDE and defines this diffusion layer of thickness δ where diffusion is the sole mode of mass transport [50] – Equation 1.24.

$$\delta = 1.61\nu^{1/6}D^{1/3}\omega^{-1/2} \tag{1.24}$$

In previous equation, ω is the rotation speed (rad s^{-1}), ν the kinematic viscosity (m^2 s^{-1}) and D the diffusion coefficient of the reacting species in the liquid (m^2 s^{-1}).

It can be seen that δ can be controlled by the rotation speed. An expression for the limiting current I_L, know as the Levich equation, is derived from the concentration profile, eq. 1.25 [44, 45, 50]:

$$I_L = 0.620nFD^{2/3}\nu^{-1/6}c_\infty\omega^{1/2} \tag{1.25}$$

where v is the kinematic viscosity ($cm^2 \ s^{-1}$), c_∞ is the bulk concentration of reacting species (mol cm^{-3}) and n the number of transferred electrons.

Normally, the hydrodynamic voltammogram is obtained by recording a linear sweep voltammogram at low scan rate (1–10 mV s^{-1}). At high overpotentials, the reaction kinetics is very fast and the reaction is limited by diffusion of the reactant through the Nernst diffusion layer. The current reaches a limit I_L that increases with rotation speed, which controls the thickness δ. A typical hydrodynamic voltammogram is shown in Figure 1.14.
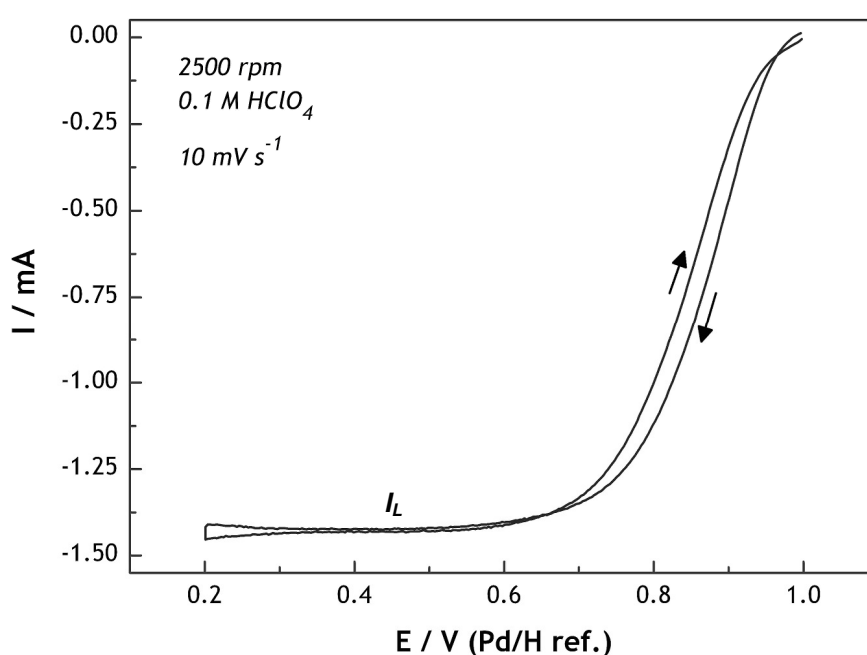

Figure 1.14 - Typical rotating disk voltammogram for a carbon-supported Pt catalyst in 0.1 M HClO$_4$, at 10 mV s^{-1} at a rotating speed of 2500 rpm [51].

For an irreversible redox process such as the reduction of oxygen, the measured current, I, can be expressed as a contribution of the kinetic current I_k and the limiting current I_L, as shown in the Koutecký-Levich equation:

$$\frac{1}{I} = \frac{1}{I_k} + \frac{1}{0.20 FAD^{2/3} v^{-1/6} c_\infty \omega^{1/2}} \tag{1.26}$$

where the kinetic current is extracted and corrected with Equation 1.27:

$$I_K = \frac{I \times I_L}{I_L - I} \qquad\qquad (1.27)$$

I_k is corrected for the effects of transport in order to enable larger sections of the voltammetric curve to be used for parameter value calculations [45].

A.3 Rotating ring-disk electrode

A rotating ring-disk electrode (RRDE) is obtained when a coaxial ring electrode is placed outside the disk electrode separated by a thin insulating ring. Since the product that forms at the disk electrode is continuously swept radially away due to the rotation of the electrode, it will be detected by the ring electrode. Typically, the potential of the ring electrode is set at a value chosen to cause the immediate reaction of the product coming from the disk electrode. The potential specified helps in the identification and quantification of the product formed at the disk electrode – Figure 1.15.
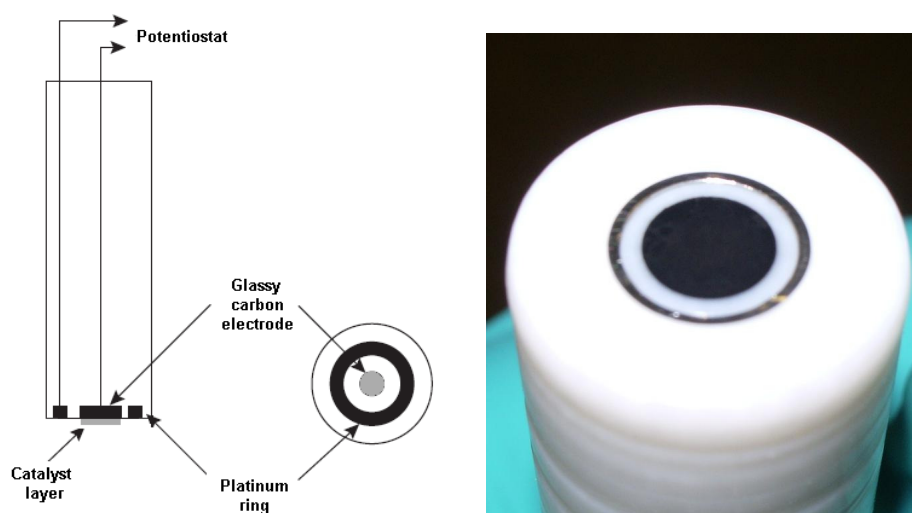

**Figure 1.7 – Scheme and photo of a RRDE electrode [47, 56].**

The flow pattern produced by rotation of the RRDE is identical to that of the RDE. The solution is drawn up to the disc and is then thrown out across the surface of the rotating structure. Therefore, the ring electrode is downstream of the disc electrode and some, but not all, of the species formed at the disc will arrive to the ring electrode. Because of the flow pattern at the rotating surface, some of them will

bypass the ring and pass into the bulk solution. The fraction of the species reaching the ring depends on the characteristics of the RRDE, and on the stability in the electrolyte of the product from the disk and as well as on the rotation rate, since this determines the time for the species to transport from the disk to the ring [50].

The collection efficiency, *N*, is defined as the fraction of a completely stable species formed at the disc (I_D) that is detected at the ring (I_R) – Equation 1.28 [45, 50].

$$N = \frac{I_R}{I_D} \qquad\qquad (1.28)$$

The collection efficiency can be determined with a redox reversible couple. In our experiments, the ferrocyanide / ferricyanide couple was used (Equations 1.29, 1.30):

$$[Fe(CN)_6]^{4-} \Leftrightarrow [Fe(CN)_6]^{3-} \qquad\qquad (1.29)$$

$$Fe(III) \Leftrightarrow Fe(II) \qquad\qquad (1.30)$$
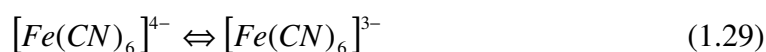
Since ferrocyanide is oxidised to ferricyanide at the disk, a ring potential is chosen such that the ferricyanide produced will be reduced to ferrocyanide at the ring – Figure 1.16.
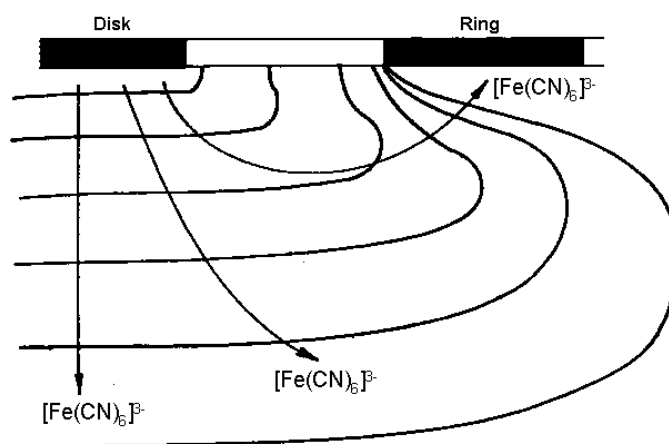

Figure 1.8 – Scheme of the RRDE for the measurement of N. Note that not all the ferrocyanide will reach the ring to be reduced [56, 57].

If both Fe(III) and Fe(II) are completely stable and the potentials of the disc and the ring are held at values where the reactions are mass transport controlled, the collection

efficiency is independent of rotation rate. While theoretical expressions relating N to the disk and ring dimensions are found in the literature, N is usually found by experiment (typical values are 0.2-0.4V vs RHE) [56, 58, 59].

Probably the most common application of the RRDE is to probe the involvement of hydrogen peroxide in the reduction of oxygen – the oxygen reduction reaction (ORR). Oxygen is reduced at the disk and the ring is held at a potential where H_2O_2 is oxidized (I_{ring} = 1.2V vs RHE). The response at the ring shows whether H_2O_2 is being formed and the fraction of the current at the disc leading to this product as a function of potential – Figure 1.17.
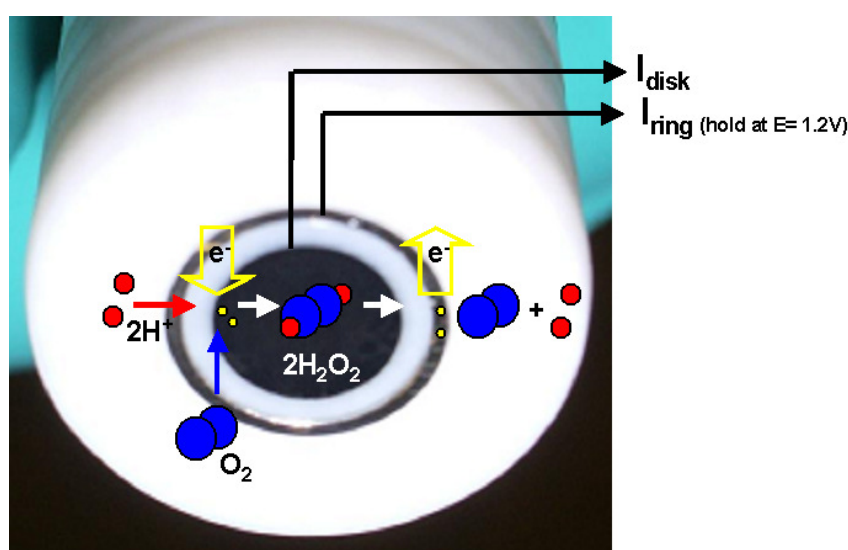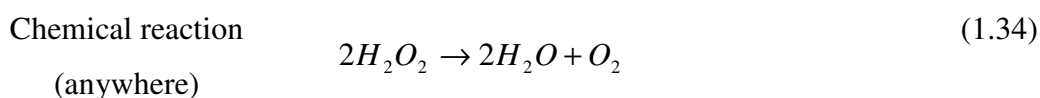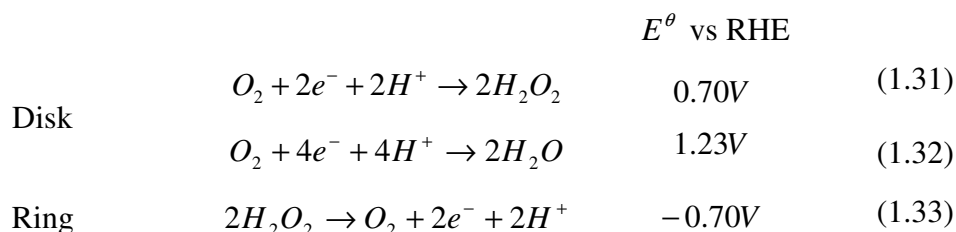

Figure 1.9 - Scheme of the reactions occurring at the RRDE [56].

The reactions occurring are,

$$E^{\theta} \text{ vs RHE}$$

Disk

$$O_2 + 2e^- + 2H^+ \rightarrow 2H_2O_2 \qquad 0.70V \qquad (1.31)$$

$$O_2 + 4e^- + 4H^+ \rightarrow 2H_2O \qquad 1.23V \qquad (1.32)$$

Ring

$$2H_2O_2 \rightarrow O_2 + 2e^- + 2H^+ \qquad -0.70V \qquad (1.33)$$

Chemical reaction (anywhere)

$$2H_2O_2 \rightarrow 2H_2O + O_2 \qquad (1.34)$$

The percentage of the current associated with peroxide generation can be calculated by Eq. 1.35.

$$\%H_2O_2 = \frac{2.I_R / N}{I_D + (I_R / N)} \tag{1.35}$$

where I_D and I_R are the disk and the ring currents, respectively, and N is the collection efficiency, has mentioned previously [60].

B. Single cell (PEMFC)

Polymer electrolyte fuel cells (PEFC), or Proton Exchange Membrane fuel cells (PEMFC), take their name from the special plastic membrane used as the electrolyte. However, the cell assembly is commonly called single cell. A single cell can be conveniently used to test a membrane electrode assembly (MEA) consisting of an anode and a cathode bonded (with noble metals) onto opposite sides of a membrane, Figure 1.18.
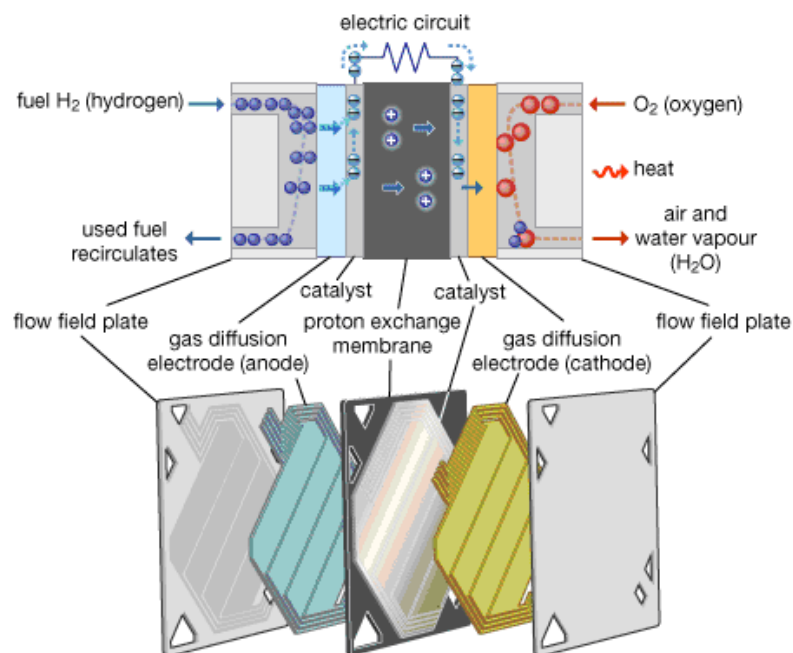

Figure 1.10 - Proton exchange membrane fuel cell [61].

The MEA is sandwiched between a pair of anode and cathode plates that have channels in which the reactants can flow. The edges of the MEA are sealed by a pair of gaskets to prevent leakage of the reactants. The plates are typically made of graphite materials to avoid the corrosion. Current collectors in contact with the outer

surface of the plates enable the measurement of the current and the voltage. Bolts and nuts are used to tighten the cell to a predetermined compression [8].

B.1 Test station

A test station is required for the single-cell test. Test stations are designed to measure and control the following parameters during the tests: (1) temperature, pressure, humidity, and flow rates of reactants, (2) temperature, pressure, and flow rate of coolant, and (3) current and voltage of the fuel cell. Usually, a test station system consists of gas control station, fuel cell, load bank, data acquisition/control unit, as well as control software. A coolant system is normally needed. The gas control station (gas meter and humidifier) is used to regulate the gas velocity, backpressure, temperature, and relative humidity. The fuel cell loads are supplied by a load bank that can provide several load modes: constant current, voltage and power – Figure 1.19 [8].
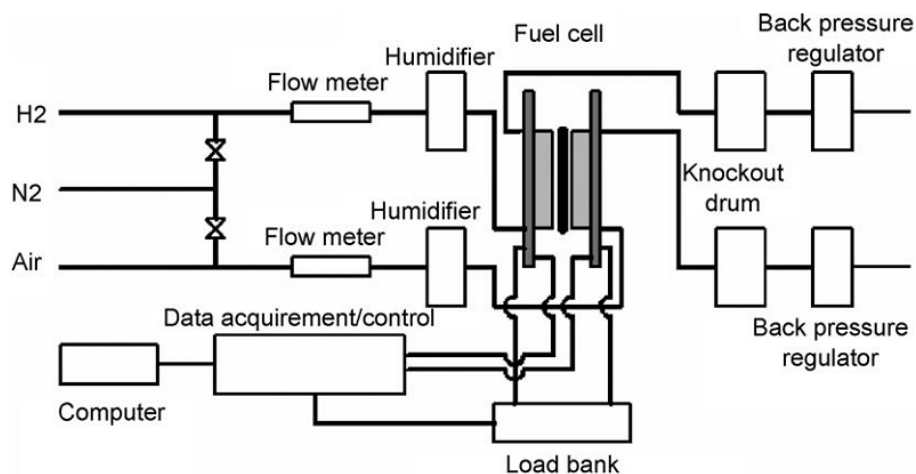

Figure 1.11 – Scheme of a test station [62].

B.2 Polarization curve

A plot of cell potential against current density under a set of constant operating conditions, known as a polarization curve, is the standard electrochemical technique to characterize the performance of fuel cells.

A steady-state polarization curve can be obtained by recording the current as a function of cell potential. By measuring polarization curves, certain parameters such

as the effects of the composition, flow rate, temperature, and relative humidity (RH) of the reactant gases can be characterized and compared systematically [63].

The fuel cell voltage losses are classified into three categories: activation polarization (ΔE_{act}), ohmic polarization (ΔE_{ohm}) and concentration polarization (ΔE_{conc}). These losses result in a cell voltage (E_{cell}) for a fuel cell that is less than its ideal value, eq. 1.36 [64].

$$V_{cell} = E_{OCV} - \Delta E_{act} - \Delta E_{ohm} - \Delta E_{conc} \qquad (1.36)$$

Figure 1.19 represents model calculations of the contributions of fuel cell voltage losses as a function of current density showing the additional contribution to voltage losses from mass transport limitation. The theoretical cell voltage is also called the theoretical open circuit voltage (OCV). The cell resistance can be due to the membrane or the electrodes and is usually called by ohmic polarization [65, 66].
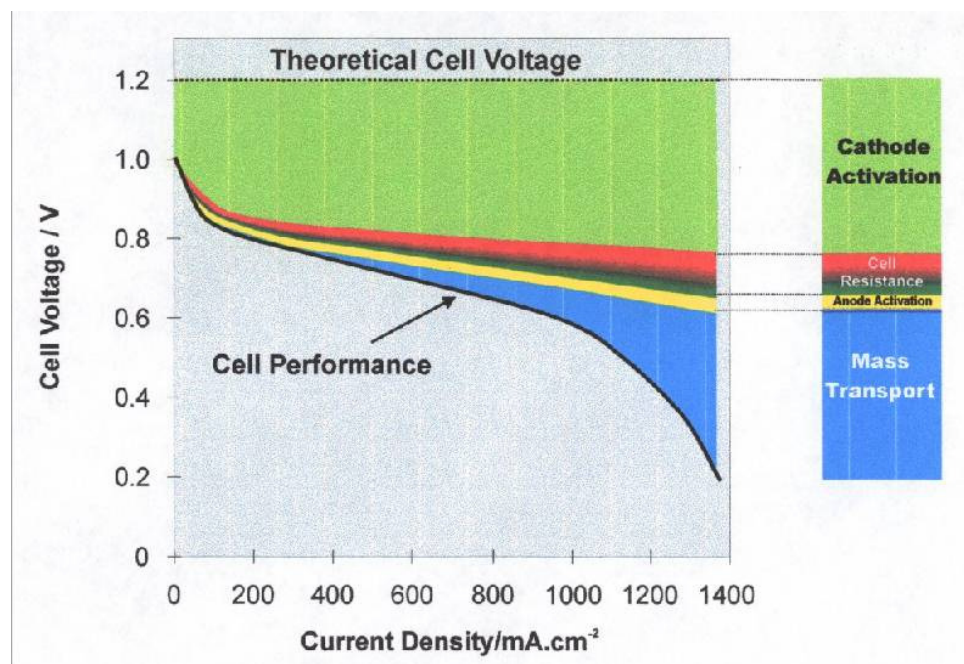

Figure 1.12 – Model calculations of the contributions to PEM losses as a function of current density with no mass transport limitation. Courtesy of JM plc.

Activation Loss

Activation loss is caused by activation polarization, which arises from the need to move electrons and to break and form chemical bonds at both anode and cathode.

In low- and medium-temperature fuel cells, activation losses are the most important cause of irreversibility and of voltage drop. The relation between activation overvoltage and current density is described by the Tafel equation [8].

Ohmic Loss

Ohmic loss arises from the resistance of the polymer membrane to the transfer of ions and the resistance of the electrode and the collector plate to the transfer of electrons. The voltage drop due to the ohmic polarization (ΔE_{ohm}) is described by Ohm's law, eq. 1.37.

$$\Delta E_{Ohm} = I.R_{Ohm} \tag{1.37}$$

where R_{Ohm} (Ω cm^2) is the internal electrical resistance, which includes ionic, electronic and contact resistances.

Open Circuit Voltage - OCV

The reversible cell potential or Nernst voltage is called the theoretical open circuit voltage (OCV). This OCV is defined as the difference between the standard potentials of the cathode (E_c^{θ}) and the anode (E_a^{θ}), and its value is 1.23 V (vs RHE) under standard conditions and considering the reaction involved, eq. 1.32. This value is strongly dependent on the temperature and pressure [67, 68].

In general, a fuel cell OCV, E_{OCV}, can be expressed as Equation 1.38.

$$E_{OCV} = E_c - E_a \tag{1.38}$$

where E_a and E_c are the Nernst electrode potentials for the cathode and anode respectively. They can be expressed in the Nernst forms Equations 1.39 – 1.41.

For the cathode, Eq. 1.32, the Nernst equation is

$$E_c = E_c^\theta + \frac{RT}{2F} . \ln(P_{O2}[H^+]^2)$$
(1.39)

For the anode, Equation 1.40,

$$H_2 \rightarrow 2H^+ + 2e^-$$
(1.40)

the Nernst equation is

$$E = E_a^0 + \frac{RT}{2F} . \ln\left(\frac{[H^+]^2}{P_{H2}}\right)$$
(1.41)

In the previous equations, as defined before, E_c^θ and E_a^θ are the standard cathode and anode potentials, respectively. E_c^θ is a temperature-dependent constant (=1.229-0.000846x(T-298.15), E_a^θ is zero at any temperature, P_{O_2} and P_{H_2} are the partial pressures (atm) of O_2 and H_2 respectively, and [H^+] is the molar concentration of protons (mol L^{-1}) [67, 68].

1.4. Objectives

The aim of this work was to investigate the electrochemical synthesis of hydrogen peroxide, by electrochemical characterization in a conventional 3-electrode cell and a single cell (fuel cell technology).

The specific objectives are to:

1. Understand the electrokinetics that determines the efficacy of the activation of dioxygen to form hydrogen peroxide of the carbon-supported cobalt catalyst (discovered by Johnson Matthey plc [29].).
2. Evaluate the catalyst in a single cell device for the electrochemical generation of hydrogen peroxide.

Electrochemical characterization methods and existing PEM fuel cell technology and materials were adopted.

The electrochemical characterization methods were cyclic voltammetry (to characterize the metal surface), the rotating disk electrode (to calculate the activity of the catalyst, the limiting current associated with the kinetics of the reaction, the

number of electrons exchanged, etc.) and the rotating ring disk electrode (to quantify the current efficiency of the catalyst to produce hydrogen peroxide).

PEM fuel cell technology was also used for electrochemical characterization. Factors directly influencing the amount of the hydrogen peroxide produced were studied, for instance, the dependence on the humidifier temperature, pressure, and cathodic gas reactant. Polarization curves were recorded to determine the current density obtained from the single cell, the resistance of the membrane, and other parameters. Afterwards, the hydrogen peroxide produced was collected and quantified by volumetric analysis. The efficiency of the catalyst was calculated.

CHAPTER 2

_____

Experimental

This chapter describes the materials used, reagents and instrumentation, and the experimental procedures for electrochemical characterisation, in a conventional 3-electrode cell and a single cell device. The fuel cell procedures include the volumetric analysis for hydrogen peroxide quantification.

2.1 Materials

This work was carried out at Johnson Matthey – Technology Centre, who provided all the reagents and equipment that will be mentioned below.

2.1.1. Reagents

The reagents used are presented in Table 2.1.

Table 2. 1 – Reagents.

Chemical reagent/material	Supplier
Different types of Carbon	Johnson Matthey
Platinum	Johnson Matthey
Cobalt	Johnson Matthey
38.1% Pt/C	Home-prepared by B. Theobald
19.5% Pt/C	Home-prepared by E. Christian
Teflonised carbon paper	Toray
0.1 M perchloric acid	VWR International Ltd
Isopropanol	Sigma-Aldrich
Nafion solution (6.11 wt%)	Home-prepared at JMTC
Nafion membranes	Dupont

O_2	Air Products
N_2	Air Products
H_2	Air Products
$K_3Fe(CN)_6$	Aldrich
KOH	Aldrich
0.2M Sulphuric acid	Fisher Scientific
Potassium permanganate	Fisher Scientific
Sodium oxalate	Aldrich
35% w/w Hydrogen peroxide	Alfa Aesar

2.1.2. Equipment

The most important equipment used is presented in Table 2.2.

Table 2.2 - Principal equipments.

Equipment	Supplier
Potentiostat / Galvanostat, PGSTAT 30	Metrohm-Autolab
Glassy carbon disc electrode	Pine
Platinum ring and Glassy carbon disc electrode	Pine
Fuel cell rig	Home-built at JMTC
Single cell	Home-built at JMTC

2.2   Conventional 3-electrode electrochemical cell

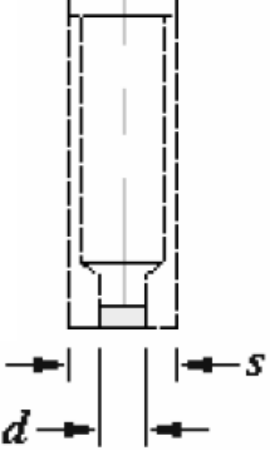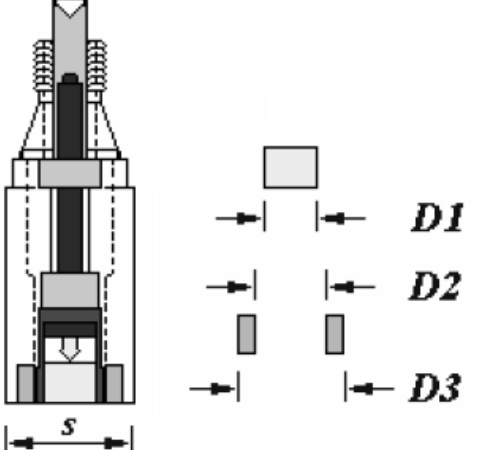A conventional 3-electrode cell – Figure 2.1, was described in Section 1.3.2.
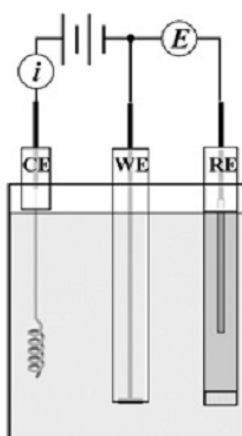
Figure 2.1 – Schematic representation of a conventional 3-electrode cell [47].

The preparation of the electrode and the set-up are common for the techniques previously referred to.

A. *Electrode preparation*

The rotating disk electrode and the rotating ring disk electrode were made of a glassy carbon disk embedded in Teflon. The RRDE also has a platinum ring, isolated from the disk (Figures1.12 and 1.15). The dimensions of these electrodes are described in Table 2.3.

Table 2.3 – Dimensions of RDE and RRDE [69, 70].

Rotating disk electrode	Rotating ring disk electrode
Shroud diameter (s): 12.0 Disk diameter (d): 5.0	Disk (D1): 5.00 Ring (D2): 6.50 Ring (D3): 7.50 Shroud (s): 15.0 Collection efficiency: 26%

The surface of these electrodes were polished with a 0.05 µm alumina paste from Pine Instruments, rinsed with Millipore water, ultrasonically cleaned in water and then rinsed again prior to use. The catalyst was dispersed ultrasonically in a mixture of isopropyl alcohol, water and Nafion®. Thin films of the electrocatalysts were prepared by placing a defined amount of catalyst suspension, onto the flat glassy carbon electrode. To ensure the thickness of the catalyst layer was thin enough to allow optimum accessibility of the catalyst by the reactant, one should aim for the following catalyst loadings:

$\qquad$ 20-25 µg cm^{-2} for catalysts containing 45-50 wt% metal

$\qquad$ 15-20 µg cm^{-2} for catalysts containing 30-40 wt% metal

$\qquad$ 10-15 µg cm^{-2}, for catalysts containing less than 30% wt% metal

The electrode was then partially dried under an infrared lamp [51].

B. Set-up

The electrochemical measurements were conducted in a standard sealed three-electrode cell with a Pine disc electrode as the working electrode. A Metrohm-Autolab potentiostat/galvanostat PGSTAT 30 and a rotation controller were also used. The reference electrode consisted of a carbon-supported Pd catalyst electrode near hydrogen bubbling (RHE) and the counter electrode of a Pt coil. The electrolyte was prepared using distilled water and concentrated $HClO_4$ to give a concentration of 0.1 M – Figure 2.2.
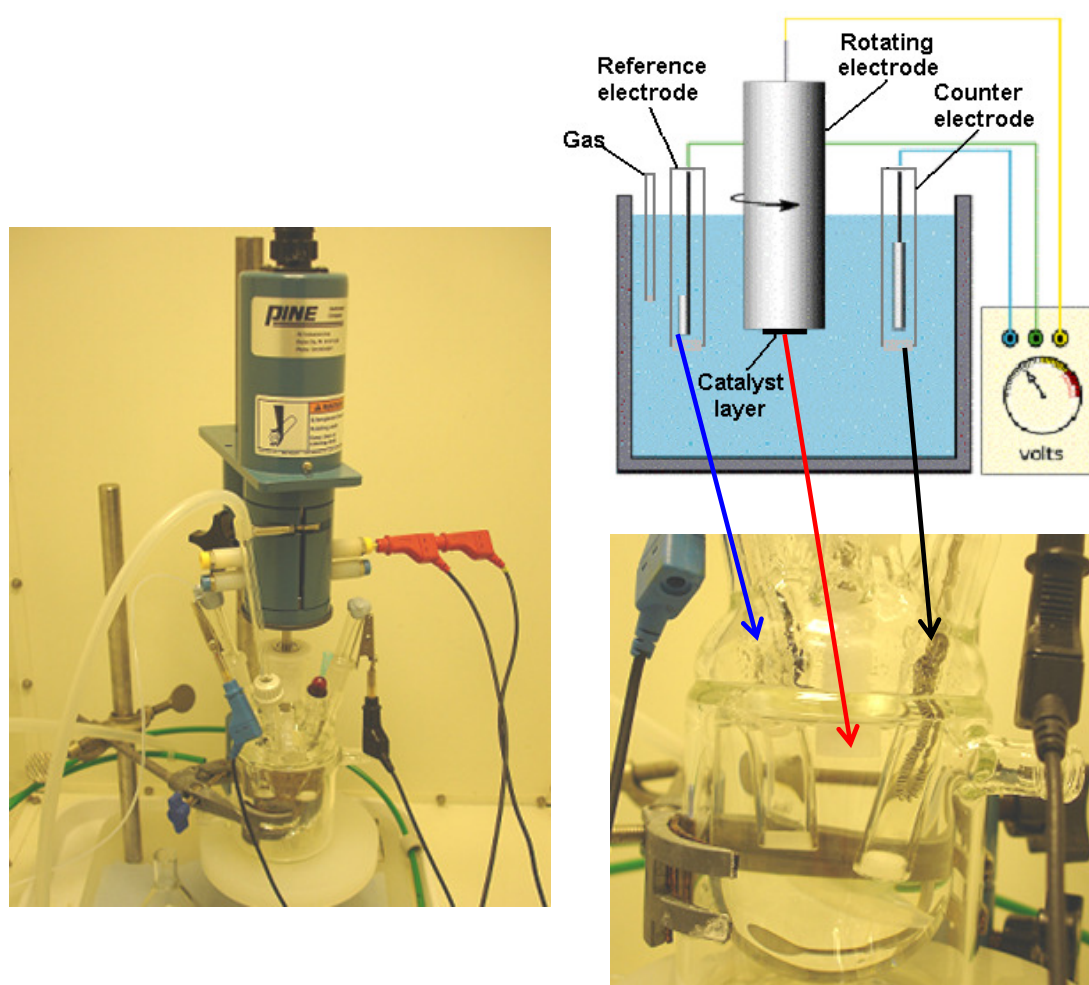
Figure 2.2 Scheme of the RDE set up [71]. Photos of the RDE set up. Courtesy of JM plc.

2.2.1 Cyclic voltammetry

The cell was purged with nitrogen or argon prior to the introduction of the working electrode in the cell. The electrode was cycled between 0.02 and 1.2 V vs RHE at 20 mV s^{-1}, until a well-defined and stable voltammogram was recorded, (typically 10 cycles were required). When possible, the electrochemically active surface area was calculated from the charge it takes to adsorb a layer of hydrogen in the H$_{adsorption}$ region (between 0.04 and 0.4 V vs RHE) – Figure 1.11.

2.2.2 Rotating disk electrode

After the cyclic voltammetry conditioning, O$_2$ was bubbled into the electrolyte for 20-30 min to ensure saturation of the electrolyte. Before evaluating the catalyst activity, the electrode was conditioned by running two cycles at a rotation rate of 400 rpm,

between 1 and 0.2 V (vs RHE) at 10 mV s^{-1}. Then two scans were run at the following rotation speeds, whilst O_2 was bubbled into the electrolyte: 400, 900, 1600 and 2500 rpm. The experiment was repeated for each catalyst to ensure reproducibility of the results.

2.2.3 Rotating ring disk electrode

The electrochemical measurements were conducted with a similar set up as described for the RDE experiments, except the PGSTAT 30 potentiostat/galvanostat was used to measure two signals independently (disc and ring) and to hold the ring at a specific potential (in this case, at +1.2V vs RHE).

For each rotation rate, hydrodynamic voltammograms were recorded, corresponding to the disc and to the ring. The ring voltammogram should not present changes between experiments as the platinum should remain clean and without contamination. The experiment was repeated for each catalyst to ensure reproducibility of the results.

A. *Collection efficiency*

The procedure followed is described by Paulus, et al.[72].

The cell was filled with a solution of 10 mM $K_3Fe(CN)_6$ and 0.1M KOH and purged with nitrogen or argon prior to the introduction of the working electrode in the cell – Figure 2.3.
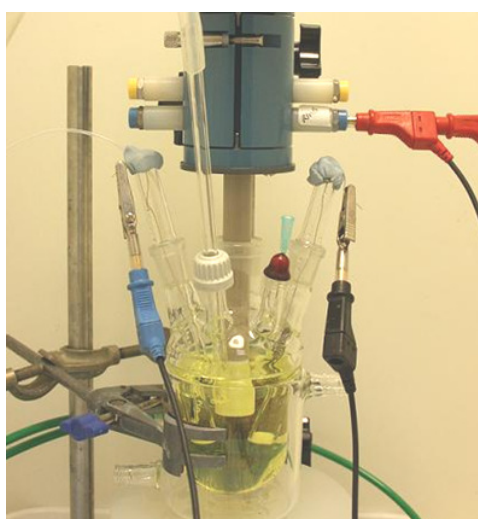

Figure 2.3 - Photo of the set up to measure the collection efficiency. Courtesy of JM plc.

The disk electrode was cycled between 0.4 and 1.55 V (vs RHE) at 10 mV s^{-1} until a well-defined and stable voltammogram was recorded, (typically 10 cycles were required). This voltammogram is used to determine the position of Fe^{III}/Fe^{II} couple.

The ring was held at a chosen potential (for this reaction, +1.6V vs RHE) and disk and ring voltammograms recorded on scanning the disk potential from 1.55 to 0.40 V (vs RHE), at 20 mV s^{-1} whilst rotating. These measurements were repeated at different rotation rates (400, 900, 1200, 1600, 2000, 2300 and 2500 rpm). The experiment was repeated for each catalyst to ensure reproducibility of the results. The collection efficiency was calculated by Equation 1.28.

2.3   Single Cell (proton exchange membrane fuel cell)

A single cell was described in Section 1.3.2. This section will start with a brief introduction of the single cell components. Afterwards, the experimental procedures for the polarization curve, the ohmic losses quantification and the determination of the dependence of the humidifiers temperature will be introduced.

A PEM single cell was designed at Johnson Matthey specifically for hydrogen peroxide production, the actual model is result of a project which has started several years ago. This single cell has some differences from the model introduced below, but the same principle. To build a fuel cell, it is necessary to make an oxygen side and a hydrogen side. Both have a graphite plate consisting of a single serpentine channel through which the gas reactants travel to the electrode catalyst layers - Figure 2.4.
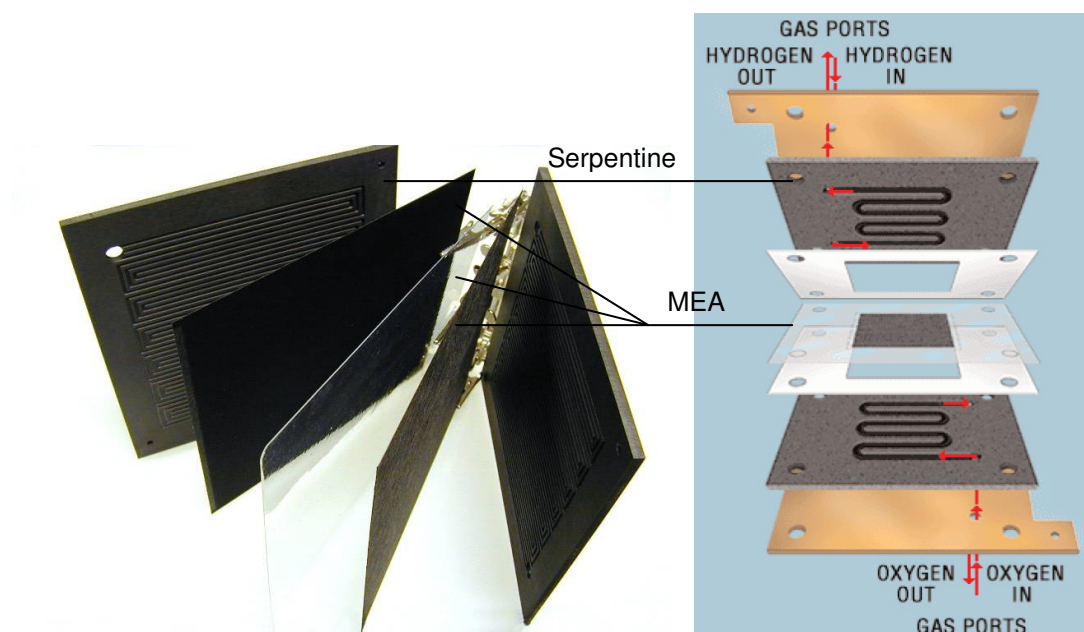
Figure 2.4 – Photo (courtesy of JM plc.) and scheme of a oxygen-hydrogen fuel cell [73].

The electrocatalysts were tested by a MEA (Figure 2.4), in which the cathodes include the catalyst under study. A standard 40%Pt/C electrocatalyst was used as the anode.

2.3.1 MEA preparation

The anode and the cathode constituting the MEA were prepared by a spraying technique. Catalyst-containing inks were sprayed onto teflonised carbon paper disks of an area of 49 cm^2 by a spraying gun. All catalysts investigated were used as cathodes.

The inks were prepared using 25 – 30 wt % Nafion® with respect to the carbon mass of the catalyst used. This was achieved by adding the required amount of 11.0 wt% Nafion® aqueous solution to 2 g of catalyst. The ink-containing plastic pots were then placed in a Speedy Mixer apparatus set at 3000 rpm for 30 seconds. A few drops of water were added to the pot to dilute the ink. The ink was processed once more in the presence of four ceramic balls in the Speedy Mixer at 3000 rpm for 3 min to help break down the catalyst particles. Each carbon paper square was first weighed and the value was recorded. Afterwards, the electrode was placed on a hot plate at less than 90°C and sprayed until the target mass was reached – Figure 2.5.
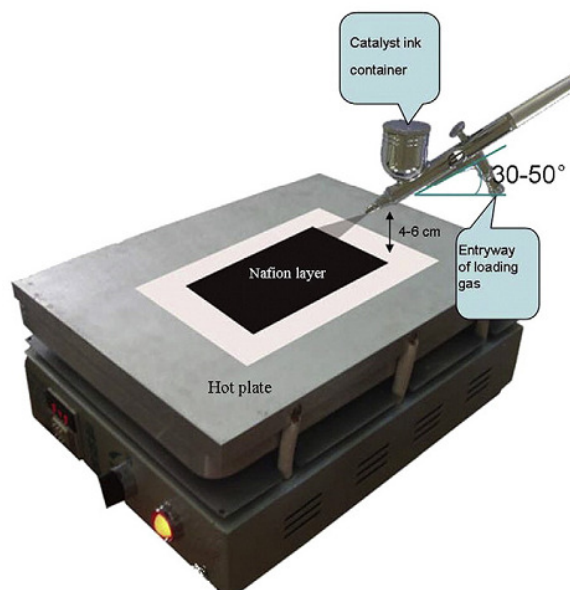
Figure 2.5 – Illustration picture of the setup for cathode preparation [74].

Different metal loadings were chosen in the range 0.5 – 2.0 mg cm^{-2} for each catalyst. The particle size of the ink was measured to control the preparation process.

It is important to refer that conductivity of fully hydrated Nafion membranes plays a key role in the performance of PEM fuel cells. Therefore, the effect of the membrane thickness on the conductivity of Nafion has been studied thoroughly [75, 76, 77, 78, 79].

To produce the MEAs, a Nafion 115 membrane was sandwiched between the cathode and anode (different Nafion membranes have been studied [39, 80] and could be used), with the catalyst layers facing the membrane. The MEAs were hot pressed between PTFE and paper sheets, above the softening point of the membrane, for 3 min, as shown in Figure 2.6.
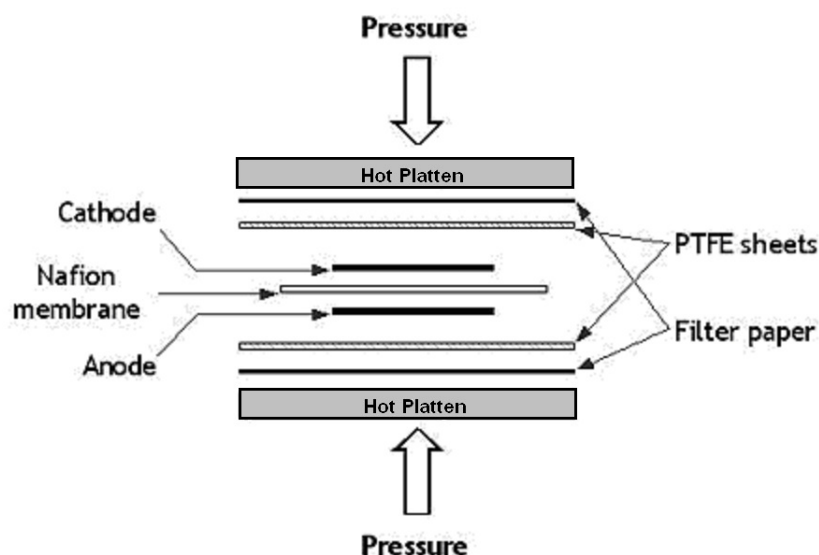
Figure 2.6 - Arrangement used for hot pressing MEAs [51].

Some studies have been done to examine the effect of the pressure and the temperature in the membrane electrode assembly. For instance, Therdthianwong et al. [81], used a Pt/Vulcan XC72 catalyst, with wet-proofed carbon as support, and a Nafion 115 membrane to study the hot-pressing parameters. Varying the conditions from 500 to 1500 psi, 1 to 5 min and 100 to 160 ºC they found that the optimum conditions for MEA fabrication were 100ºC, 1000 psi and 2 min.

2.3.2 Single Cell set up

For performance testing, the MEAs were assembled within the fuel cell. In the fuel cell assembly, the MEA sits between two graphite current collector plates – Figure 2.4. It is compressed to 80% thickness by tightening the bolts used to hold the plates together and measuring the distance between the plates until the desired compression is achieved.

The MEA/graphite plate body is then sandwiched between two membrane substrate assembly components (MSA), whose role is to humidify the fuel and oxidant gases. Water is pumped through tubes from a water bath or a cooler depending on the temperatures studied (this is one of the changes that have been implemented from the well-know PEM fuel cell which has best performance at high temperatures).

The hydrogen peroxide collection was done with collectors specially designed to avoid chemical decomposition.

This set-up was used to study the dependence on the temperature of the humidifiers, the cathodic reactant gas and the catalyst performance by a polarization curve. The gases, hydrogen and oxygen/air, were humidified and passed into the apparatus at different flow rates.

2.3.3 Dependence of the humidifier temperature

The humidification of the gases in a fuel cell system directly influences the concentration of hydrogen peroxide produced. In order to estimate the volume of water produced from gas humidification, calibration of the humidifiers was carried out. To ensure the reliability of the theoretical calculations a study was done which consisted in by-passing the cell and changing the operating conditions such as temperature and flow rates [67, 68, 82, 83].

The methodology followed can be seen in Figure 2.7. Consider a gas passing through the humidifier, which is at constant temperature. From the humidifier temperature (T_{hum}) it is possible to calculate the Saturated Vapour Pressure (SVP) and thence assuming that the Relative Humidity (RH) is 100%, the vapour pressure.

The vapour pressure in this case is equal to the water partial pressure (W_{PP}) and it is necessary to compensate the flow rate of the gas to obtain a specific pressure at the outlet (P_{anode} or $P_{cathode}$ are chosen previously).

Equation 2.1 is used to calculate the fraction of water flowing into the fuel cell (W_{inlet}) with the W_{PP} and the total pressure gauge (P_{total}) in Pa units [67, 68, 82, 83].

$$W_{inlet} = \frac{W_{PP}}{P_{total}} \tag{2.1}$$

From the ideal gas law and the flow rate, the molar quantity of dried gas, n_{air}, can be calculated and Equation 2.2 is used to calculate the amount of water produced in moles.

$$n_{water} = \frac{W_{inlet} \times n_{air}}{1 - W_{inlet}} \tag{2.2}$$

Finally, from the molar amount of water it is possible to estimate the volume of water obtained, from Equation 2.3.

$$m_{water}\,(g/h) = n_{water} \times MW\,(H_2O) \tag{2.3}$$

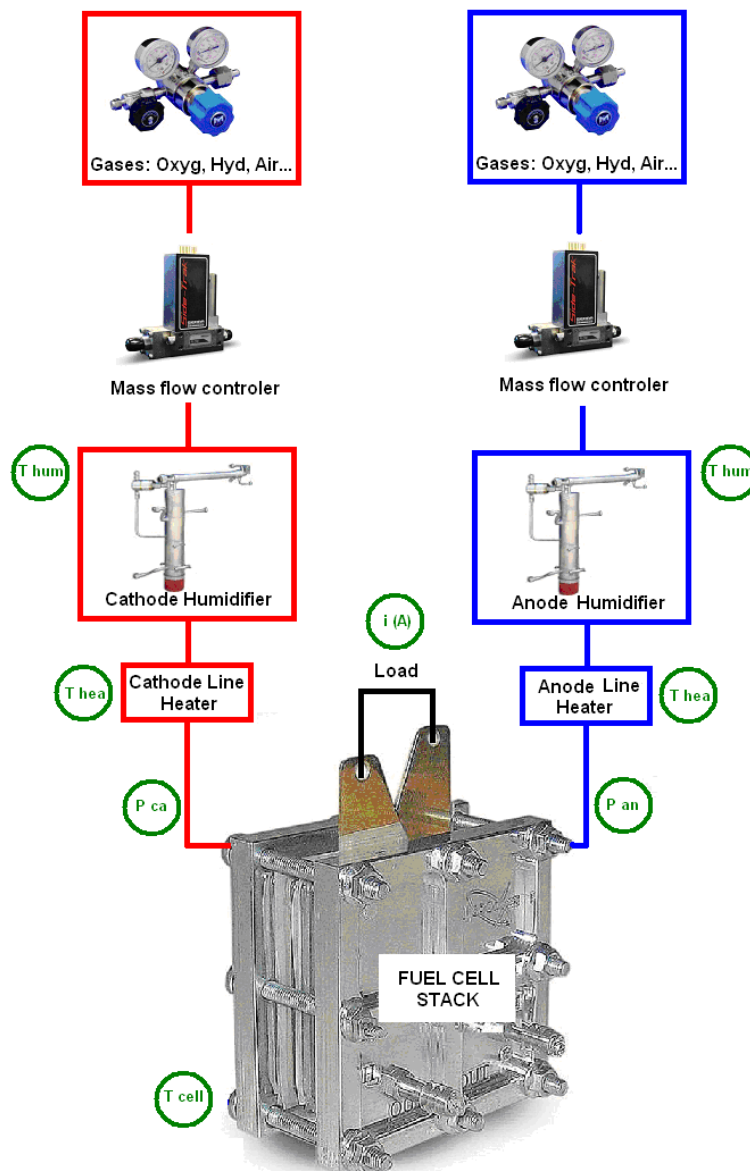The calculations were done at different temperatures: 80, 60, 40, 20 °C.

Figure 2.7 - Fuel Cell scheme. Green balls represent the variables to set-up.

To ensure the reliability of this theoretical calculations, the fuel cell was by-passed, and different conditions were tested by changing the temperature and flow rates.

2.3.4   Dependence of the total gauge pressure

The theoretical model was also used to measure the effect of the pressure on the volume of water collected. The variation of P_{total} alters the water fraction W_{inlet} – Equation 2.1, and consequently the volume of water expected.

2.3.5   Polarization curves

The performance of the MEAs that were fabricated was characterised by polarisation measurements. The performance depends primarily on the activity of the electrocatalyst layer, the quality of the material components, the flow rate and purity of the reactant gases. The best performance is obtained when pure oxygen is fed to the cathode, but in most practical systems air is used. By pressurising the air on the cathode side, substantial gains in performance may be obtained.

A. *Flow rates*

A polarization curve can be obtained by changing the load (Figure 2.7) and measuring the cell voltage of the fuel cell.

To estimate the flow rates consider a current of 1 C s^{-1}. From the definition of Faraday's constant, the number of electrons per second will be:

$$n = \frac{I}{F} = \frac{1}{96485} = 1.04 \times 10^{-5} \, moles/s \qquad (2.4)$$

so per minute, 6.22×10^{-4} mol of electrons will be obtained.

Taking into account the reaction occurring – Equation 1.32 (in the fuel cell H_2O and H_2O_2 will be produced, however is assumed that the hydrogen peroxide solution will be diluted, water is the major product), from the stoichiometry, 1.55×10^{-4} molecules of O_2 will react.

For an ideal gas, the molar volume V_m = 24.4 L mol^{-1} at 0 °C, 1 atm [84], and so the volume was 3.48 mL min^{-1}.

To evaluate the dependence on the cathodic reactant (O_2 or Air) a stoichiometry of 10 times more than the required by the reaction is used for the cathode. This value is used because it permits the use of automatic program in the rig, as it does not need to change flow rates (however, different concentrations of O_2 will be studied). This means, from the previous calculations, that the volume of O_2 necessary for a current of 1 A is 34.8 mL min^{-1}. The same calculations were done for the anode side; however, in this case, only twice the volume of H_2 is required (stoichiometry of 2).

The set up used was that presented in Section 2.3 B.

For these studies, a temperature of 60°C for the humidifiers and a pressure gauge of 1700 mbar (170000 Pa) were chosen.

B. Volume collected (Co catalyst)

In the case of using Co catalysts, it is also important to estimate the volumes collected on the cathode side, to be sure that the volume collected will be enough for volumetric analysis. Calculations considering the currents applied and the duration of the experiment were done (Eq. 2.4). As previously, from the stoichiometry of the reaction (Eq. 1.32) the molar quantity of water produced was found. Therefore, the volume of water produced could be calculated.

Before this, from the calibration of the humidifiers (Section 2.3.1) bypassing the cell, the volume expected (depending on P_{total}, flow rate and temperature of humidification) was calculated. These values should be added to the volume due to the passage of current.

2.3.6   Ohmic losses – current interrupt

The current interrupt method is normally used to measure the ohmic losses (ΔE_{ohm}) in a PEM fuel cell. An example of a voltage transient during current interruption is shown in Figure 2.8.
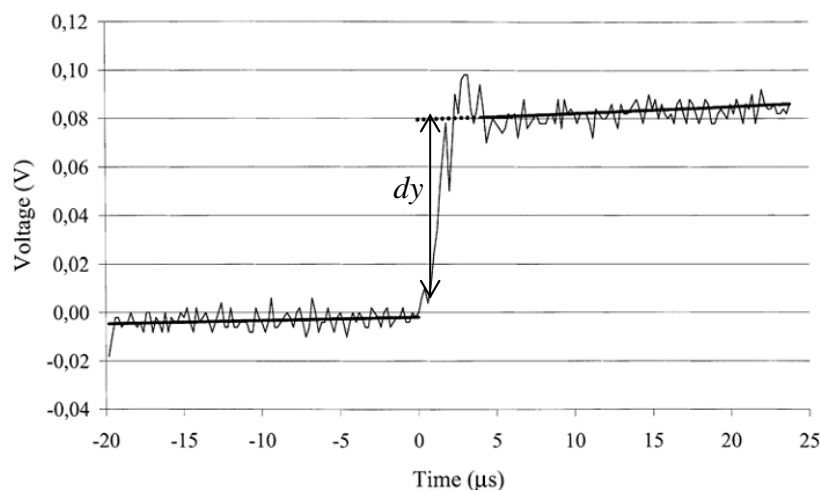
Figure 2.8– Voltage transient for individual cell in a PEM stack during current interruption [85].

The principle behind the use of the technique is that ohmic losses vanish much faster than the electrochemical overpotentials when the current is interrupted [85]. It is therefore important that the data acquisition for the voltage transient is as rapid as possible in order to adequately separate the ohmic and activation losses.

From Figure 2.8, interrupting the current the decay in the slope (*dy*) can be quantified. The resistance can be calculated in accordance with Ohm's law [86], Equation 2.5:

$$R(\Omega) = \frac{dy(V)}{I(A)} = \frac{I}{\eta_{ohm}}$$ (2.5)

where *dy* (V) is the value measured from the current interrupt, and *I* (A) is the load applied.

2.3.7   Hydrogen peroxide quantification

Potassium permanganate is a valuable and powerful oxidising agent, first introduced into titrimetric analysis by F. Margueritte for the titration of iron (II).

For volumetric analysis, sulfuric acid is the most suitable acid, as it has no action upon permanganate in dilute solution. For the titration of colourless or slightly coloured solutions, the use of an indicator is unnecessary, since as little as 0.01 cm^3 of 0.002 M potassium permanganate imparts a pale-pink colour to 100 cm^3 of water [87]. The basis of the method for hydrogen peroxide analysis can be represented by:

$$2MnO_4^- + 5H_2O_2 + 6H^+ \Leftrightarrow 2Mn^{2+} + 5O_2 + 8H_2O \qquad (2.6)$$
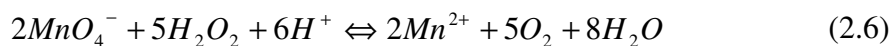
At the end-point, the solution colour changes to pale pink due to the presence of unreacted MnO_4^-.

2.3.8 Open circuit voltage (OCV)

The cell voltage at open circuit (OCV), which is the difference between the standard potentials of the cathode (E_c^θ) and the anode (E_a^θ), is strongly dependent on the temperature and pressure.

Under standard conditions (25 ℃, 1 atm), considering the reaction from Eq. 1.32, the electrode potential (E_a^θ) is 0.0 V (vs. RHE) and the cathode electrode potential (E_c^θ) is 1.23 V (vs RHE). The fuel cell OCV, E_{OCV}, can be expressed as Equation 1.38. with Eqs. 1.39 and 1.41. From these equations a theoretical OCV, E_{OCV}^t for the case in which the ORR leads to water (4-electron reduction) can be expressed as:

$$E_{OCV}^t = 1.23 - 0.000846(T - 298.15) + \frac{RT}{4F}.\ln(P_{O2}.(P_{H2})^2) \qquad (2.7)$$

The same calculations can be done considering a 2-electron ORR to give hydrogen peroxide, and the E_{OCV}^t is:

$$E_{OCV}^t = 0.70 - 0.000846(T - 298.15) + \frac{RT}{2F}.\ln(P_{O2}.P_{H2}) \qquad (2.8)$$

To calculate the partial pressures of O_2 and H_2 (P_{anode} or $P_{cathode}$) a theoretical model similar to the ones defined in Sections 2.3.1 and 2.3.2 is needed [8, 36, 67, 68]. An estimate of P_{O_2} or P_{H_2} can then be made considering the stoichiometry of the reaction.

CHAPTER 3

_____

Results and Discussion

This chapter is divided into experiments carried out in a conventional 3-electrode electrochemical cell and in a single cell (fuel cell), including hydrogen peroxide quantification.

The aim is to characterize and compare two catalysts, a standard and well-known platinum catalyst and a cobalt catalyst (discovered by Johnson Matthey for hydrogen peroxide production[1]), the first being used as reference.

3.1   Characterization measurements in the 3-electrode cell

Amongst the most frequently-used techniques for ORR catalysis studies cyclic voltammetry, rotating disk electrode (RDE), and rotating ring-disk electrode (RRDE) were all used.

3.1.1   Cyclic voltammetry

Cyclic voltammetry was used to characterize the metal catalyst surface.

A.   *Carbon/baseline voltammetry*

The catalyst supports, carbon 1 and carbon 2, were examined by cyclic voltammetry. The baseline response was close to zero, which means that the supports will not interfere in the results – see Figures 3.1 and 3.2.

B. Pt catalyst voltammetry

Figure 3.1 shows the cyclic voltammogram (CV) of a carbon-supported Pt catalyst in 0.1 M $HClO_4$. The voltammetric features are less sharp than expected (compare with Figure 1.11). The characteristic pair of peaks related to hydrogen adsorption/desorption and Pt oxide formation and reduction are very small even though they can be found. The double layer region is seen between 0.35 – 0.43V (vs RHE) [50, 88]. A "weak" adsorption of hydrogen can be attributed to the particle size and dispersion on the carbon support, which may change the number of adsorption sites. Mayrhofer, et al. [89], found that the Pt-H interactions appeared to be weaker on smaller particles and also that at the same potential the surface coverage by oxygenated species increases by decreasing the particle size.
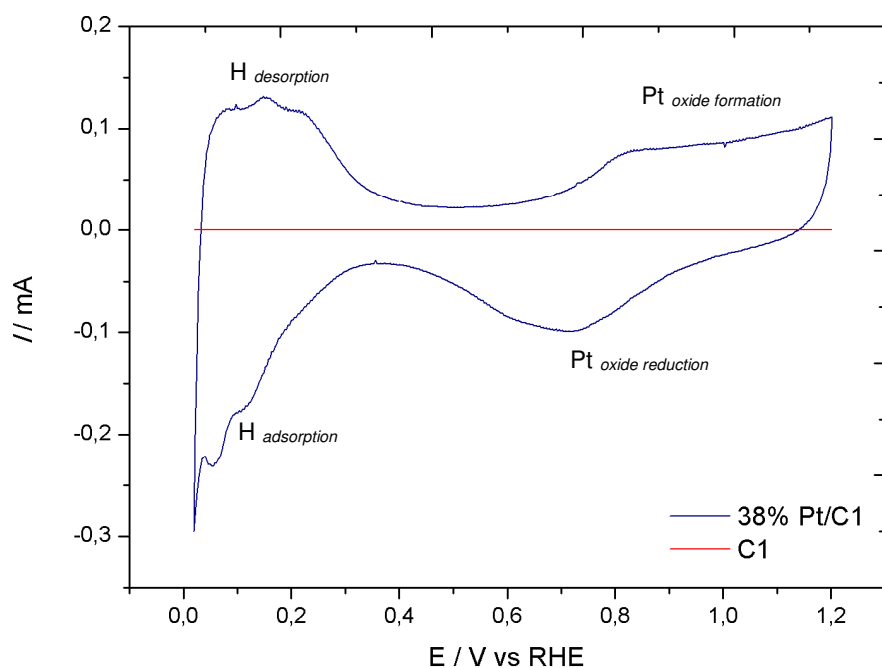
Figure 3.1 - Cyclic voltammogram of 38% Pt/C1 (0.019 mgPt cm^{-2}) in 0.1 M HClO$_4$.

C. Co catalyst voltammetry

Figure 3.2 shows the CV of the carbon-supported cobalt catalyst in 0.1 M $HClO_4$. The CV does not reveal any features, and no relation with Co metal characteristics can be found. The treatment of the catalyst is the reason for this absence - using the same analytical technique in pre-treated catalysts, Fox et. al. [90] found similar results.
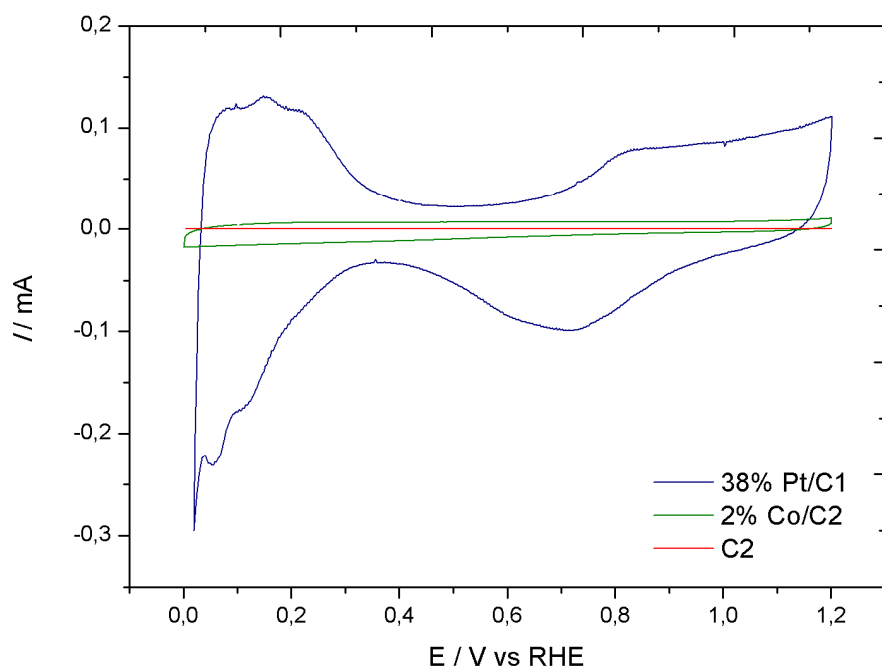
Figure 3.2 - Cyclic voltammogram of 38% Pt/C1 (0,019 mgPt cm^{-2}), 2% Co/C2 (0.001 mg Co cm^{-2}) in 0.1 M HClO$_4$.

D. Active surface of metals (EPSA and ECSA)

The number of Pt surface atoms is commonly estimated from the charge consumed for adsorption/desorption of underpotential-deposited hydrogen Q_H, in the potential between 0.05 – 0.35 V (vs RHE), assuming one adsorbed H per Pt surface atom [89] Equation 1.21.

The hydrogen adsorption charge, Q_H, can be determined from Equation 3.1.

$$Q_H = 0.5 \times (Q_{Total} - Q_{DL}) \tag{3.1}$$

where Q_{total} is the total charge transfer in the hydrogen adsorption/desorption potential region and Q_{DL} stands for the capacitance of the high-surface area carbon support which is also called "double layer" in the voltammogram – 1.11 [85]. So, integrating the corresponding CV in the anodic sweep, after subtracting the charge density required for the charging of the double layer [91, 92, 93, 94] the total charge density transferred through the metal/electrolyte interface, Q_H (μC cm^{-2}) is determined, Eq. 3.2.

$$Q_H = \frac{\int i.dE}{\upsilon} \tag{3.2}$$

However, the most correct value can be found as the average value between the amounts of charge exchanged during the electroadsorption and electrodesorption of H_2 on Pt sites.

In this case, and from Figure 3.1,

$Q_H = 311\mu C$ (for a loading of 0.019 mg Pt cm^{-2})

This value is in agreement with Schmidt et al [91], who found a 3 mC cm^{-2} value for Q_H (for a loading of 28 µg Pt cm^{-2}). It is important to mention that Mayrhofer et al [93] found that the value of Q_H increases linearly in proportion with the loading of Pt. The determination of Q_H allows the evaluation of the electrochemical platinum active surface area (EPSA) [95]. Applying Equation 1.22 to this case,

$$EPSA = \frac{3.11 \times 10^{-4}}{0.196 \times 2.10 \times 10^{-4}} = 7.54 cm^2\,_{Pt}\,cm^{-2} \tag{3.3}$$

Using EPSA, it is also possible to determine the ECSA, the electrochemically active surface area (ECSA) [95]. Applying Equation 1.23,

$$ECSA = \frac{7.54}{0.019} = 397 cm^2 mg^{-1} Pt \tag{3.4}$$

The absence of features in the Co-Carbon 2 cyclic voltammogram does not permit this calculation.

3.1.2   Rotating disk electrode

The understanding of the kinetic limitations of the oxygen reduction reaction (ORR) on different catalysts is of outstanding interest in fuel cell research [96]. The use of the rotating disk electrode (RDE) has great advantages in that it can eliminate and control

mass-transfer and enable the accurate evaluation of kinetically controlled ORR activity [97].

A. Pt hydrodynamic voltammograms

Figure 3.3 shows hydrodynamic voltammograms of the carbon-supported platinum catalyst in 0.1 M $HClO_4$. The baseline was also determined to correct the data. The ORR currents at the disc commence at ca. 1.0 V in the negative direction (oxygen starts reacting and producing water by the four electron reaction). This region is called "mixed control". The concentration of O_2 decreases until it becomes "zero" close to the disk electrode [50, 98] (the O_2 that goes through the catalyst will react automatically); at this point the diffusion-limiting current is reached as a plateau region [94]. For different rotation rates, different limiting currents are achieved (from the Levich equation (Eq. 1.25), j is directly proportional to $\omega^{1/2}$.
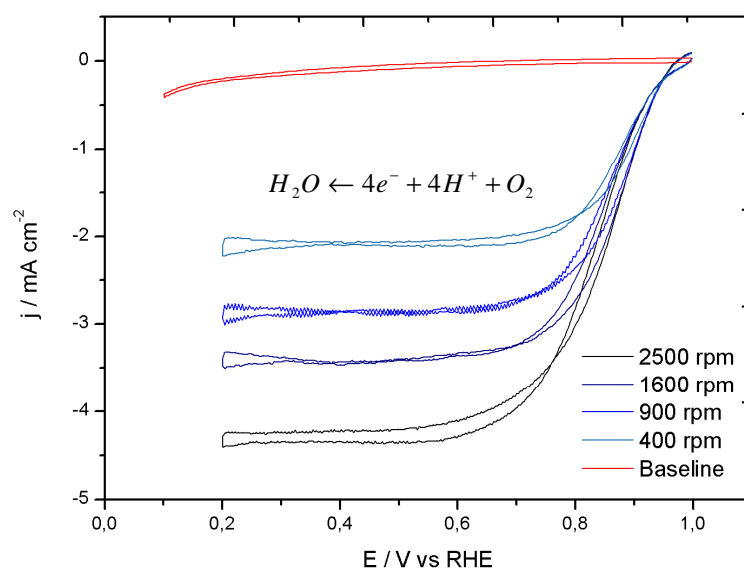
Figure 3.3 – Hydrodynamic voltammogram of 38% Pt/C (0.019 mgPt cm^{-2}) in 0.1M HClO$_4$.

B. Co hydrodynamic voltammograms

Figure 3.4 shows hydrodynamic voltammograms of the carbon-supported cobalt catalyst in 0.1 M $HClO_4$. The baseline was also recorded to correct the data. Below 0.6 V the oxygen starts reacting and producing water (by the four electron reaction), the production of hydrogen peroxide is the reason for the change from 1.0 V

(platinum catalyst) to the 0.6 V, where both reactions should be occurring. This behaviour is typical of a hydrogen peroxide catalyst. A diffusion-limiting current plateau was not found, the diffusion is too slow to be a diffusion-limited catalyst.

The sloping plateau currents in steady-state voltammograms was studied by Ziang et al. [99], who found that in catalyst-substrate complexes the distribution of catalytic sites for reduction will lead to inclined plateaux on current-potential curves. Furthermore, some studies done with carbon-supported cobalt catalyst revealed the absence of limiting currents. Similar results were found by Fox et al. (Pt-Co/C catalyst) [90], or Lee et al [100], with a Co-PPy/C. With the Co-PPy/C there was also found a limiting current of -1.0 mA cm^{-2} for a 400 rpm rotation rate (loading of 0.122 mg cm^{-2}).
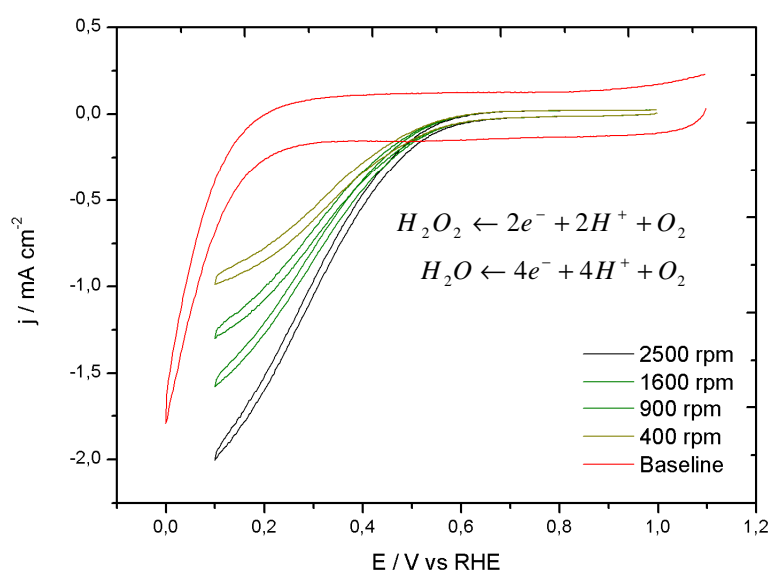
Figure 3.4 - Hydrodynamic voltammogram of 2% Co/C2 (0.001 mgCo cm^{-2}) in 0.1M HClO$_4$.

The absence of limiting currents is a fact common to other studies, and is explained mainly by the porous electrode behaviour (the distribution of active sites) and the influence of the Nafion in the catalyst layer.

According to the porous electrode explanation, the depth of O_2 penetration inside the electrode structure changes with potential. If the electrocatalyst is platinum, the O_2 reaction is limited only to the outer part of the porous electrode and a flat limiting current plateau is observed. Macrocycle molecules are poorer electrocatalysts than platinum[12]. In the cobalt catalyst no well-defined diffusion limiting current has been

82

found, which means that the distribution of active sites on these catalysts is less uniform and the oxygen reduction reaction rate is slower [28, 93].

3.1.3   Ink composition study – amount of Nafion

The amount of Nafion in the catalyst-containing ink for the fuel cell cathode can influence the efficiency of the reduction process.

Figures 3.3 and 3.4 showed two types of hydrodynamic voltammogram. This difference is related with the presence or absence of diffusion limiting currents (scheme below).
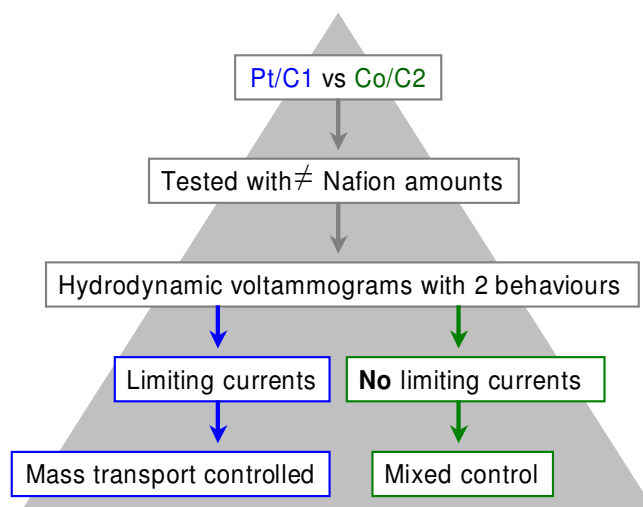
To understand the absence of the limiting currents, a study of the effect of the amount of Nafion in the ink composition was done. Similar studies have been done in carbon-supported platinum catalysts by Chu [98], Ayad et. al [101] and Paulus et. al [72]. However, Chu and Ayad used a Pt rotating disk electrode covered with Nafion ionomer and Paulus used a glassy carbon rotating disk electrode in which he pipetted an aliquot of catalyst suspension, and after the evaporation of water he added a drop of diluted Nafion on top – Figure 3.5.
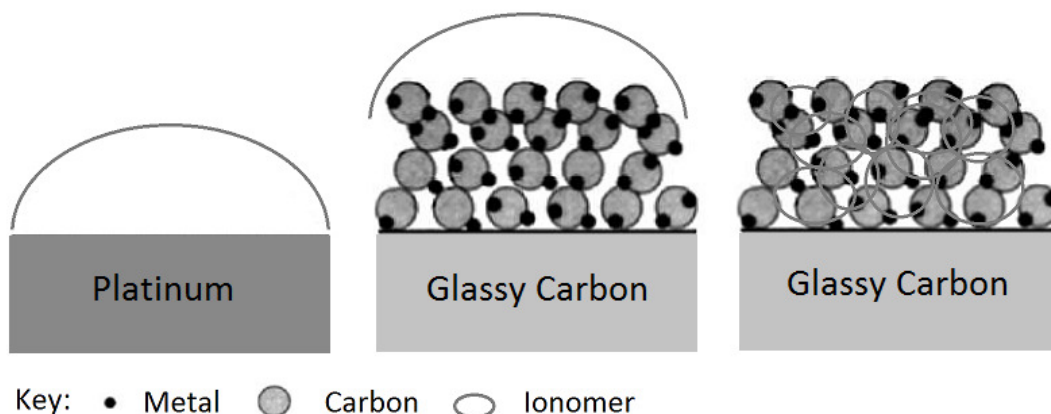
Figure 3.5 – Scheme representing the different studies about the infuence of Nafion in RDE studies. On the left the method used by Chu [98] and Ayad et. al [101] , in the middle the method used by Paulus et. al [72] and on the right the method used in this work.

In this work, different amounts of Nafion were added to the catalyst ink solution. The standard and well-known platinum catalyst and the cobalt catalyst were studied using this configuration.

A. *Pt catalyst*

Two carbon-supported platinum catalysts were used with metal percentages of 20% and 38%. The amounts of 17.8%, 9.8%, 1.7% of Nafion in the solvent were added to the ink composition. The aspect of the layers obtained for 39% Pt/C1 with 1.7% Nafion are shown in Figure 3.6: the one on the right was not completely covered (the higher the Nafion amount, the better coverage the layers will have).

The hydrodynamic voltammograms are presented in Figure 3.7.

Figure 3.6 – RDE layers of a 38%Pt/C1 catalyst, 0.019 mgPt cm^{-2} (1.7% Nafion).

Figure 3.7 shows the diffusion limiting currents found. As expected, the best value is related to the lowest amount of Nafion. The Nafion content adds a film diffusion resistance which changes the diffusion of O_2 through the catalyst layer. The thicker the layer, the higher the resistance, the lower the O_2 reacting, and the worst will be the limiting current. This effect can be determined by the Koutecky-Levich equation [72].

The effect of the metal loading on the limiting currents was tested with the 20% and 38% Pt/C1 catalysts (using the same amount of Nafion), and the limiting currents found are close - Figure 3.7. This result is in agreement with Gojkovic et al. [102], who found that the limiting current does not depend on Pt loading of the electrocatalyst.
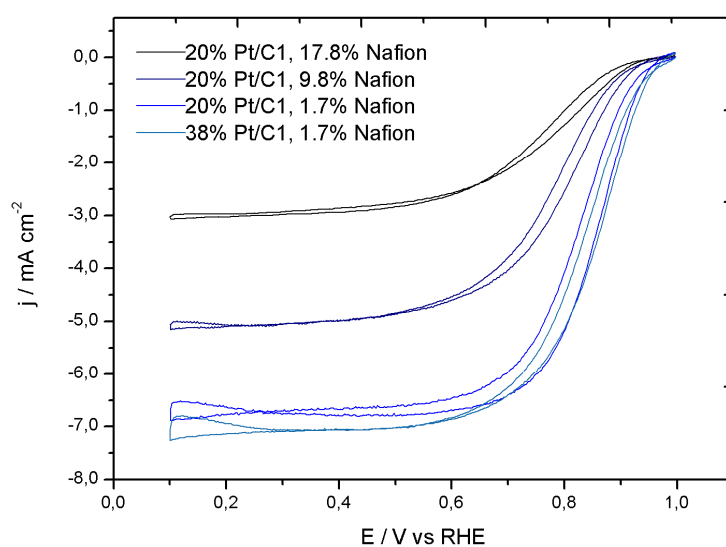
Figure 3.7 - Hydrodynamic voltammograms of 20% Pt/C1 (17.8%, 9.8%, and 1.7% Nafion) and 38%Pt/C1 (1.7% Nafion), 2500 rpm, scan rate 20 mV/s, in 0.1M HClO₄.

From the previous results and in relation to the 20%Pt/C1, the relation between the Nafion amount used in the inks and the limiting currents can be represented by Figure 3.8.
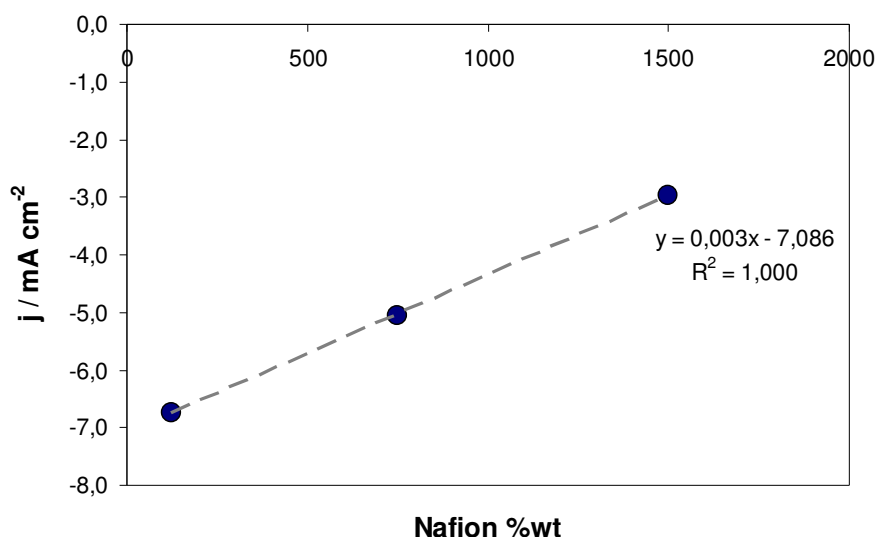
Figure 3.8 – Relation between Nafion amount and limiting currents for 20%Pt/Cl.

Extrapolating the curve, it was found that when the Nafion amount is zero, the limiting current value is -7.01 mA cm^{-2}. Comparing this value with the literature, using 0.5 M, H$_2$SO$_4$ as electrolyte, Ayad et. al [101] obtained -0.317 mA cm^{-2}, Chu [98] found, with a 85% conc. H$_3$PO$_4$ as electrolyte -0.152 mA cm^{-2}, and finally Paulus, et. al [72], found -0.388 mA cm^{-2}, evidence that the intercept value will in practice be different from zero.

A.1 Mass activity (Pt catalysts)

The mass activity reflects the gain/cost factor of a catalyst and is therefore of major importance in the development of economical catalysts [103]. The mass activity i.e. the reaction rate per mg catalyst [103, 104, 105] can be determined by Equation 3.5.

$$Mass.activity = \frac{I_k}{L_{Pt}} \tag{3.5}$$

where I_k is the limiting current corrected (Eq. 1.27), L_{Pt} the platinum catalyst loading. Assuming that all the geometric area of the electrode is covered (since the diffusion limiting current is dependent on the geometric area), the different inks/layers can be compared.
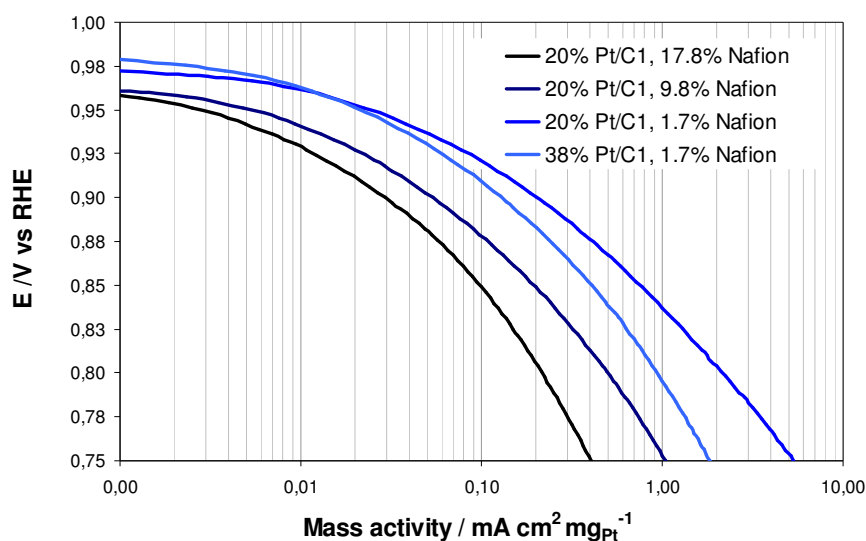
Figure 3.9 - Mass activity of the catalysts studied, 20% Pt/C1 (17.8%, 9.8%, and 1.7% Nafion) and 38%Pt/C1 (1.7% Nafion), 2500 rpm, scan rate 20 mV/s, in 0.1M HClO$_4$.

Figure 3.9 shows that the 38% Pt/C1 with 1.7% Nafion is most active and that the Nafion loading influences the results.

A.2 Specific activity – platinum catalysts

The specific activity, i.e. the reaction rate per unit active area of the catalyst [93, 104, 105] can be determined from Equation 3.6.

$$Specific.activity = \frac{I_k}{L_{Pt}\big/Q_H} = \frac{Mass.activity}{Q_H} \qquad (3.6)$$

where I_k is the corrected limiting current (Eq. 1.27), L_{Pt} the platinum catalyst loading and Q_H is 2.10 x 10^{-4} C cm^{-2}.

Figure 3.10 shows that 38% Pt/C1 with a 1.7% Nafion is the most active. At 0.9V, a specific activity of 0.16 mA cm^{-2} was found.
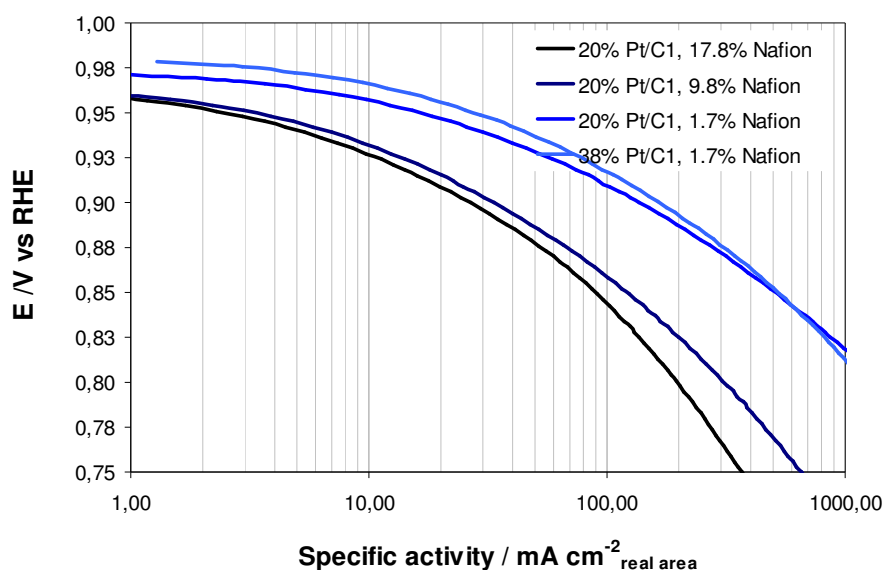
Figure 3.10 - Specific activity of the catalysts studied, 20% Pt/C1 (17.8%, 9.8%, and 1.7% Nafion) and 38%Pt/C1 (1.7% Nafion), 2500 rpm, scan rate 20 mV/s, in 0.1M HClO₄.

Wang et al. [106] and Mayrhofer et al. [93] found that the specific activity increases with the particle size. Mayhofer also found that this result is independent of the temperature. For polycrystalline Pt, at 0.9 V, using 0.1M HClO₄ as electrolyte and a rotatition rate of 1600 he found a specific activity of 1.5 mA cm^{-2}. Carbon-supported Pt nanoparticles with mean diameters of 1-1.5 nm, 2-3 nm and 5 nm were also analysed. For a 1 nm Pt catalyst a specific activity of 0.125 mA cm^{-2} was found. At 0.85 V, Mayrhofer found a specific activity of 0.5 mA cm^{-2}, for the 1 nm Pt catalyst, the same value obtained at the same potential in this work (Figure 3.10).

A.3 Levich analysis

Levich analysis was done on the results presented in Figure 3.11, plotting the diffusion-limited current densities j_L vs $1/\omega^{-1/2}$. This plot should be linear and should pass through the origin. The slope is commonly used to estimate the diffusion coefficient of the electroactive species (D), and the number of electrons involved (n).

Using Eq. 1.25, and considering that F is 96485 C mol^{-1}, D is 1.9 x 10^{-5} cm^2 s^{-1}, ν is 0.011 cm^2 s^{-1} and c_∞ *is* 1.25 x 10^{-6} mol cm^{-2} (using literature data [96]), the theoretical

values for *n* equal to 2 and 4 electrons exchanged were calculated and are presented in Figure 3.11 (labelled Levich n = 4, n = 2).
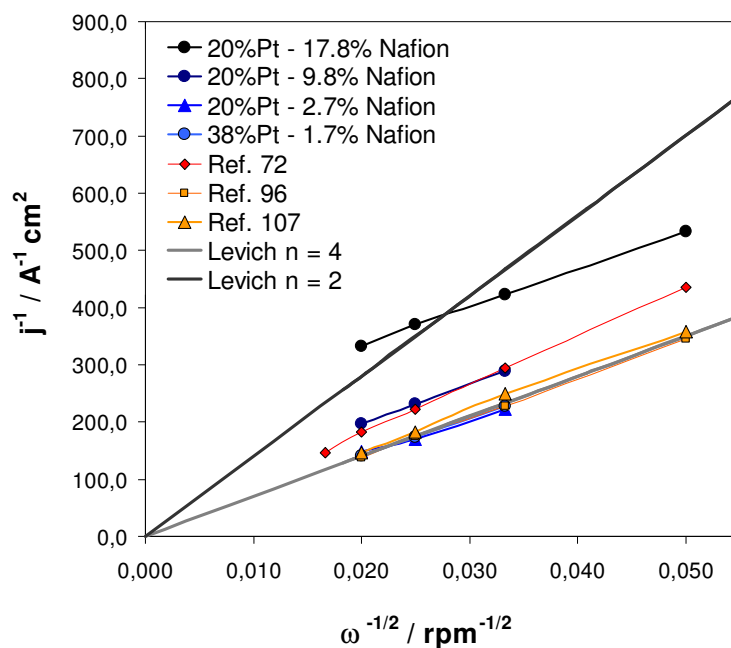

Figure 3.11 – Levich plot for the 20%Pt/C1 and the 38%Pt/C1 catalysts, with different amounts of Nafion. References and theoretical values for 2 or 4 electrons exchanged are also presented.

Figure 3.11 shows the Levich plot for the carbon-supported platinum catalysts studied. As expected, the lower the amount of Nafion, the closer to the literature values. Considering again Eq. 1.25, I_L is proportional function of n, D, v, c_∞ ω. In this case, v, c_∞ and ω should remain constant between measurements (inks/layers). The different intercepts in Figure 3.11 cannot be related with *n*, as it should not vary since the same catalyst is being used.

From previous studies [72, 98, 101] it is known that Nafion blocks the active sites of the catalyst, creating a resistance against the diffusion of O_2.

Analysing the results, theoretically and varying *D,* two different curves were found, which are represented in Figure 3.12.
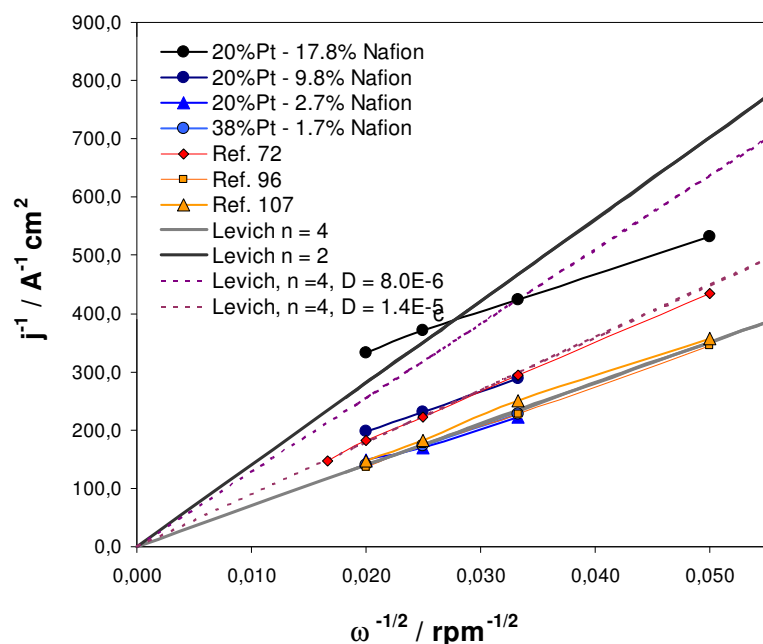
Figure 3.12 - Levich plot for the 20%Pt/C1 and the 38%Pt/C1 catalysts, with different amounts of Nafion. References and theoretical values for 2 or 4 electrons exchanged and for different diffusion coefficients (in cm^2 s^{-1}) are also presented.

Figure 3.12 shows that for the 20% Pt with 9.8% of Nafion (considering that n, ν, c_∞ ω remain constant), D should be around 1.4 x 10^{-5} cm^2 s^{-1}, which is slightly smaller than the literature value. Relative to the 20% Pt with 17.8% of Nafion, considering a D around 8.0 x 10^{-6} cm^2 s^{-1} for 900 rpm (0.030 rpm$^{-1/2}$), the curve overloads the result found. However, for the other rotation rates the results do not fit the theoretical model.

A.2 Koutecky-Levich equation

For a rotating disk electrode coated with polymer film, a more general expression for the current, I, would include the kinetic current, I_k. A plot of j^{-1} versus $\omega^{-1/2}$, the Koutecky-Levich plot, should give a straight line which intercepts the y axis at j_k^{-1}. The value of this intercept is usually justified by an additional resistance (for instance related with the Nafion film). The extrapolation to infinitely fast mass transport, for which surface and bulk concentrations would be equal, allows determination of the kinetic current density j_k - Figure 3.13.

In this case, and from Figure 3.13, $j_k \neq 0$, so representing j^{-1} vs $\omega^{-1/2}$ follows the relation [105, 108].

$$\frac{1}{j} = \frac{1}{j_k} + \frac{1}{0.20FAD^{2/3}\nu^{-1/6}c_\infty\omega^{1/2}} \Leftrightarrow y = b + a.x \qquad (3.7)$$

where b is the intercept (j_k) with the y axis and a is the slope of the curve.

From Equation 3.7 the number of electrons exchanged can be determined

$$a = slope = \frac{1}{B} = \frac{1}{0.20nFAD^{2/3}\nu^{-1/6}c_\infty} \qquad (3.8)$$

So,

$$n = \frac{a^{-1}}{0.20FAD^{2/3}\nu^{-1/6}c_\infty} \qquad (3.9)$$

Figure 3.11 shows a Koutecky-Levich plot for the 38% Pt/C1 catalyst (1.7% Nafion), at the potentials 0.85, 0.80, 0.75 and 0.70 V vs RHE, all in the diffusion-mixed control region.

For all rotation rates, a series of essentially parallel straight lines indicates that the number of electrons transferred per O_2 molecule and active surface area for the reaction rate are not changed significantly between the potential range 0.70 - 0.85V vs RHE and the limiting current plateau [12, 72, 105, 109, 110].

The intercepts with the y axis can be related with the effect of the Nafion in the catalyst layer [72, 98]. Gojkovic et al.[102] found similar results (intercept $\neq$ 0) and considered that diffusion control is not established, probably due to two reasons, the distribution of the active sites, and the Nafion film which acts as an additional barrier to O_2 diffusion.
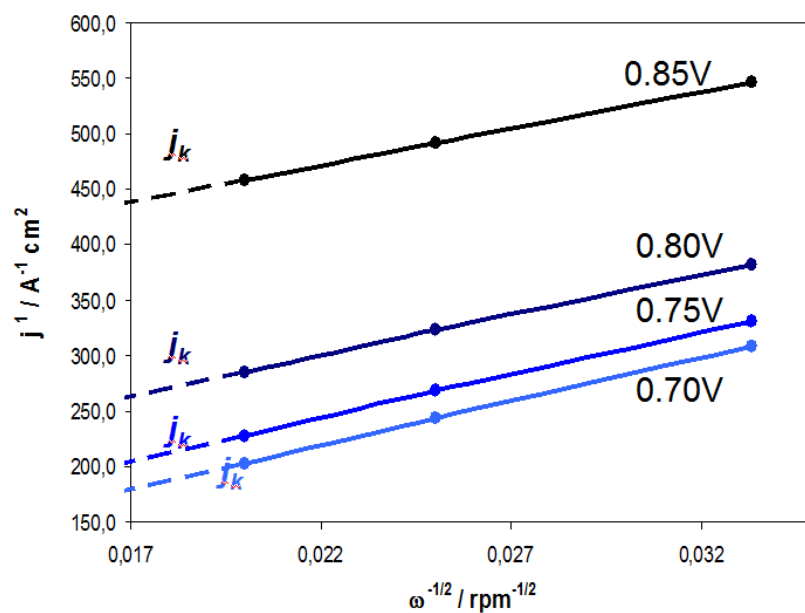
Figure 3.13 – Koutecky-Levich plots for the 30%Pt/C1 (1.7% Nafion); potential range studied 0.70 – 0.85 V.

Figure 3.14 shows a direct relation between the film resistance caused by the Nafion and the kinetic currents. Again, kinetic currents increase as the amount of Nafion increases, the same as found by Chu [98].
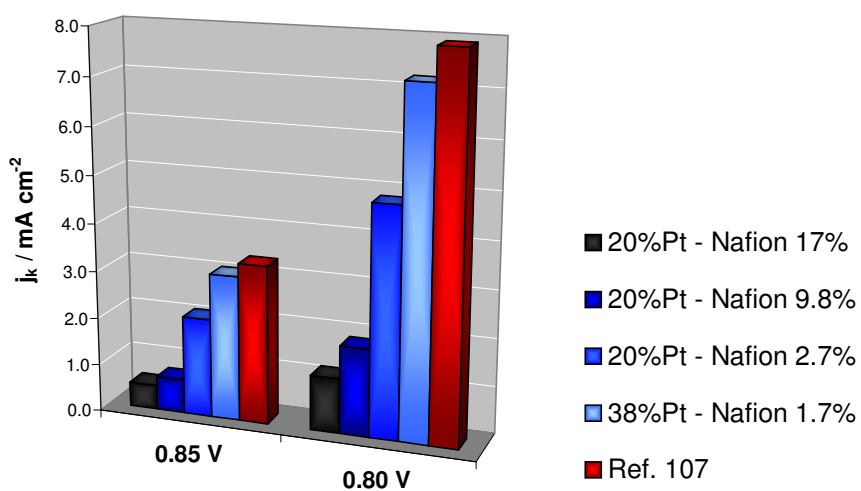

Figure 3.14 – Relation between Nafion amount and the kinetic current densities from Figure 3.11 [107].

A.3 Number of electrons transferred

Finally, from Equation 3.9, is possible to calculate the number of electrons exchanged in the reaction over the limiting current potential range. Figure 3.15 shows the results found for the 38% Pt/C1 catalyst, and the 4 electron reaction was verified.
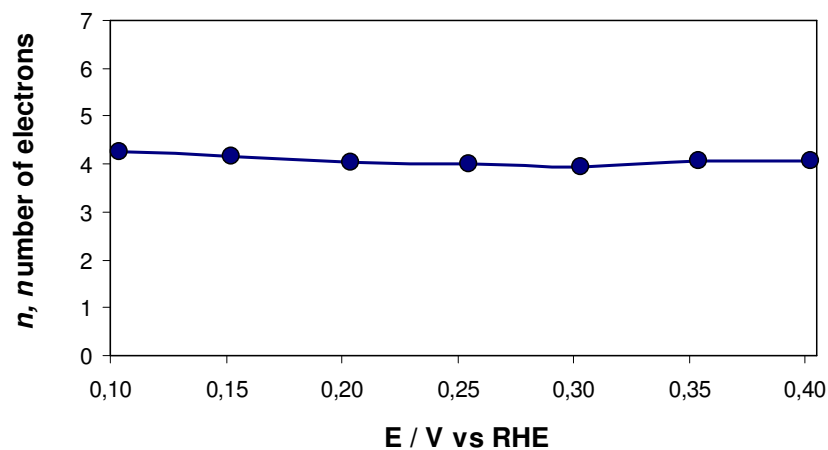

Figure 3.15 – Number of electrons exchanged in the reaction for the 38%Pt/C1 (1.7% Nafion).

A.4 Tafel analysis

Using a limiting form of the Tafel equation, due to the high negative overpotentials (see Section 1.3.1 C.) the Tafel slope can be determined. From the plot for the 38%Pt/C1 catalyst (with 1.7% Nafion), Tafel analysis was done and is shown in Figure 3.16.
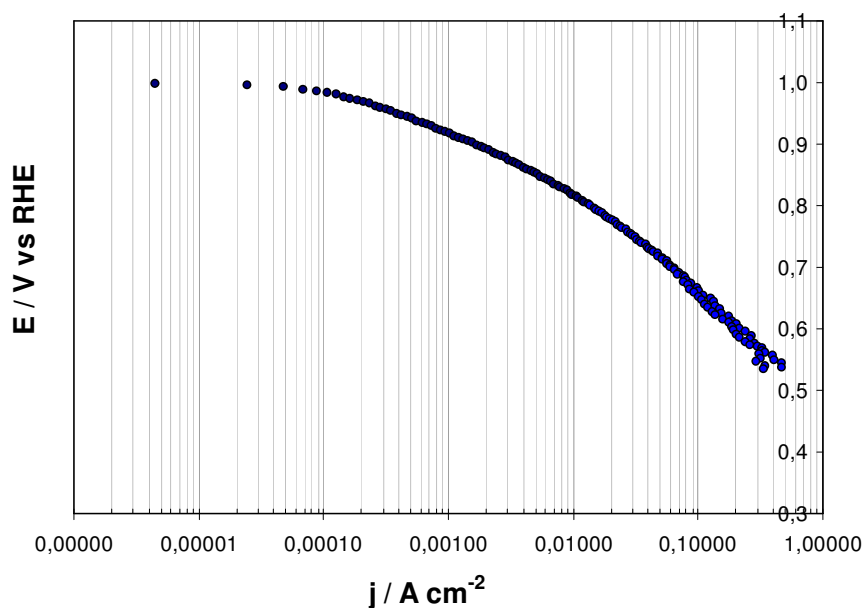
Figure 3.16 – Tafel plot for 38%Pt/C1 (1.7% Nafion), in oxygen saturated 0.1M HClO$_4$, corrected for mass-transfer resistance, at 900 rpm.

At higher potentials (> 0.85 V) the Tafel slope was found to be 76 mV dec^{-1}, and at lower potentials (< 0.85 V), it was 186 mV dec^{-1}. The results obtained for the platinum catalyst are in agreement with the literature results presented in Table 3.1.

Tabela 3.1 – Literature results for the Tafel plot in carbon-supported platinum catalysts.

References	Electrolyte, Catalyst	Tafel slope (mV/dec) Higher / Lower
72	0.5M H$_2$SO$_4$, Pt/Vulcan	62 / 123
107	0.1M HClO$_4$,Polycrystalline Pt	64 / 126
111	0.5M H$_2$SO$_4$, Pt/XC-72R	69 / 120
112	0.1M HClO$_4$, Pt/Vulcan	78 / -

The Tafel slopes are ascribed to two different rate determining steps [12].

B. Co catalyst

A carbon-supported cobalt catalyst was used, with metal loadings of 2% and amounts of Nafion of 10%, 2.7%, 1.3% and 0.7% of Nafion related to the solvent added to the ink solution. The visual aspect of the layers obtained for 39% Pt/C1 with 1.7% Nafion are shown in Figure 3.17, the one on the left was not completely covered (as before, the higher the Nafion amount, the better the coverage).

Figure 3.17 – RDE layers of a 2%Co/C2 catalyst. On the left the ink composition with 10% Nafion, on the right 1.7% Nafion was added to the ink solution.

Figure 3.18 shows hydrodynamic voltammograms for the Co catalyst. Similarly to Figure 3.4, no limiting current plateau was found.
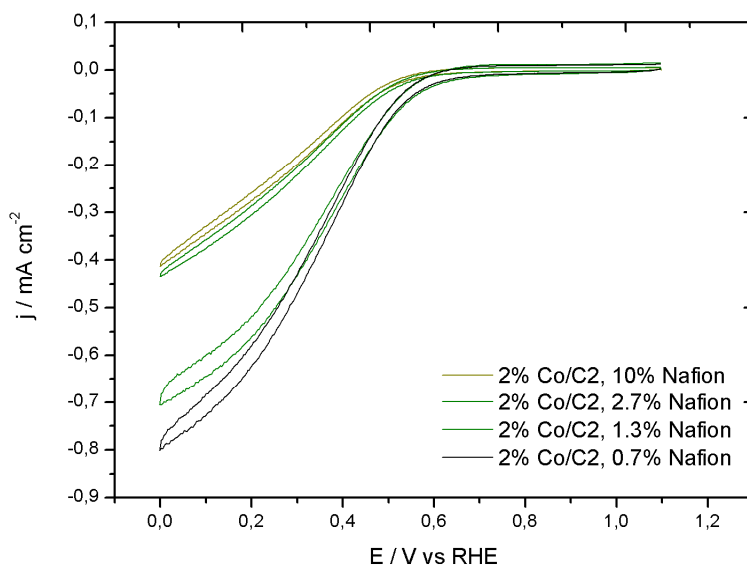

Figure 3.18 - Hydrodynamic voltammograms of 2% Co/C (0.001 mgCo cm^{-2}) in 0.1M HClO$_4$, at 2500 rpm.

B.1 Levich equation

Figure 3.19 represents a Levich plot for the 2% Co/C2 catalyst with different ink compositions. As expected, and as for the platinum catalysts, the lower the amount of Nafion, the closer to the theoretical values.
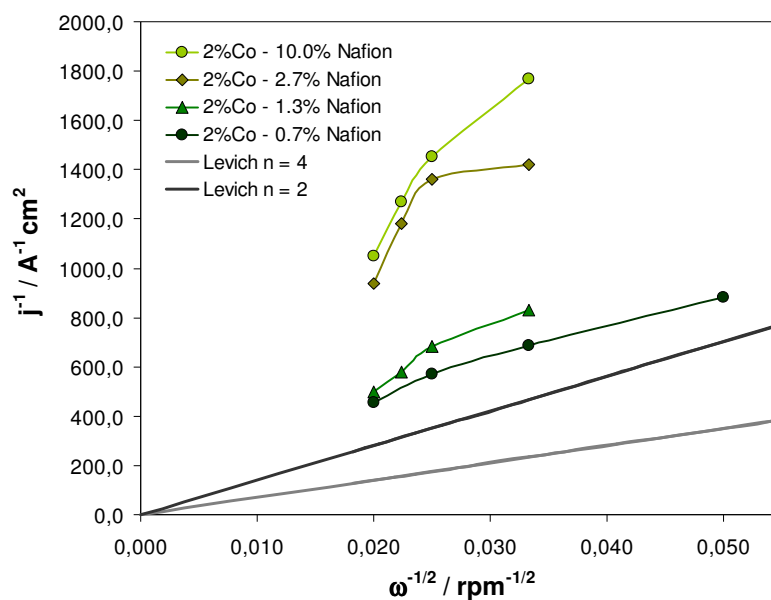

Figure 3.19 – Levich plot for the 2%Co/C2 catalyst, with different amounts of Nafion.

The linearity of the Levich curves increases with the decrease of Nafion, which seems to be related to the blockage of the active sites in the catalyst layer, which influences more than the homogeneity/coverage of the layer. This effect is maximized at lower rotation rates and could explain the observed dependence of the limiting currents on rotation rate.

B.2 Koutecky-Levich equation

Figure 3.20 shows the Koutecky-Levich plot for the 2% Co/C2 catalyst (1.3% Nafion) at 0.30, 0.25, 0.20 and 0.15 V vs RHE (all in the diffusion-mixed control region). The intercepts with y axis are related to the effect of the Nafion in the catalyst layer.
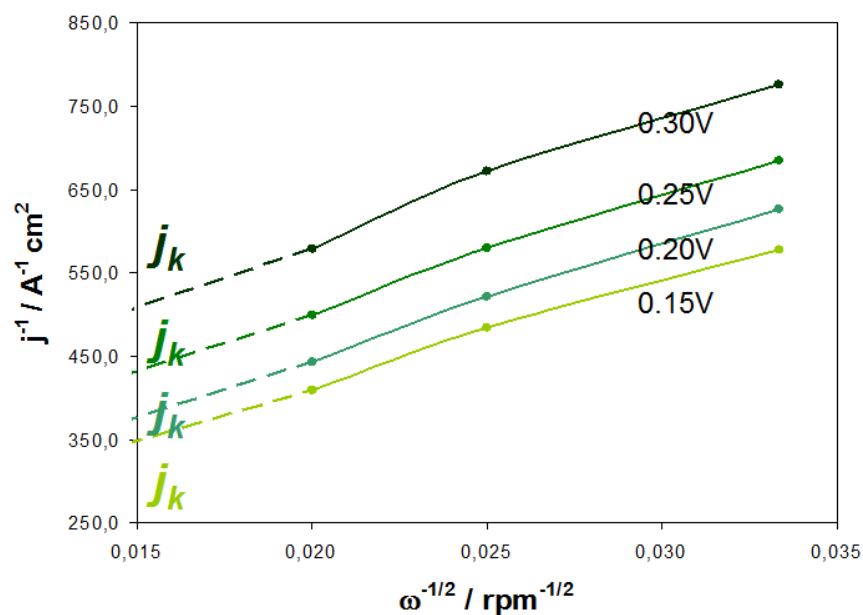
Figure 3. 20 – Koutecky-Levich plot of the 2%Co/C2 catalyst with 1.3%Nafion.

Figure 3.21 shows the direct relation between the film resistance caused by the Nafion and the calculated kinetic currents.
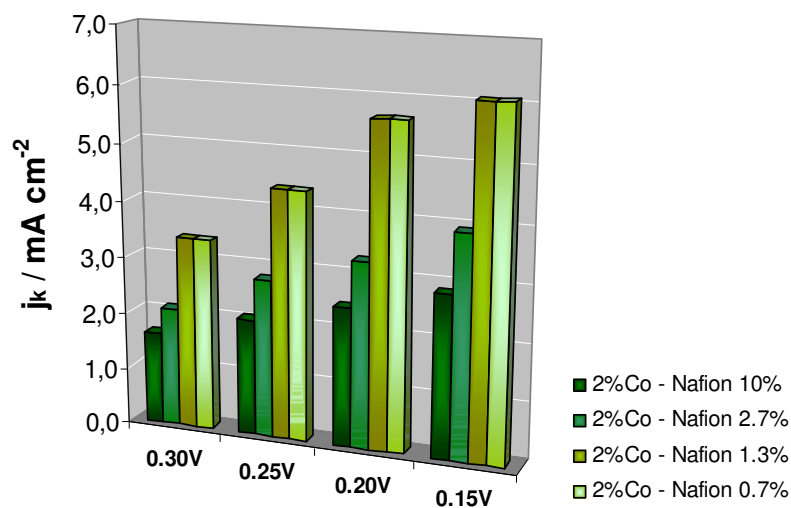

Figure 3.21 - Relation between Nafion amount and kinetic currents results from Figure 3.18.

Again, the kinetic currents increase as the Nafion amount increases, as was found with the Pt catalysts [91].

B.3 Number of electrons

Assuming that the effect of the Nafion can be ignored, the number of electrons exchanged can be calculated from Equation 3.9. Figure 3.20 shows the results for the 2%Co/C2 (1.3% Nafion) catalyst and a 2 electron reaction was verified [93].
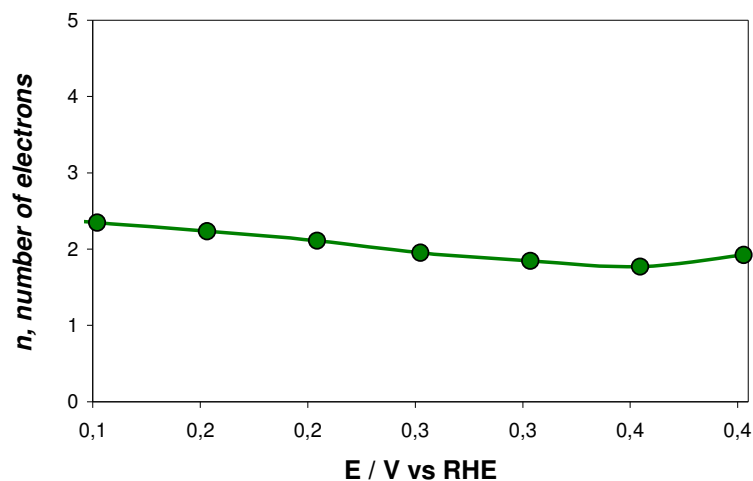

Figure 3. 22 – Number of electrons exchanged in the reaction for the 2%Co/C2 (1.3% Nafion).

For the cobalt catalyst, even without the limiting currents, this analysis confirmed that two electrons are exchanged during the process.

B.4 Tafel analysis

Following the procedure for the platinum catalyst, a Tafel slope can also be calculated for the 2%Co/C2 (Nafion 1.3%). The results are represented in Figure 3.23. From the plot it was verified that at higher potentials (> 0.95 V), 419 mV dec^{-1}, intermediate potentials 514 mV dec^{-1} and at lower potentials (> 0.80 V), 191 mV dec^{-1}.
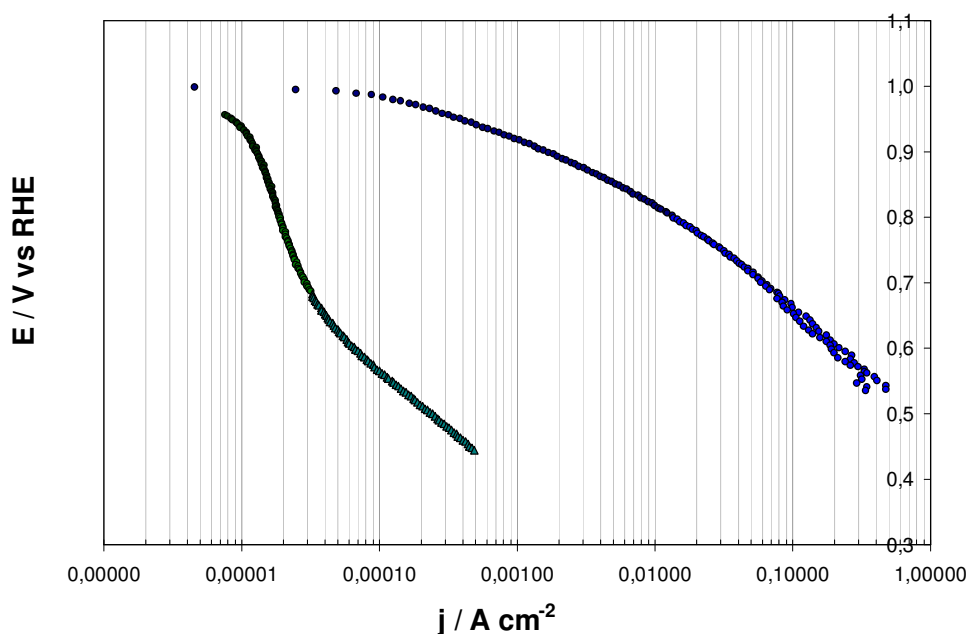
Figure 3.23 – Tafel plots for 38%Pt/C1 (1.7% Nafion) and 2%Co/C2 (1.3% Nafion), in oxygen saturated 0.1M HClO₄, corrected for mass-transfer resistance, at 900 rpm.

Figure 3.23 shows the Tafel plots. Comparing the values found with the 10%Co/TETA catalyst studied by Zhang et al. [28]. Zhang found for higher potentials (>0.95 V) a Tafel slope of 409 mV dec⁻¹ and for intermediate potentials 654 mV dec⁻¹. From theory, the higher the Tafel slope, the slower the reaction kinetics [8], so we can assume that the cobalt catalyst reactions will be much slower when compared with platinum. The very similar values found for the Tafel slopes of the two different cobalt catalysts can be assumed as proof of the 2 electron pathway. Zhang et al. also found some predominance of the 2-electron reduction in their study.

3.1.4   Rotating ring disk electrode

These experiments were undertaken to probe the products of the electrode reaction at the disk electrode at the ring electrode and the fraction of species undergoing reaction in homogeneous solution.

A. Collection efficiency

The fraction of the species formed at the disk reaching the ring electrode, the collection efficiency, depends on the characteristics of the RRDE [50, 107], and has to be determined for each electrode used, according to Eqn. 1.28. The steady-state collection efficiency can be measured using a couple such as ferrocyanide (Fe^{3+}) / ferricyanide (Fe^{2+}), Eq. 3.10.

$$[Fe(CN)_6]^{4-} \leftrightarrow [Fe(CN)_6]^{3-} \Leftrightarrow Fe^{3+} \leftrightarrow Fe^{2+} \qquad (3.10)$$
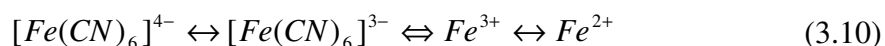
The results are presented in Table 3.2 and the corresponding hydrodynamic voltammograms in Figure 3.24.

Tabela 3.2 – Limiting currents, after background subtraction, for the different rotation rates (disk and ring) and collection efficiencies using 0.1M KOH and 10 mM K$_3$Fe(CN)$_6$ solution;

Rotation rate rpm	I_L ring mA cm^{-2}	I_L disk mA cm^{-2}	Collection efficiency %
400	1.28	-4.45	28.8
900	0.87	-2.99	29.2
1200	1.45	-5.10	28.4
1600	1.66	-5.86	28.4
2000	1.81	-6.46	28.0
2300	1.90	-6.87	27.7
2500	2.00	-7.10	28.2

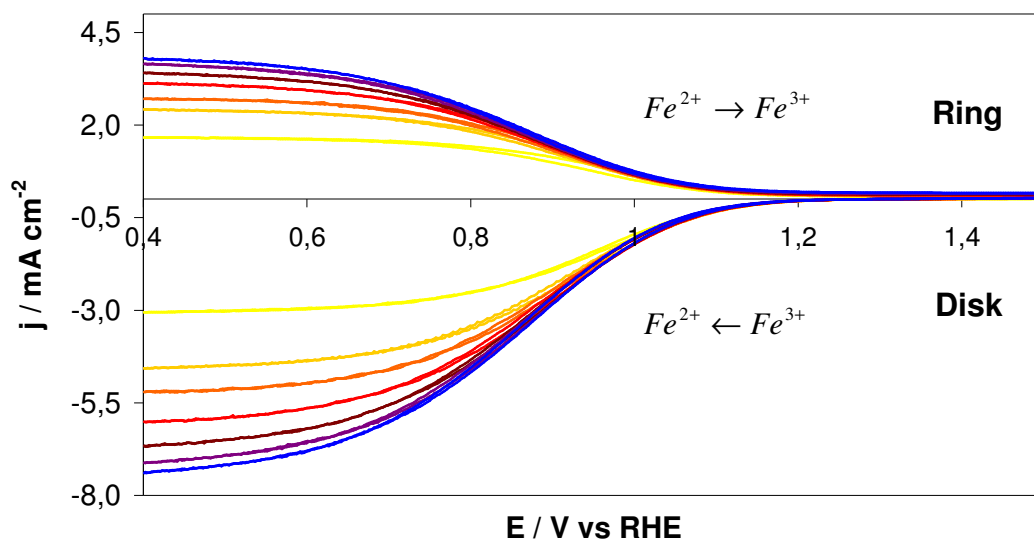The collection efficiency was found to be around 28.4%.

Figure 3.24 - Collection efficiency for the ferrocyanide (Fe^{3+}) / ferricyanide(Fe^{2+}) couple. Rotation rates of 400, 900, 1200, 1600, 2000, 2300 and 2500 rpm were studied.

A.1 Collection efficiency – layer influence

To determine the effect of the catalyst layer some experiments were done with another RRDE electrode (again with 5 mm diameter). This study consists of analysing the collection efficiency with a 38%Pt/C1 catalyst layer. The results are presented in Figure 3.25.
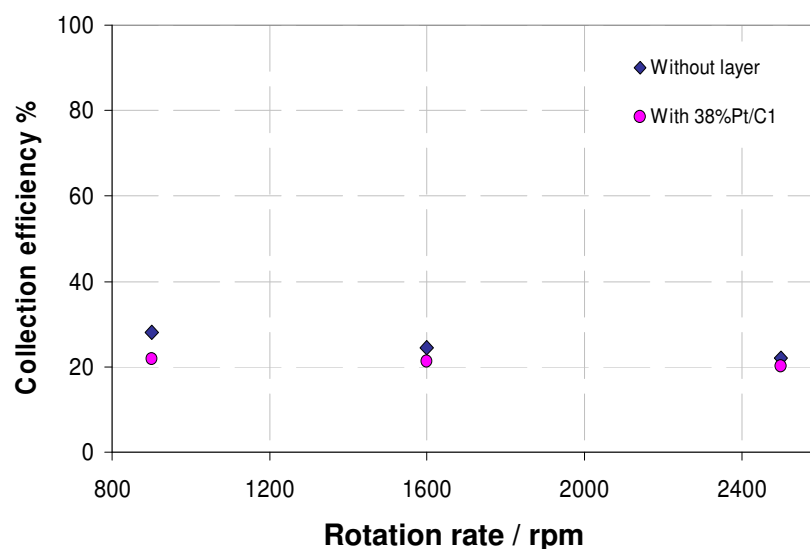

Figure 3. 25 – Collection efficiency for the rotation rates 900, 1600 and 2500 rpm. Interference of the catalyst layer study [56].

Statistical calculations from the results shown in Figure 3.25 found an average collection efficiency of 26% with a RSD of 11% without the layer, and an average of 22% with a RSD of 4% with a Pt layer. Thus, the difference between both measurements is not significant. Gojkovic et al. [113] also studied the effect of the layer on the collection efficiency but found an increase of 18% for the disk coated with ink.

B. Pt catalyst

The behaviour of the 38%Pt/C1 catalyst was studied at the RRDE. Figures 3.26 and 3.27 represent the results found for the disk and the ring respectively.
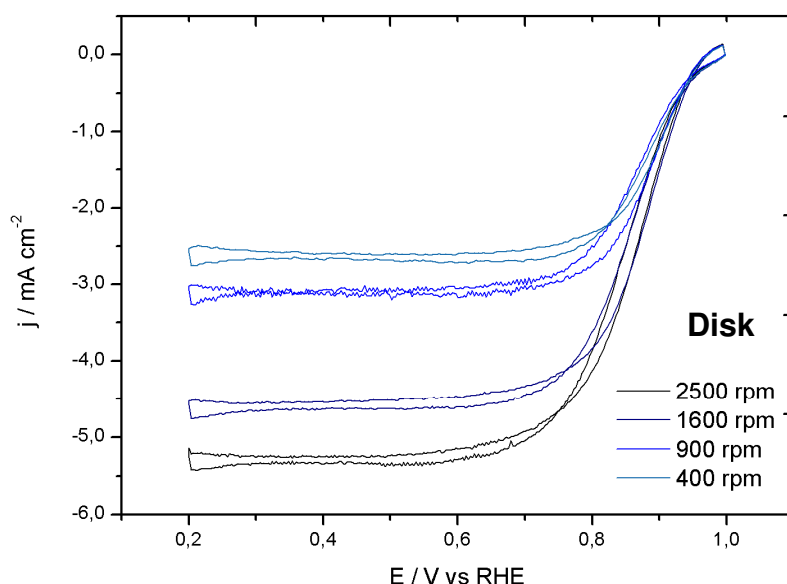

Figure 3.26 - Hydrodynamic voltammograms at the disk, for the 38% Pt/C1, rotation rates 2500, 1600, 900 and 400 rpm, scan rate 20 mV s^{-1}, in 0.1M HClO$_4$.

In the disk hydrodynamic voltammograms the limiting current plateau was found to be -5.0 mA cm^{-2}, at 2500 rpm. The same value was found by Schmidt et al. [114], with 20%Pt/XC72 and 0.5 M HClO$_4$ solution as electrolyte. Furthermore, Paulus et al [72], with 20%Pt/XC72 at 60ºC with 0.5 M H$_2$SO$_4$ as electrolyte also obtained the same result.
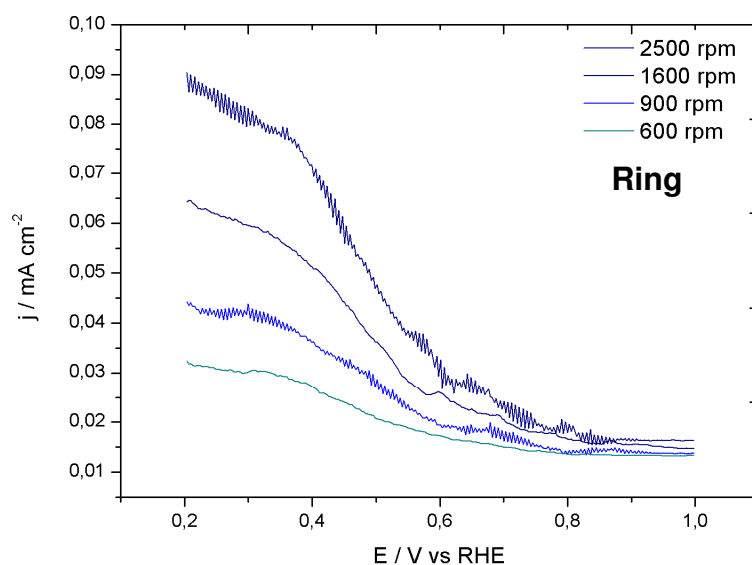
Figure 3. 27 - Hydrodynamic voltammograms at the ring, for the 38% Pt/C1, rotation rates 2500, 1600, 900 and 400 rpm, scan rate 20 mV s^{-1}, in 0.1M HClO$_4$.

The noise of the analytical system used is visible in Figure 3.27, a current of 90 µA cm^{-2} was found for a 2500 rpm rotation rate. This plot also shows that hydrogen peroxide decomposition starts at around 0.85 V. Similar results were obtained by Schmidt et al. [114] and Paulus et al [72].

C. Co catalyst

The 2%Co/C2 catalyst was analysed by the RRDE technique. Hydrodynamic voltammograms for the disk are presented in Figure 3.28 - limiting current plateaux were not found at this negative potential limit. Yamanaka et al. [33], found similar results for an activated carbon (0.6 M H$_2$SO$_4$ as electrolyte), reaching a disk current of -0.6 mA at 2000 rpm (in our case a -0.5 mA at 2500 rpm was found) also without the limiting current plateaux.

Figure 3.28 - Hydrodynamic voltammograms of the disk, for the 2% Co/C2, rotation rates 2500, 1600, 900 and 400 rpm, scan rate 20 mV s^{-1}, in 0.1M HClO$_4$.

The signal of the ring is related to the decomposition of H_2O_2. Figure 3.29 shows the higher values for the decomposition of H_2O_2 at the disk. A ring current of 95 µA was found for a 2500 rpm rotation speed. Yamanaka et al. [33] measured a ring current of 120 µA at 2000 rpm.
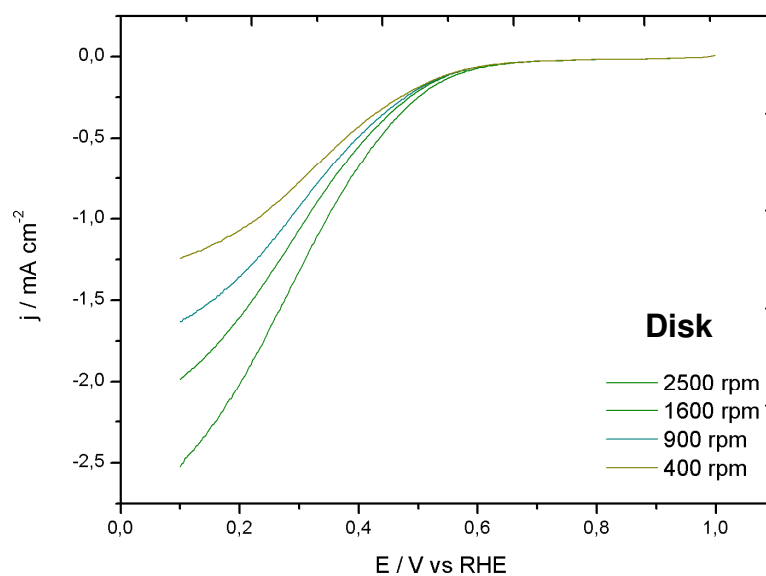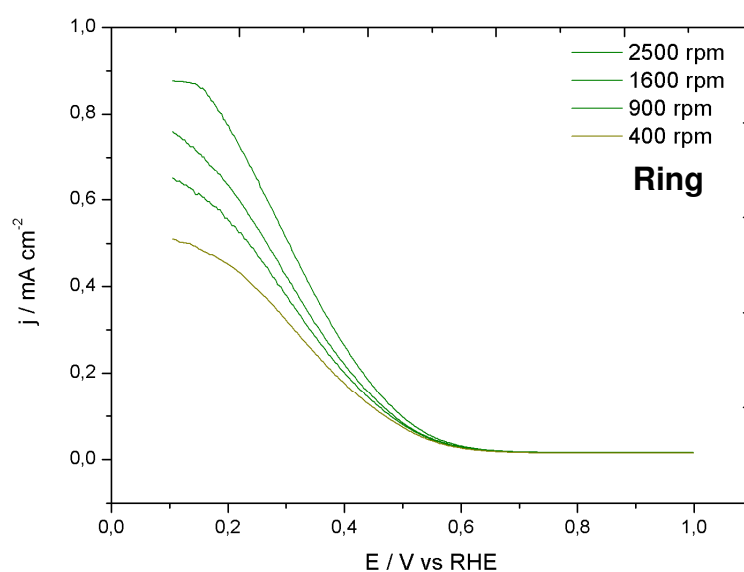

Figure 3.29 - Hydrodynamic voltammograms of the ring, for the 2% Co/C2, rotation rates 2500, 1600, 900 and 400 rpm, scan rate 20 mV/s, in 0.1M HClO$_4$.

C.1 Negative scan limits

In order to try to understand the absence of limiting currents with the 2%Co/C2 catalyst a more negative potential limit was tested. The hydrodynamic voltammograms are shown in Figure 3.30.
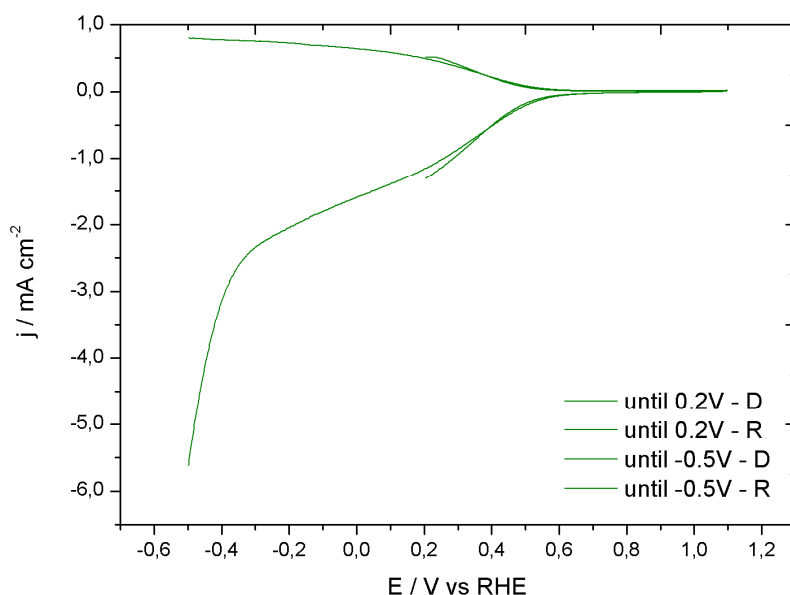

Figure 3.30 - Hydrodynamic voltammograms of the 2%Co/C2 catalyst (0.0008 mg Co cm⁻²). Disk and Ring signals were recorded at different rotation rates 2500 rpm.

From the previous plot it can be seen that the 2%Co/C2 catalyst is highly sensitive to the oxygen reduction reaction, and that hydrogen evolution only starts with nearly 400 mV overpotential at pH = 0 before any limiting current plateau has appeared.

D. H_2O_2 current efficiency %

From Equation 1.35 it is possible to determine the H_2O_2 current efficiency. Figure 3.31 shows the results at potentials between 0.2 and 0.7 V vs RHE, for the 38%Pt/C1 and the 2%Co/C2 with a 95% confidence interval, which was calculated for 3 runs each (Pt, Co) at 2500 rpm rotation rate. The current efficiency for the production of H_2O_2% range for the cobalt catalyst was found to be up to 82%, and for the Pt catalyst up to 4%.
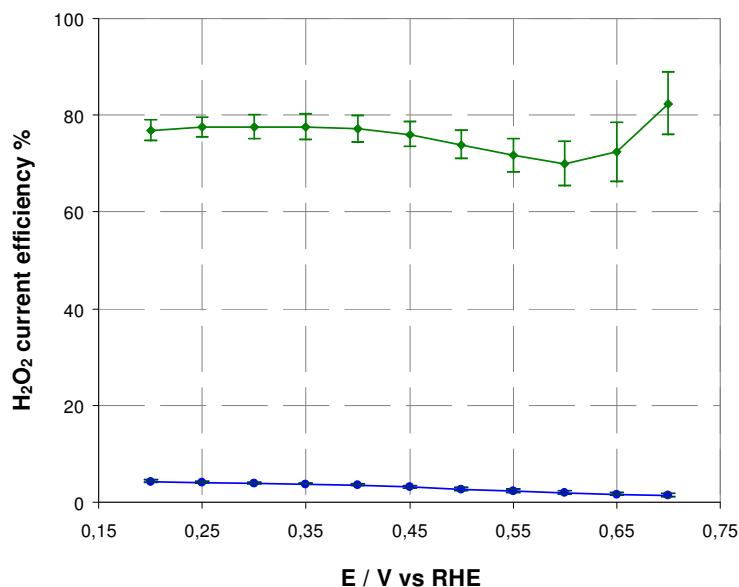
Figure 3. 31 – Hydrogen peroxide current efficiency %, for the 38% Pt/C1 (blue line) and 2% Co/C2 (green line) with confidence intervals of 95% probability.

At more negative potentials, and relating to the cobalt catalyst, variations in the %H_2O_2 were found this could be due to the noise, or other reactions occurring.

The influence of the rotation rate can be evaluated by plotting the H_2O_2 current efficiency against the rotation rate – Figure 3.32.
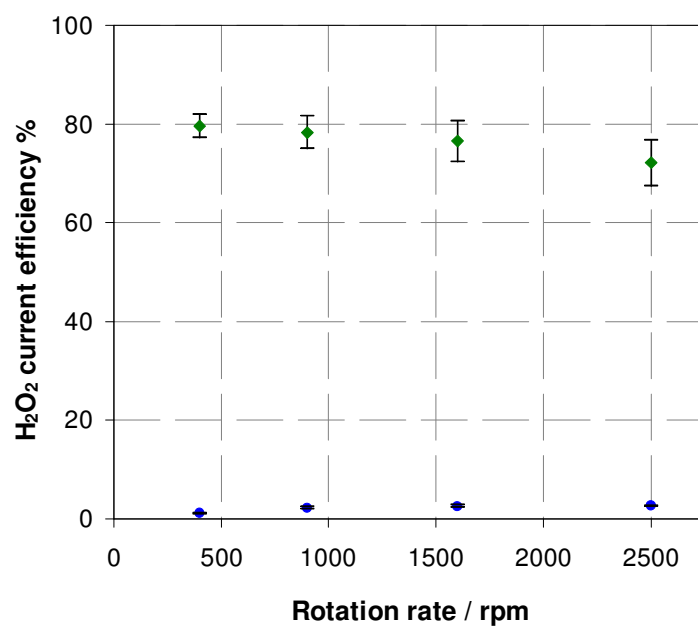

Figure 3. 32 - Hydrogen peroxide current efficiency in %, for the 38% Pt/C1 and 2% Co/C2 with 95% confidence intervals, for 0.25 V.

The Levich equation (Eq. 1.25) considers that I_L is proportional to $\omega^{1/2}$. Consequently, the ratio between I_D and I_R should not vary with the rotation rate. However, Figure 3.32 shows a small variation. This difference is probably due to problems of turbulence at high rotation speed, the layer was not homogenously covered. Statistical analysis proves that this difference is not significant. According to Contamin et al.[115], when an electrode is locally blocked (or inactivated), the electrode surface "seen" by the electroactive species varies with the increase of the disk rotation speed.

3.2   PEM single cell measurements

Higher performance of a PEM fuel cell requires maintaining optimal temperature, membrane hydration, and partial pressure of the reactants across the membrane to avoid any degradation of performance. These critical operation parameters must be controlled over a wide range of current [41, 116, 117].

3.2.1. Dependence of the humidifier temperature

The humidification of the gases in a fuel cell system directly influences the concentration of hydrogen peroxide produced.

The dependence of the humidifier temperature was studied by theoretical calculations, in which the volume of water expected from the humidification, was calculated [62, 63, 64, 120, 121]. Practical experiments were done to verify the model defined.

A. *Theoretical model analysis*

Following the methodology described in Section 2.3.1, some results for the calculations at different humidifier temperatures: 80, 60, 40, 20 °C, are shown in Figure 3.33.

From the theoretical model (Figure 2.7) it can be deduced that if we change the temperature, increasing it at constant flow, the amount of dry gas will be constant, so the molar amount of air is constant. W_{PP} will increase (due to the saturated vapour pressure increase), so W_{inlet} will increase, and consequently the volume collected will increase. This is because a high saturated pressure will be produced at higher T for the same conditions of P and gas flow rate.

Decreasing the temperature, W_{PP} will decrease, and W_{inlet} will decrease, so the volume collected will decrease [68, 82, 83].
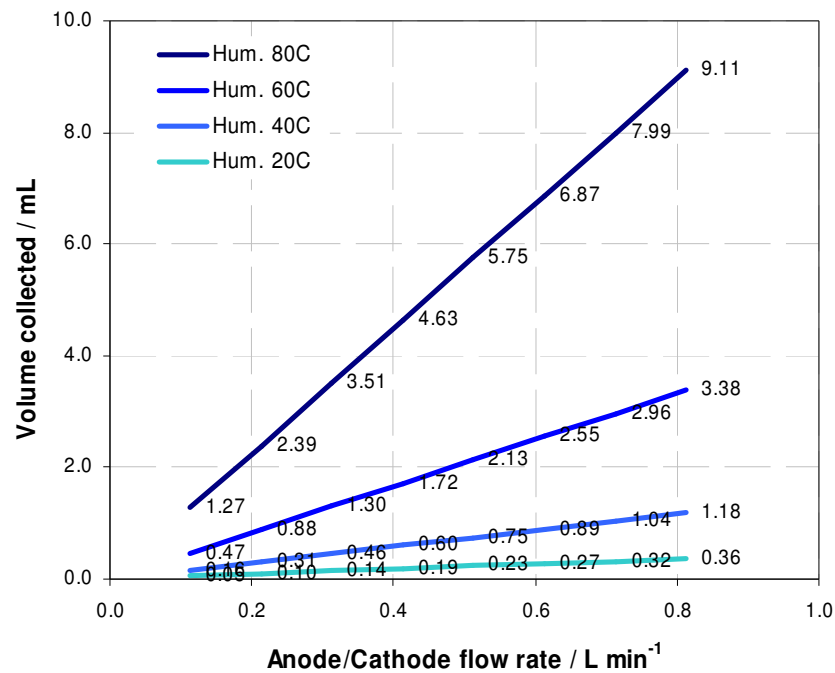
Figure 3.33 – Relation between the volume expected on the anode / cathode side for different humidifiers temperatures (80, 60, 40 or 20ºC) considering different flow rates of the gas.

The theoretical model shows that, as expected, the higher humidification of the gases the higher saturation and condensation of water. This a important factor that is related directly with the cell resistance losses (Fig. 1.20). The membrane requires water to keep its hydration, so it can be more conductive and less resistive.

B. Testing of the theoretical model

In order to test the reliability of the model, the cell was by-passed and different conditions were tested, changing temperatures and flow rates. The procedure is described in Table 3.1.

Table 3.1 - Procedure to verify the theoretical model. Varying the flow rates, different volumes of water will be collected.

Flow rate		Volume expected		Volume collected	
L min^{-1}		mL		mL	
Cathode, O_2	Anode, H_2	Cathode	Anode	Cathode	Anode
0.313	0.130	3.5	1.5	5.0	1.8
0.813	0.340	9.1	3.8	8.0	2.4
0.213	0.089	2.4	1.0	3.4	1.2
0.713	0.298	8.0	3.3	6.8	2.0
0.813	0.340	9.1	3.8	7.6	2.4
0.513	0.215	5.8	2.4	6.2	2.8
0.413	0.173	4.6	1.9	4.2	2.1
0.113	0.047	1.3	0.5	1.9	1.4
0.613	0.256	6.9	2.9	5.4	1.6

The volumes collected for the cathode side, at 80 °C, are presented in Figure 3.34.

Figure 3.34 - Volume expected on the cathode side for a humidifier temperature of 80ºC considering different flow rates of the gas (theoretical value). Volumes collected for a humidifier temperature of 80ºC considering different flow rates of the gas (Vol. collected).

Figure 3.34 show that the practical results differ from those expected from the model. This difference appears a little bigger at higher (0.6 – 0.8 L min^{-1}) and lower flow rates (0.1 – 0.3 L min^{-1}). This difference can be attributed to two reasons:

condensation of gases and the 'build up' of water inside the rig (water gets stuck and affects the next measurement).

B.1 Reproducibility

To investigate the reproducibility of the measurements, the same measurement was repeated three times. The results are shown in Figure 3.35.
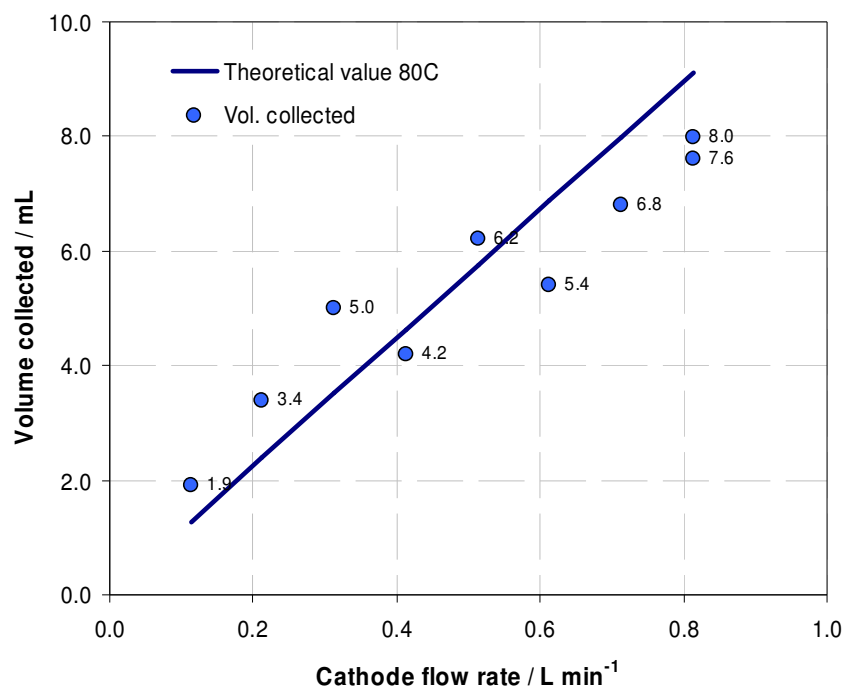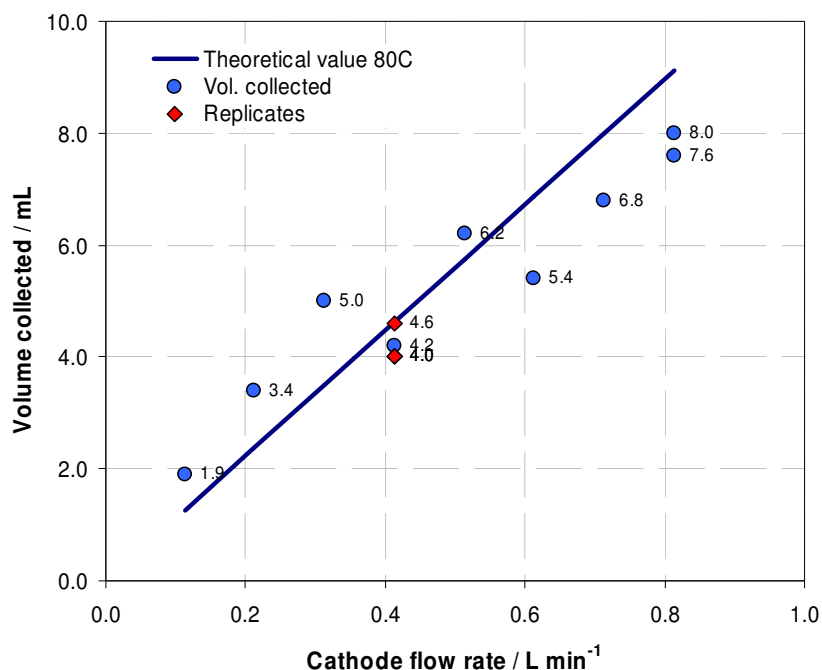

Figure 3.35 Volume expected on the cathode side for a humidifier temperature of 80ºC considering different flow rates of the gas (theoretical value). Volumes collected for a humidifier temperature of 80ºC considering different flow rates of the gas (Vol. collected). Replicates (green dots) same measurement repeated three times.

From Figure 3.35 it is possible to see that even though the volumes collected are close to each other, smaller differences can be found.

3.2.2. Dependence of the pressure gauge

The theoretical model was also used to measure the effect of pressure on the volume of water collected [118, 119, 120]. The results are presented in Figure 3.36.
.

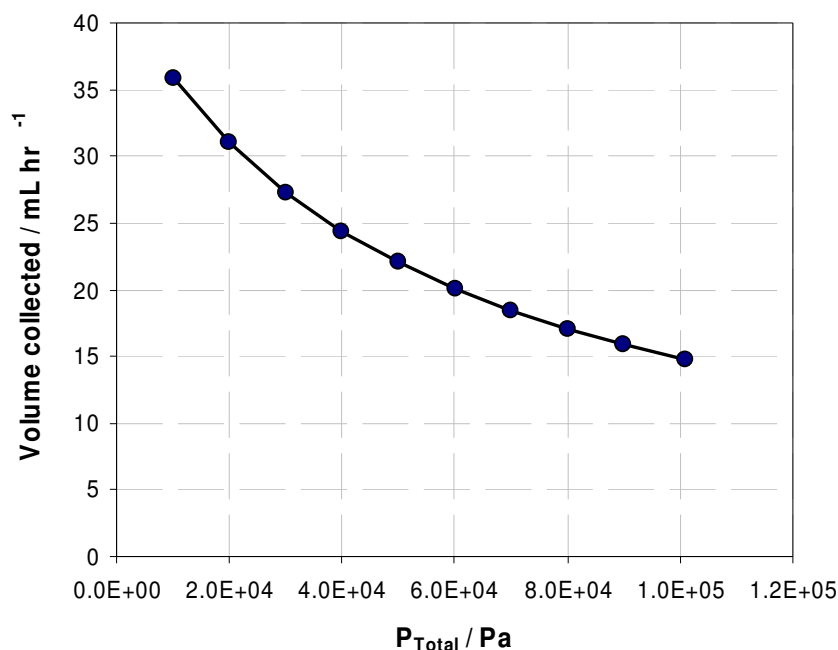**Figure 3.36 - Relation between the volume expected on the anode / cathode side for a humidifier temperature of 80ºC, considering different pressures, from 1×10^4 to 1×10^5 Pa (100 to 1000 mbar).**

Observing the scheme in Figure 2.7, it is possible to conclude that if we change P_{total}, increasing it at constant flow rate, n_{air} will be constant. W_{PP} will decrease, so W_{inlet} will decrease, and thence the water volume collected. This is because W_{PP} does not change with the increase of the pressure gauge.

Decreasing P_{total}, n_{air} will be constant, W_{PP} will remain constant, but W_{inlet} will decrease, and consequently the volume collected will increase. This is because for the same W_{PP} a lower P_{total} is required [72, 82, 83].

3.2.3. Polarization curves

In order to evaluate the single cell performance a polarization curves were recorded. Between measurements for the Co catalyst, sample collections on the cathode and anode side were done, and the cathode samples were quantified by volumetric analysis to determine the H_2O_2 wt% produced. The data were corrected for ohmic losses.

A. Pt catalyst

Table 3.2 shows the procedure, type of gas, flow rates and applied current density, and the results obtained (cell voltage and resistance).

The MEA tested has as cathode, a 40% Pt/C1 and as anode a 40% Pt/C1. Each measurement should be taken every 3 min (minimum) so the MEA will remain hydrated (even at lower flow rates). The volumes of water/hydrogen peroxide collected in the cathode and anode side were thrown away.

Table 3.2 – Results of the standard procedure followed for a 40% Pt/C1 / 40% Pt/C1 MEA.

Anode Gas	Anode Flow mL/min	Cathode gas	Cathode flow mL/min	j, current density A / cm^2	E_{cell} V	R_{Ohm} Ω / cm^2
H_2	340	O_2	813	0.50	0.517	0.79
H_2	408	O_2	976	0.60	0.474	0.43
H_2	476	O_2	1138	0.70	0.462	0.39
H_2	544	O_2	1301	0.61	0.523	0.36
H_2	272	O_2	650	0.40	0.581	0.44
H_2	136	O_2	488	0.30	0.636	0.46
H_2	136	O_2	325	0.20	0.701	0.48
H_2	136	O_2	325	0.10	0.783	0.42
H_2	136	O_2	325	0.05	0.829	0.42
H_2	136	O_2	325	0.02	0.882	0.54
H_2	136	O_2	325	0.00	0.978	0.00

Figure 3.37 shows the results related to the cell resistance [47].
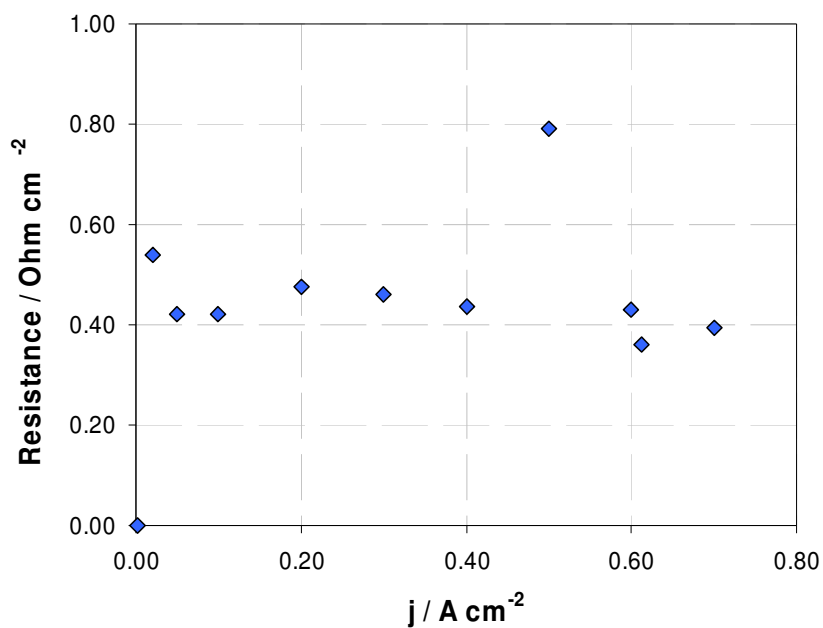
Figure 3.37 – Resistance (which causes ohmic losses) for the 40% Pt/C1 / 40% Pt/C1 MEA (cathode loading 0.4 mg cm^{-2}).

At 0.5 A cm^{-2} a higher resistance was found - this measurement is probably an outlier. The simplest way to correct the MEA performance is by adding the *dy* (*dy* is the result of the current interrupt described on Section 2.3.4.) to the cell voltage obtained. Figure 3.38 shows the polarization curve for the platinum MEA, both corrected for ohmic losses and uncorrected.
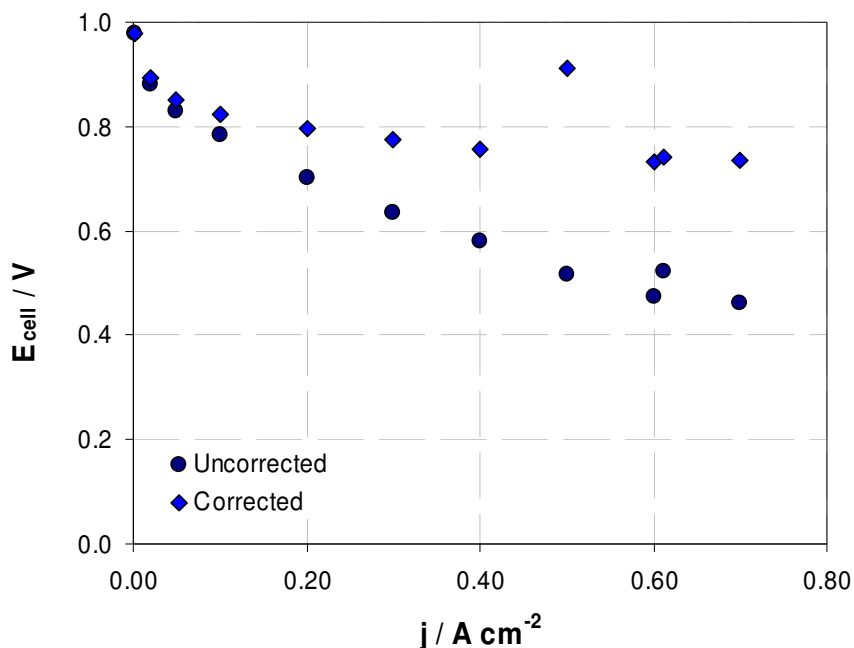
**Figure 3.38 – Polarization curve for the 40% Pt/C1 / 40% Pt/C1 MEA
(cathode loading 0.4 mg cm^{-2}).**

At 0.5 A cm^{-2}, the correction is dubious as is related with the Dy (which also affected the resistance).

At open circuit voltage, the cell voltage was 0.975 V (see explanation in Section 1.3.2, B.2).

B. Co catalyst

Table 3.3 shows the procedure followed: type of gas, flow rates and applied current density, and the results obtained (cell voltage and resistance).

Table 3.3 - Standard procedure followed for a 2% Co/C2 / 40% Pt/C1 MEA.

Anode Gas	Anode Flow	Cathode gas	Cathode flow	Current density	E_{cell}	R_{Ohm}
	mL/min		mL/min	A / cm^2	V	Ω / cm^2
H$_2$	139	O$_2$	348	0.20	0.075	0.38
H$_2$	111	O$_2$	279	0.16	0.118	0.37
H$_2$	84	O$_2$	209	0.12	0.152	0.34
H$_2$	84	O$_2$	209	0.08	0.218	0.34
H$_2$	84	O$_2$	209	0.04	0.292	0.29
H$_2$	84	O$_2$	209	0.02	0.354	0.34

Figure 3.39 shows the results related to the cell resistance.
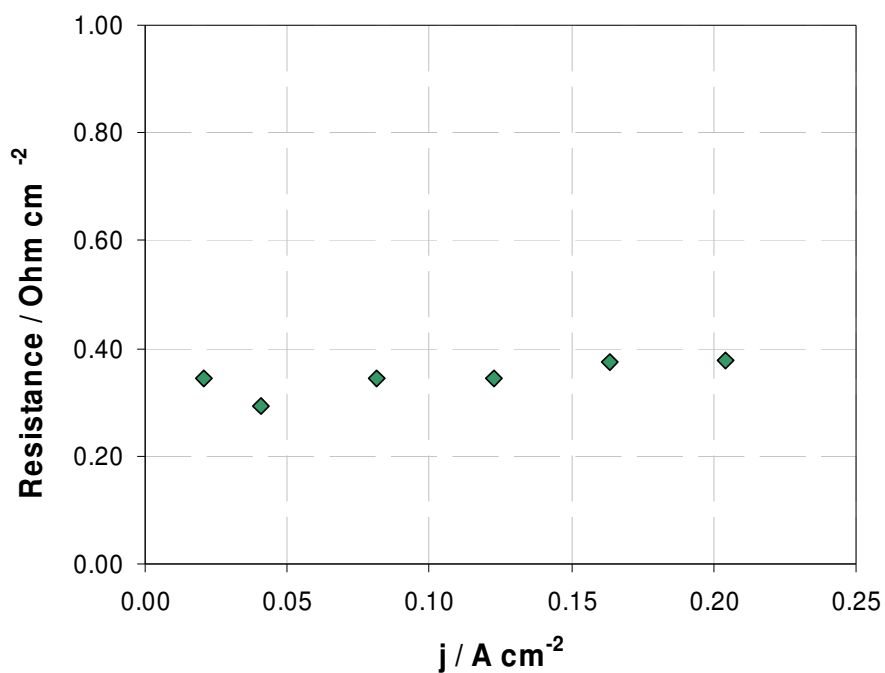

Figure 3.39 – Resistance for the 2%Co/C2/ 40% Pt/C1 MEA (cathode loading 0.887 mg cm^{-2}).

The values for the resistance are not very different from the platinum MEA, which indicates that the system is working well.

Figure 3.40 shows the polarization curve for the cobalt MEA, both corrected for ohmic losses and uncorrected.
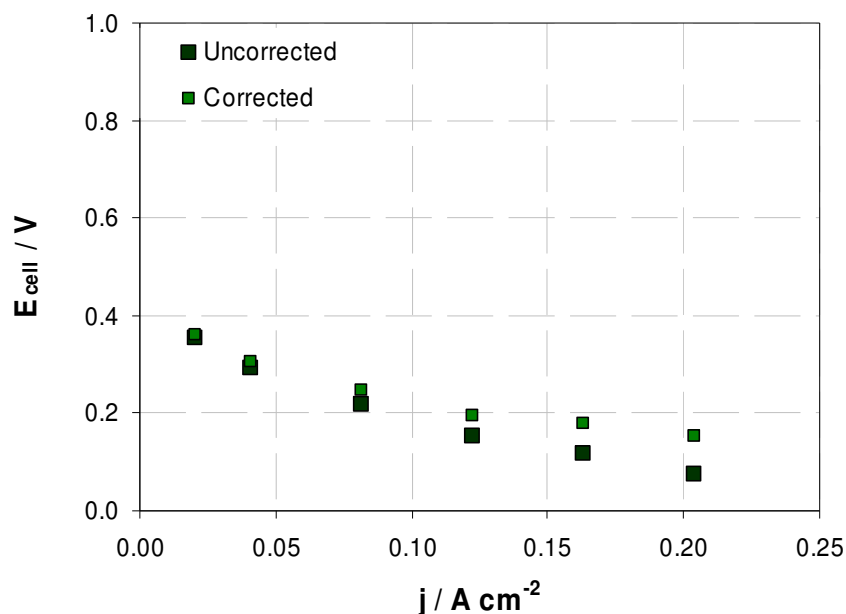
Figure 3.40- Polarization curve 2% Co/C2/ 40% Pt/C1 MEA (cathode loading 0.887 mg cm^{-2}).

Ma et al. [26], found similar results for a cobalt based non-precious electrocatalyst, starting with an OCV of 0.82 V vs RHE. However, in his study, a current density of 1000 mA cm^{-2} was found for a 1.0 mg cm^{-2} MEA loading (in this study, from Figure 3.40, a current density of 200 mA cm^{-2} was found).

At the open circuit voltage, the cell voltage is 0.83V vs RHE.

B.1 H_2O_2 maximum percentage produced

Using volumetric analysis, it is possible to determine the concentration of the hydrogen peroxide solution produced.

As an example, Table 3.4 presents the results for the three replicate collections (current density 0.20 A cm^{-2}).

Table 3. 4 - Volumetric analysis of H₂O₂ solution collected *at 0.20 mA cm⁻²) in the fuel cell system.

Trials	V. H₂O₂ titrated mL	V. KMnO₄ used mL	n H₂O₂ mol	[H₂O₂] M	% H₂O $_{(m/m)}$ %
1	0.1	3.90	0.00022	2.15	7.3
2	0.1	4.00	0.00022	2.21	7.5
3	0.1	3.90	0.00021	2.10	7.1

The concentrations of the H_2O_2 solutions collected in the single cell during the measurements for the polarization curve are presented in Figure 3.41.
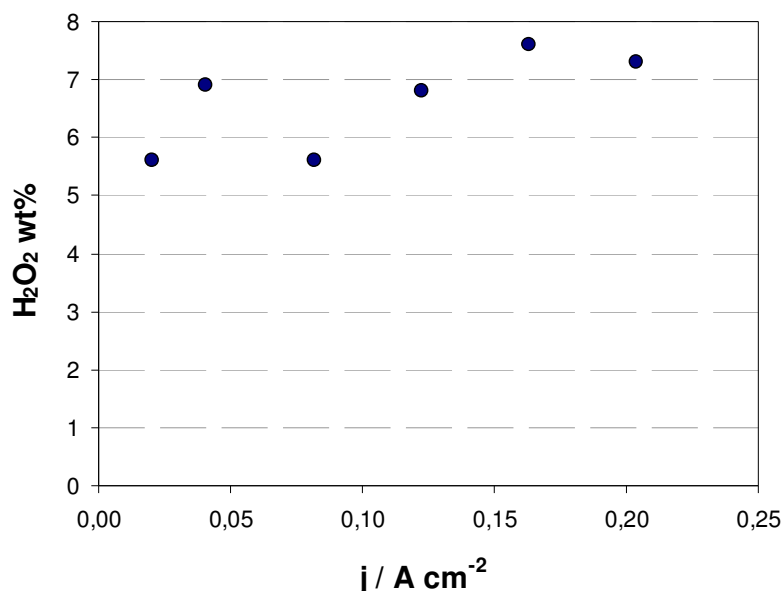
Figure 3.41 – H₂O₂%, in the solutions collected in the fuel cell system.

The lower concentration of H_2O_2 obtained can be related with the chemical decomposition process inside the rig. The decomposition process of H_2O_2 is thermodynamically favorable, furthermore the rate of decomposition is dependent of the temperature (a PEM FC was working at 30ºC), the presence of impurities and stabilizers (the materials that constitute the rig or residual particles of catalyst should be considered) and its concentration.

B.2 Efficiency of the catalyst

The efficiency of the catalyst can easily be calculated by comparison between the theoretical/expected values for the molar quantity of H_2O_2 produced with the real value obtained - Equation 3.11.

$$Efficiency(\%) = \frac{n \cdot_{H_2O_2.real}}{n \cdot_{H_2O_2.theoretical}} \times 100 \qquad (3.11)$$

Table 3.5 shows the results found and the efficiencies are represented in Fig.3.42.

Table 3.5 – Efficiency of the 2%Co/C2 catalyst.

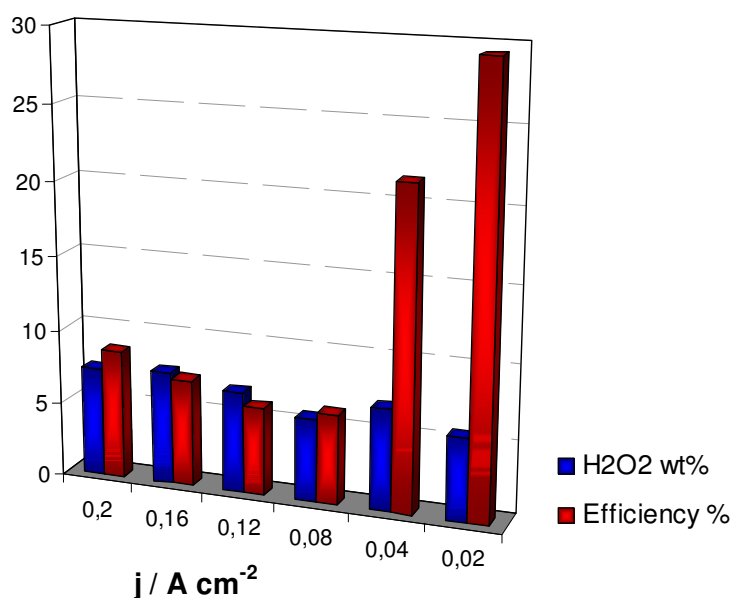| Current density A / cm2	n H_2O_2 expected mol	n H_2O_2 obtained mol	Efficiency %
0.20	0.124	0.011	8.6
0.16	0.124	0.009	7.2
0.12	0.112	0.007	5.9
0.08	0.149	0.009	6.1
0.04	0.075	0.016	21.5
0.02	0.037	0.011	29.4

Figure 3.40 – H_2O_2% and Efficiency (%) for the 2% Co/C2 catalyst, during the polarization curve.

A possible explanation for the higher efficiency at lower current densities can be related with the flux of water due to the current. A lower current produces less

electrons and consequently less water. Even though the reaction will be faster, probably the water flux is the biggest factor, diluting the final product.

3.2.4. Open circuit voltage (OCV)

The cell voltage at open circuit (OCV) is strongly dependent on the temperature and pressure. First, theoretical calculations were done to evaluate which pathway is occurring (2 or four electrons).

A. Theoretical calculations

To calculate the E_{OCV}^{t} it is necessary to calculate the partial pressures of O_2 and H_2 (P_{anode} or $P_{cathode}$). Therefore, the theoretical model described in Section 2.3.6 A was used and the results obtained are shown in Figure 3.43.
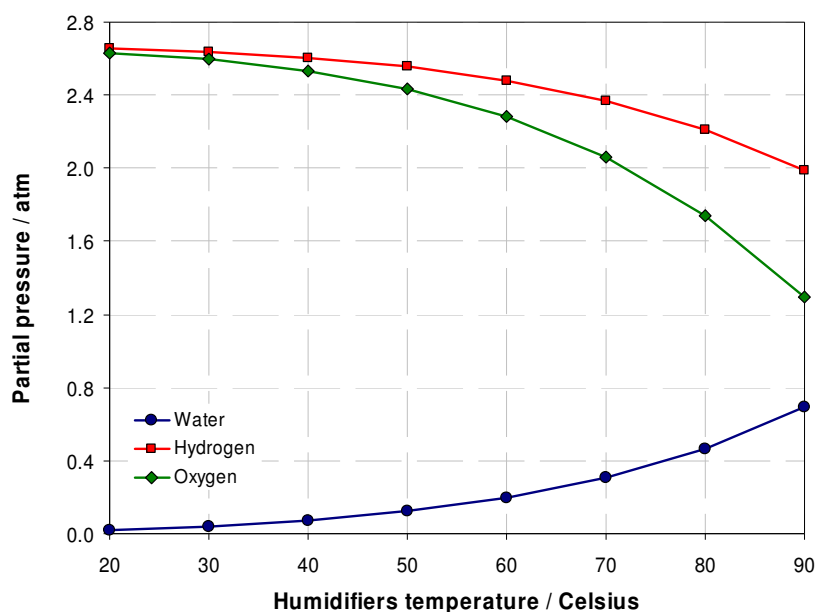

Figure 3.43 - Partial pressures of O_2, H_2 and H_2O in the fuel cell streams as a function of operating temperature (humidifiers), 1 atm and 100% RH.

From this, E_{OCV}^{t} was calculated and is presented in Figure 3.44.
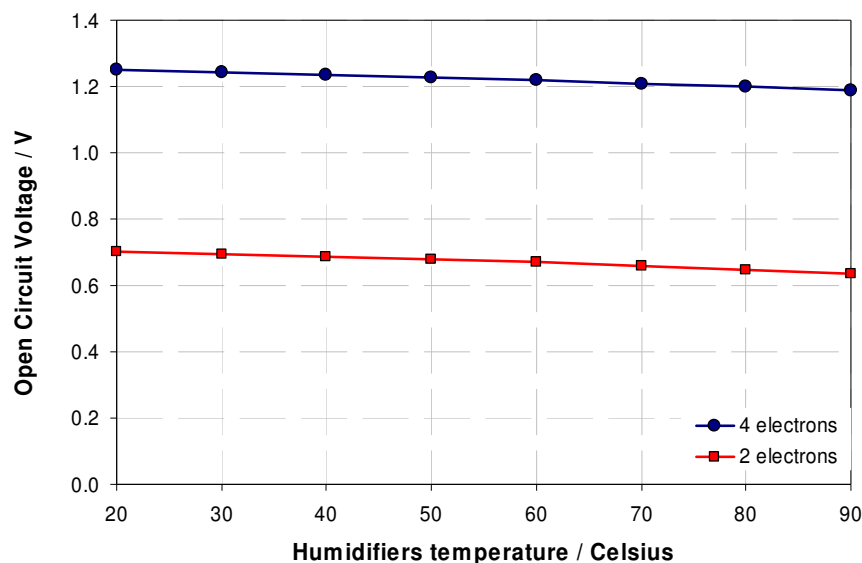
119

Figure 3.44 – Single cell theoretical E^t_{OCV} as a function of temperature, 1.0 atm absolute pressure and 100% RH, considering a 4 electrons and a 2 electrons pathway reaction.

B. Pt catalyst

For the 40% Pt/C1 catalyst tested at 60 ºC, the E_{OCV} found was 0.975 V, whereas the theoretical value is 1.23 V. The value is between the two and four electron reaction, but is understandable and is explained in Section 1.3.2 C2. The cell voltage losses, classified into three categories, activation polarization, ohmic polarization, and concentration polarization, will result in a cell voltage that is less than its ideal value.

C. Co catalyst

The 2%Co/C2 catalyst at 60 ºC lead to a value of E_{OCV} of 0.83 V. The theoretical value is 0.67 V so this value is close to that for the two electron reaction.

The E_{OCV} value for the RDE analysis should be similar to the E_{OCV} value for the single cell analysis. The E_{OCV} value for the platinum catalyst is between 0.95 and 1.0 V and for the cobalt catalyst, is around 0.65 – 0.85 V. The values found from the 3 electrode cell and the single cell seemed to be in agreement.

3.2.5. Electrode kinetics – Tafel analysis

Considering the Tafel concept described in Section 1.3.1 C, Tafel plots were made of the results shown in Figures 3.45 and 3.46.

A. *Pt catalyst*

Figure 3.45 shows the Tafel plot for the Pt catalyst.
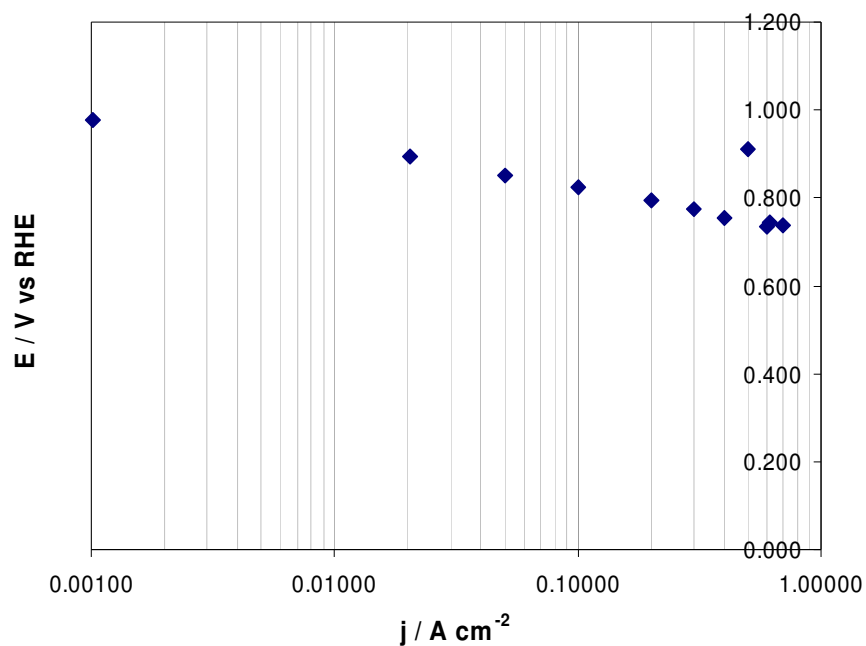

Figure 3.45 – Plot of $E_{corrected}$ vs. ln |j| with α = 0.5, for the Pt/C1.

A Tafel slope of 76 mV dec^{-1} was found at more negative potentials (> 0.85 V). The results obtained are in agreement with Section 3.1.3 and the literature results are presented in Table 3.1 [72, 107, 111, 112].

B. *Co catalyst*

Figure 3.46 shows the Tafel plot for the Co catalyst.
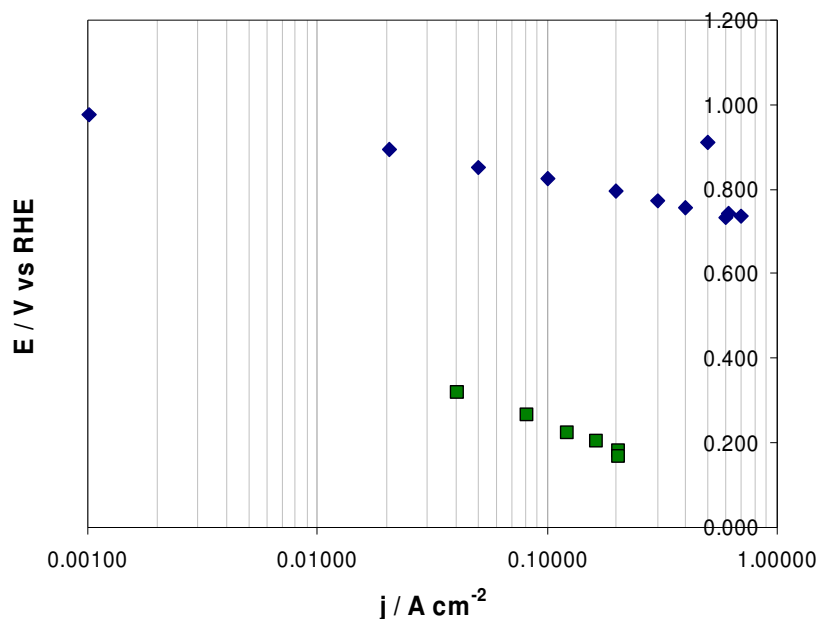
Figure 3.46 - Plot of $E_{corrected}$ vs. ln |j| with $\alpha = 0.5$, for the 38%Pt/C1 and the 2%Co/C2.

From the plot at lower potentials (> 0.80 V), a slope of 206 mV dec^{-1} was found. This value is close to the results presented in Section 3.1.3.

3.2.6. Gains O$_2$/Air

The best performance is obtained when pure oxygen is fed to the cathode, but in most practical systems air is used. In this study a stoichiometry of 10 (see page 70) was used to the O$_2$/Air (the anode stoichiometry did not change). The huge difference between the O$_2$ concentrations can influence the polarization curves.

A. Pt catalyst

Two polarization curves, using two different cathodic reactants, O$_2$ and Air (in the cathode) and H$_2$ (in the anode) for the Pt/C1 catalyst were determined. The results are shown in Figure 3.47.

Figure 3.47 - Polarization curves (cell voltage corrected) 38% Pt/C1 / 40% Pt/C1 MEA (cathode loading 0.4 mg cm^{-2}), on the cathode side O$_2$ and Air were used.

Comparing both curves at two different current densities

j A cm^{-2}	Gains in E_{cell} V
0.1	0.102
0.4	0.094

The gain seems to be stable along the polarization curve, the highest concentration of pure O$_2$ gas compared with the 22% of O$_2$ present in the compressed air is the principal reason for the difference in the results. Around 0.1 V gain in cell voltage for pure O$_2$ was found, i.e. a increase of 12%.

B. Co catalyst

Two polarization curves, using two different cathodic reactants, O$_2$ and Air (in the cathode) and H$_2$ (in the anode) are shown in Figure 3.48.
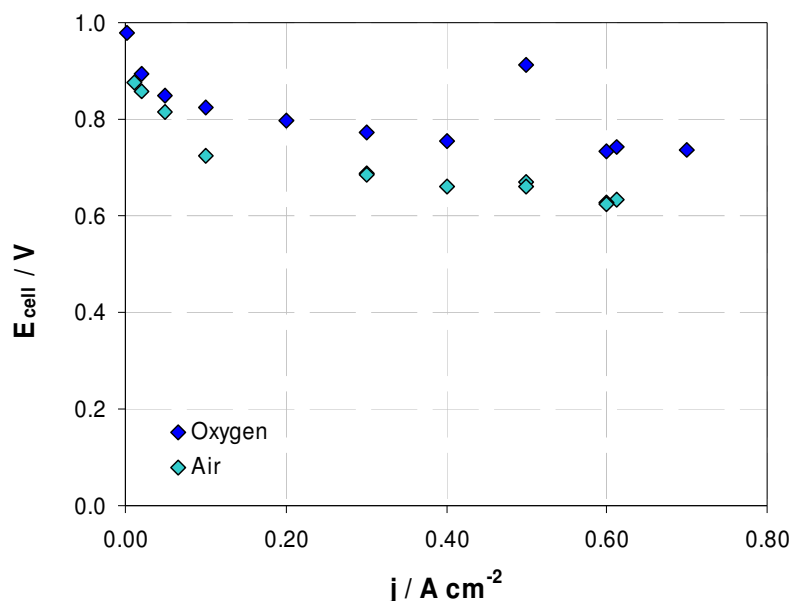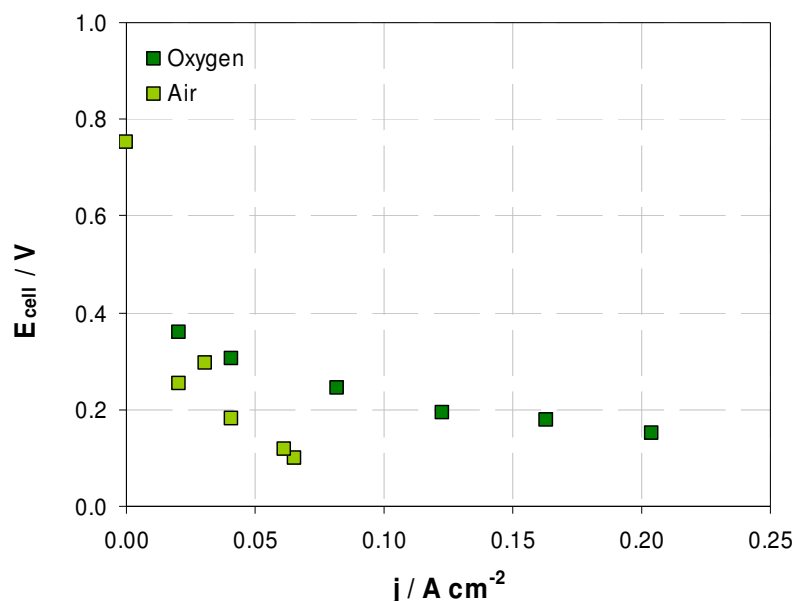
Figure 3.48 - Polarization curves (cell voltage corrected) 2% Co/C2 / 40% Pt/C1 MEA (cathode loading 0.887 mg cm^{-2}), on the cathode side O$_2$ and Air were used.

Comparing both curves at two different current densities

j A cm^{-2}	Gains in E_{cell} V
0.02	0.106
0.04	0.122

The gain does not seem to be stable along the polarization curve. Around 0.1 V gain in cell voltage for O$_2$, was found corresponding to an increase of 30% and 40% for 0.02 and 0.04 A cm^{-2} respectively.

3.2.7. Parameters interfering in the Single Cell

The dependence of the humidifier temperature (3.2.1), the dependence of the pressure gauge (3.2.2) and the dependence of the cathodic reactant, both directly influence the concentration of the hydrogen peroxide solution produced by the fuel cell rig.

The factors referred to were studied, but other factors can influence the behaviour, see the scheme below,
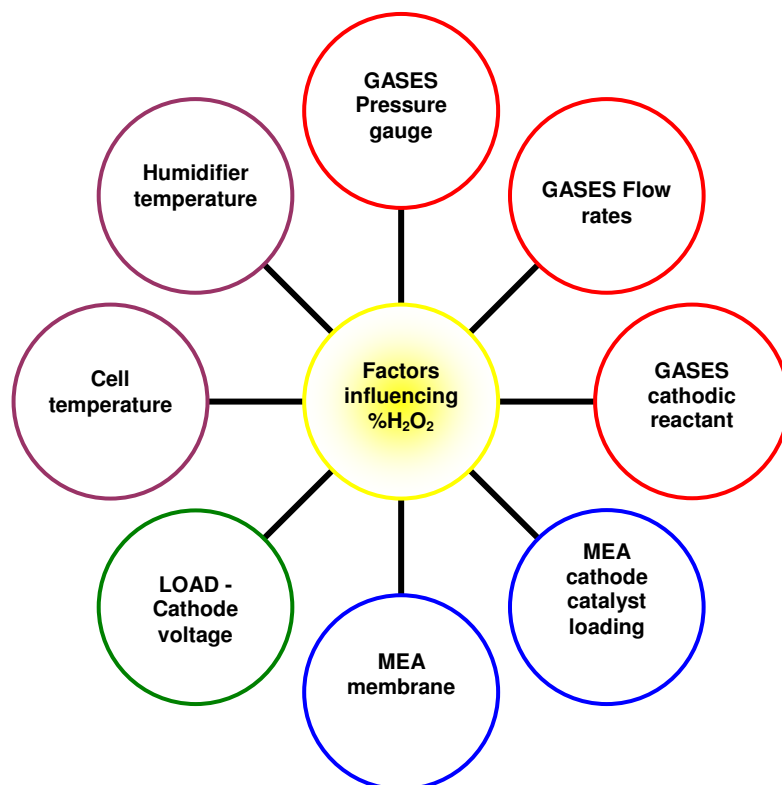
These parameters are:

- Flow rates of the gases, influencing the pressure gauge and the humidifier temperature. A higher flow rate does not mean a more efficient reaction. The percentage of gases reacting does not have to be 100% [109, 118].

- Cathode catalyst loading. According to Li et al. [27] after a certain point the concentration of active sites for the ORR can reach saturation, and after that, no matter how much more metal is put into the catalyst, the concentration of the active sites will remain constant. Borakdarpour et al. [121], studying the impact of the loading considered that along the diffusion path, some H_2O_2 molecules produced may further react at catalytic sites, to produce only water. A higher loading can also interfere with the thickness. Feng et al. [122], considered that in a thicker layer, the hydrogen peroxide molecule has additional time to chemically react to water. However, a number of catalytic sites is necessary to produce a higher reaction rate [122], so the opposite effect, also has to be taken into account.

- MEA membrane closely related with the thickness and the resistance of the MEA. Usually Nafion membranes are used for fuel cell devices; however,

these ones can have different thicknesses. The MEA resistance can be evaluated with different membranes and loadings at cathode and anode sides. A higher MEA thickness is related to a higher resistance, this means that the gases will not go through so easily, and do not reach the active sites.

- Load – Current density, the current applied, or the current density applied can be defined in a fuel cell. The higher the current density, the faster the reaction and the higher the volume of water collected.

- Cell temperature can interfere with the rate of hydrogen peroxide decomposition [109].

3.2.8. Comparison between RDE and SC

In order to compare the RDE and SC techniques, the results were plotted in Figure 3.49, after normalizing for the loading of the catalyst (mg of metal per cm^2). Factors such as concentration of O_2, residence time, mass transport effects (in the single cell), and the concentration of H are considered to be equal in both systems.
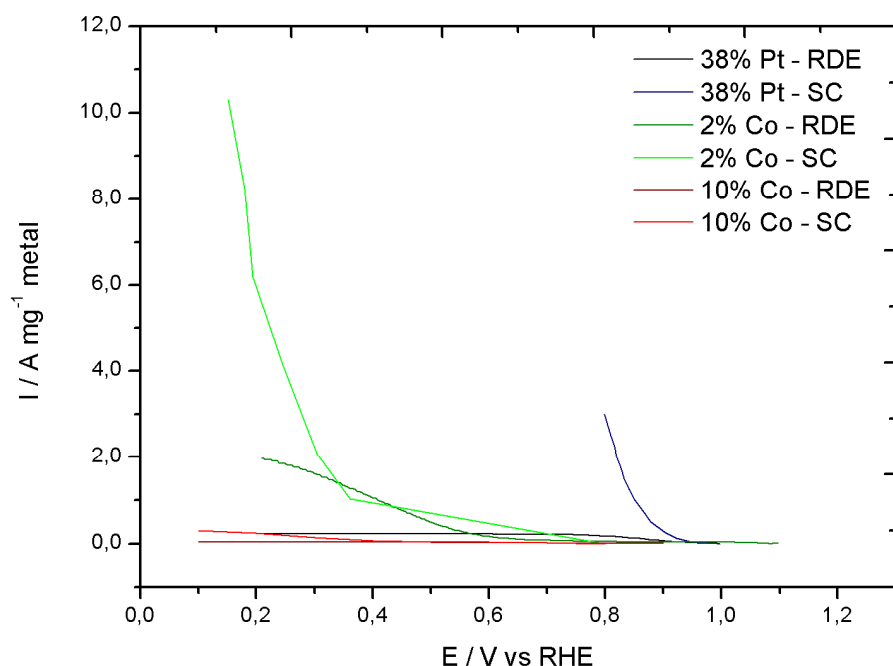
Figure 3.49 - Comparison between RDE and SC analysis. The platinum and the cobalt catalyst were analysed. A 10 % Co/TETA catalyst, published by H.-J. Zhang [28] is also presented. RDE data is present in absolute values.

The cobalt catalyst shows the best performance for both techniques. This difference can be explained by the loadings used – Table 3.6.

Table 3.6 – Loadings used for the different catalyst in RDE and Single Cell measurements.

Technique / loadings (mg cm^{-2})	38% Pt	2% Co	10%Co/TETA
RDE	0.019	0.0008	0.08
Single Cell	0.4	0.0198	2.96

In order to compare the catalysts using each technique, the results were plotted for the RDE, Figure 3.50, and for the SC, Figure 3.51.

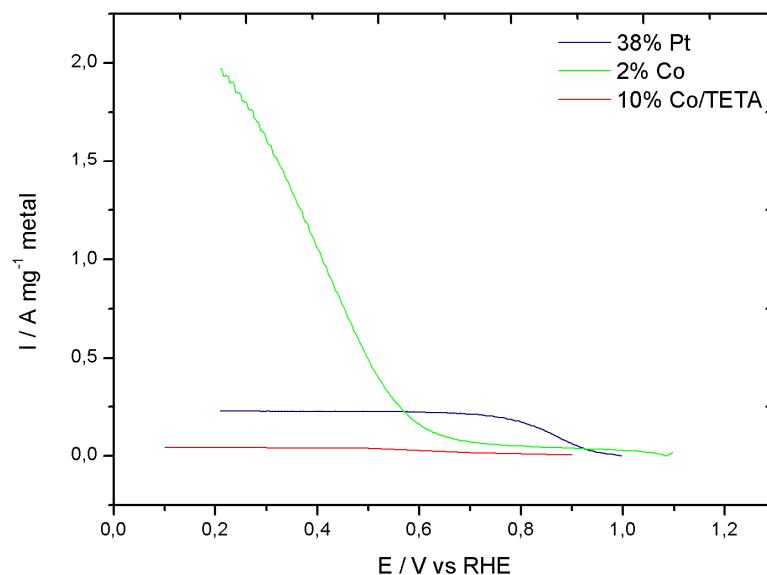**Figure 3.50 - Comparison between the platinum and the cobalt catalyst. The 10%Co/TETA catalyst published by Zhang [28] is also presented. RDE results.**
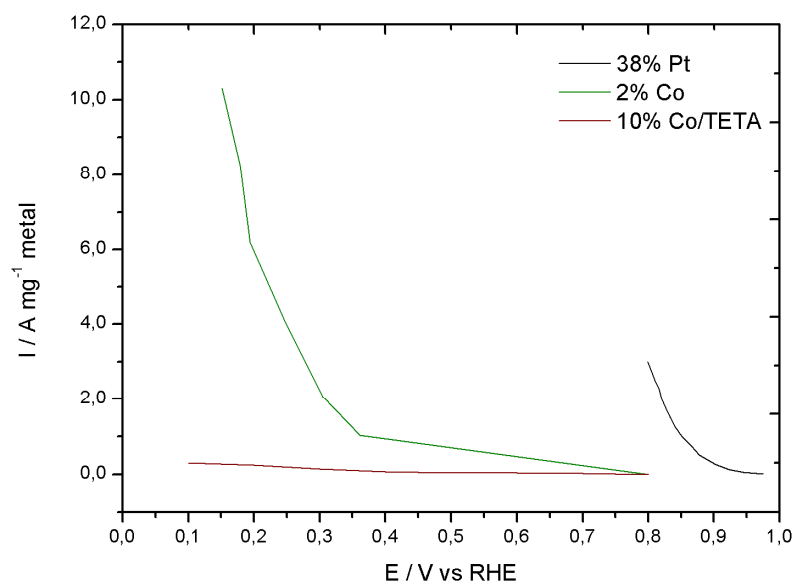
Figure 3.51 - Comparison between the platinum and the cobalt catalyst. The 10%Co/TETA catalyst published by Zhang [28] is also presented. SC results.

Figures 3.50 – RDE - shows clearly that the cobalt catalyst discovered by Johnson Matthey reaches a maximum current of 2 A mg^{-1} Co, well above that of the platinum catalyst, with 0.25 A mg^{-1} Pt.

Platinum reaches a limiting current in Figs. 3.50 at around 0.8 V (vs RHE), this value is not clear in Single Cell analysis, Fig.3.51. However the OCV value is similar for both techniques (around 1.0 V).

Regarding cobalt, the absence of limiting currents is clear in both figures, the potential when the catalyst became active, was found from RDE analysis to be at 0.6 V vs RHE, which seems to be shifted for the Single Cell to around 0.4 V vs RHE. The cobalt catalyst is slightly sensitive to potential variations.

Several studies concerning PEM fuel cells and Platinum catalysts have been done. For instance, Ralph et al. [123], found at 0.2 V a current density of 1.2 A cm^{-2} for a 20% Pt/Vulcan XC72R (loading 0.25 mg cm^{-2}) - this means that a current of 4.8 A mg^{-1} Pt was reached. Equipment limitations did not permit the determination of this value in our platinum catalyst. However, considering the value found by Ralph and comparing it with our RDE analysis (0.25 A mg^{-1} Pt), the value from the Single Cell is 20 times larger.

For instance, at 0.2 V, a current of 2 A mg^{-1} Co was found with RDE analysis and 6 A mg^{-1} Co was found for Single Cell analysis (3 times bigger for the Single Cell). The results published for Co/TETA [28] seem to have similar performances in both techniques.

The difference between RDE and Single Cell for the catalysts used in this work is not yet fully understood due to the influence of many different parameters.

CHAPTER 4

_____

Conclusions

In this work a new cobalt catalyst for the production of hydrogen peroxide was investigated and compared with a platinum catalyst using several electrochemical characterization techniques - cyclic voltammetry, the rotating disk electrode (RDE) and the rotating ring disk electrode (RRDE) - and PEM fuel cell technology.

The cyclic voltammetry of the cobalt catalyst does not reveal any metal characteristic features. However, the platinum catalyst showed features that allowed the calculation of the active surface area.

From RDE studies, the platinum catalyst hydrodynamic voltammogram was shown to be active and to be faster than cobalt, reaching a well defined steady state (mass transport controlled). The absence of the limiting currents is common to other studies, and is explained mainly by the porous electrode behaviour (the distribution of active sites) and the influence of the Nafion in the catalyst layer.

The influence of Nafion in RDE/RRDE measurements was studied, and it was found that the lower the amount of Nafion, the worse the layer homogeneity and coverage but the better the diffusion of O_2 through the catalyst layer.

Levich analysis was used to calculate the number of electrons exchanged. For the platinum catalyst a four electron pathway and for the cobalt catalyst a two electrons pathway, were deduced. From Koutecky-Levich analysis, the parallelism of the straight lines indicates that the number of electrons transferred is always the same, for either catalyst. Tafel analysis for the platinum catalyst agrees with the literature. For the cobalt catalyst, the Tafel slopes were much higher than for the platinum catalyst (slower reaction kinetics).

Rotating ring disk (RRDE) studies were used to determine the current efficiency for the production of hydrogen peroxide: for the platinum catalyst up to 4%, and for the

cobalt catalyst up to 82%. In the case of the Co catalyst, the remaining 20% can be associated with chemical or electrochemical decomposition of H_2O_2.

Regarding the high current efficiency for the cobalt catalyst and the absence of limiting currents the limits of the scan range were widened, and RRDE experiments were done from +1.0 V (vs RHE) down to -0.5 V (vs RHE). These experiments showed that the cobalt catalyst is highly sensitive to the oxygen reduction reaction.

The single cell (PEN fuel cell) studies involved the study of effects such as humidifier temperature, pressure gauge and the cathodic reactant, in order to find the optimum conditions to record polarization curves. Polarization curves were used to compare the platinum and cobalt catalysts. The platinum catalyst can reach high current densities, whereas the cobalt only goes up to 0.3 A cm^{-2}.

For the cobalt catalyst the amount of hydrogen peroxide produced was determined by volumetric analysis, the maximum of concentration of H_2O_2 found was roughly 8% (factors such as the increase of the water flux or the residence time which promotes the thermodynamically favourable decomposition can explain the low value).

Comparison of the normalized values obtained from RDE and PEM showed a good performance for the cobalt catalyst by both techniques.

Future work includes the optimisation process of this promising catalyst, for instance, by the preparation method (raw materials used, loading of the catalyst, heat-treatment effect, should be studied thoroughly). The PEM FC also needs to be improved: studies of the residence time of H_2O_2 and materials used that interact with the H_2O_2 can be done. The use of analytical techniques, to examine the MEA or the structure of the catalyst need to be used, such as transmission electron microscopy) should throw further light on the structure and morphology of the materials and permit the development of strategies to improve contact with the catalyst surface.

REFERENCES

1. D. Schiffrin, *New Role for fuel cells?*, Research Intelligence, University of Liverpool, 2003

2. Chemical and Material Sciences Department, Research Division, *Hydrogen peroxide handbook*, 1967

3. J. Campos-Martin, G. Blanco-Brieva, J. Fierro, *Angew. Chem. Int*., 2006, Vol. 45, 6962

4. B. Cook,, *Introduction to fuel cells and hydrogen technology*, Engineering science and education journal, 2002

5. Kink-Othmer, *Encyclopedia of Chemical Technology*, Wiley-interscience, 5th Ed., Vol. 14, 2007

6. G. Hoogers, *Fuel Cell Technology – Handbook,* CRC Press, 2002

7. B. Steele, A. Heinzel, *Nature*, 2001, Vol. 414, 345

8. J. Zhang, *PEM Fuel Cell Electrocatalysts and Catalysts layers, Fundamentals and Applications*, Springer, 2008

9. F. Alcaide, P.-L. Cabot, E. Brillas, *Journal of Power Sources*, 2006, Vol. 153, 47

10. R. Bashyam, P. Zelenay, Nature, 2006, Vol. 443, 63

11. *Internet*: http://www.matthey.com/, Access date: 20/06/10

12. H.-J. Zhang, X. Yuan, W. Wen, D. Zhang, L. Sun, Q.-Z. Jiang, Z.-F. Maa, *Electrochemistry Communications II,* 2009, 11, 206

13. A. Widelov, *Electrochimica Acta*,1993, Vol. 38, 2493

14. P. Gourérec, M. Savy, *Electrochimica Acta*, 1999, Vol. 44, 2653

15. R. Jasinski, *Nature,* 1964, Vol. 201, 1212

16. E. Yeager, *Electrochimica Acta*, 1984, Vol. 29, No. 11, 1527

17. E. Claude, T. Addou, J.-M. Latour, P. Aldebert, *Journal of Applied Electrochemistry*, 1998, Vol. 28, 57

18. G. Faubert, G. Lalande, R. Côté, D. Guay, J. P. Dodelet, L. T. Weng, a, P. Bertrand and G. Dénès, *Electrochimica Acta*, 1996, Vol. 41, No. 10, 1689

19. P. Gouéred, A. Biloul, O. Contamin, G. Scarbeck, M. Savy, J. Riga, L. Weng, P. Bertrand, *Journal of Electroanalytical Chemistry*, 1997, Vol. 422, 61

20. T. Okada, S. Gotou, M. Yoshida, M. Yuasa, T. Hirose, I. Sekine, *Journal of the Electrochemical Society*, 1998, Vol. 145, No. 3, 2411

21. P. Gouérec, M. Savy, *Electrochimica Acta*, 1999, Vol. 44, 2653

22. T. Okada, S. Gotou, M. Yoshida, M. Yuasa, T. Hirose, I. Sekine, *Journal of Inorganic and Organometallic Polymers*, 1999, Vol. 9, No.4, 199

23. A. Lin, J. Huang, *Journal of Electroanalytical Chemistry*, 2003, Vol. 541, 147

24. S. Yamazaki, Y. Yamada, T. Ioroi, N. Fujiwara, Z. Siroma, K. Yasuda, Y. Miyazaki, *Journal of Electroanalytical Chemistry*, 2005, Vol. 576, 253

25. N. Guillet, L. Roue, S. Marcotte, D. Villers, JP Dodelet, N. Chhim, S. Trevin,, *Journal of Applied Electrochemistry*, 2006, Vol. 36, 863

26. Y. Ma, H. Zhang, H. Zhong, T. Xu, H. Jin, Y. Tang, Z. Xu, *Electrochimica Acta,* 2008 (article in press)

27. S. Li, L. Zhang, H. Liu, M. Pan, L. Zan, J. Zhang, *Electrochimica Acta*, 2010, Vol. 55, Issue 15, 4403

28. H.-J. Zhang, Q.-Z. Jiang, L. Sun, X. Yuan, Z.-F. Ma, *Electrochimica Acta*, 2010, Vol. 55, 1107

29. S. Lopez, R. Potter, *Improvements in catalysts*, WO 2009/081183 A1, 2009

30. J. McIntyre, R. Phillips, *Method for electrolytic production of alkaline peroxide solutions,* US Patent 4,431,494, 1984

31. J. McIntyre, S. Webb, *Composite membrane for chemical* synthesis, WO 95/30474, 1994

32. S. Webb, J. McIntyre, *Composite membrane and use thereof for chemical synthesis,* WO 97/13006, 1995

33. I. Yamanaka, T. Hashimoto, R. Ichihashi, K. Otsuka, *Electrochimica Acta*, 2008, Vol. 53, 4824

34. C. Oloman, A. Watkinson, *Journal of Applied Electrochemistry*, 1979, Vol. 9, 117

35. K. Otsuka, I. Yamanaka, *Electrochimica Acta*, 1990, Vol. 35, No. 2, 319

36. F. Alcaide, E. Brillas, P.-L. Cabot, J. Casado, Journal of the *Electrochemical Soc*iety, 1998, Vol. 145, No. 10, 3444

37. E. Brillas, F. Alcaide, P. Cabot, *Electrochimica Acta,* 2002, Vol. 48, 331

38. P. Piela, P. Wrona, *Journal of Power Sources*, 2006, Vol. 158, 1262

39. R. Gopal, *Electrochemical synthesis of hydrogen peroxide,* US 6,712,949 B2, 2002

40. D. Schiffrin, K. Kontturi, R. Nichols, J. Paprotny, *Electrochemical cell,* US 2004/0053098 A1, 2004

41. D. Pletcher, *Industrial Electrochemistry*, 2nd edition, Kluwer

42. T. Bligaard, J. Norskov, S. Dahl, J. Matthiesen, C. Christensen, J. Sehested, *Journal of Catalysis,* 2004, 224-206

43. J. Norskov, J. Kitchin, T. Bligaard, H. Jonsson, *Journal of Physical Chemistry B,* 2004, 108, 17886-17892

44. C.M.A. Brett, A.M. Oliveira-Brett, *Electrochemistry. Principles, Methods and Applications*, Oxford University Press, Oxford, 1993.

45. C.M.A. Brett, A.M. Oliveira-Brett, *Electroanalysis*, Oxford Chemistry Primers, Oxford, 1998

46. M. Perry, J. Newman, E. Cairns, *Journal of the Electrochemical Society,*1998, Vol. 45 No. 1, 5

47. C. Zoski, *Handbook of Electrochemistry*, Elsevier, 1st Edition, 2007

48. J. Wang, *Analytical electrochemistry*, Wiley-VCH, 2006

49. D. Harvey, *Modern Analytical Chemistry*, McGraw-Hill, 1st Ed., 2000

50. D. Pletcher, *A first course in electrode processes,* RSC Publishing, 2nd Ed., 2009

51. B. Tessier, *Preparation, Characterisation and Evaluation of Core-Shell Electrocatalyst for PEMFCs*, PhD Thesis, 2009

52. K. Juttner, *Technical Scale of Electrochemistry, Encyclopedia of Electrochemistry* - Electrochemical Engineering, Wiley-VCH, Vol. 5, 2007

53. F. Will, *Journal of the Electrochemical Society*, 1965, Vol. 112, 451

54. D. Lowde, J. Williams, *Applied Surface Science*, 1978, Vol. 1, 215

55. L. Bregoli, *Electrochimica Acta*, 1978, Vol. 23, 489

56. M. Campos, *ELCAT presentation* – ELCAT Training course on Training course on advanced instrumental and spectroscopic techniques applied to electrocatalysis, University of Birmingham, 2009

57. Adapted from: W. Albery, M. Hitchman, *Ring-Disc electrodes*, Oxford Science Research Papers, Oxford University Press, 1971

58. Southampton Electrochemistry Group, University of Southampton, *Instrumental methods in electrochemistry*, Horwood Publishing, Chemical Science Series, 2001

59. R. Holze, *Experimental Electrochemistry – A laboratory Textbook*, Wiley-VCH, 2009

60. M. Shao, T. Huang, P. Liu, J. Zhang, K. Sasaki, M. Vukmirovic, R. Adzic, *Langmuir*, 2006, Vol 22, No 25, 10409

61. *Internet:*http://www.britannica.com/EBchecked/topic/221374/fuel-cell,Access date: 20/06/10

62. J. Zhang, Z. Xie, J. Zhang, Y. Tang, C. Song, T. Navessin, *Journal of Power Sources*, 2006, Vol. 160, 872

63. W. Schmittinger, A. Vahidi, *Journal of Power Sources*, 2008, Vol. 180, 1

64. X. Yuan, C. Song, H. Wang, J. Zhang, *Electrochemical Impedance Spectroscopy in PEM Fuel Cells – Fundamentals and Applications*, Springer, 2010

65. D. Bernardi, M. Verbrugge, *Proc. of the Symposium on Modeling of Batteries and Fuel Cells*, The Electrochemical Society, Phoenix, U.S.A., 1991

66. T. Mennola, M. Mikkola, M. Noponen, T. Hottinen, P. Lund, *Journal of Power Sources*, 2002, Vol. 112, 261

67. J. Zhang, Y. Tang, C. Song, Z. Xia, H. Li, H. Wang, J. Zhang, *Electrochimica Acta*, 2008, Vol. 53, 5315

68. J. Zhang, Y. Tang, C. Song, J. Zhang, H. Wang *Journal of Power Sources*, 2006, Vol. 163, 532

69. Internet:http://www.pineinst.com/echem/viewproductpage.asp?pageID=8&productID=45655, Access date: 20/06/10

70. Internet:http://www.pineinst.com/echem/viewproductpage.asp?pageID=36&productID=46525, Access date: 20/06/10

71. *Internet*:http://www.cheng.cam.ac.uk/research/groups/electrochem/JAVA/electrochemistry/ELEC/l7html/hydro.html, Access date: 20/06/10

72. U. Paulus, T. Schmidt, H. Gasteiger, R. Behm, *Journal of Electroanalytical Chemistry*, 2001, 495, 134

73. P. Hurley, *Build Your Own Fuel Cells,* Wheelock Mountain, 2002

74. L. Sun, R. Ran, G. Wang, Z. Shao, *Solid State Ionics*, 2008, Vol. 179, 960

75. M. Tsampas, A. Pikos, S. Brosda, A. Katsaounis, C. Vayenas, *Electrochimica Acta*, 2006, Vol. 51, 2743

76. V. Sethuraman, S. Khan, J. Jur, A. Haug, J. Weidner, *Electrochimica Acta*, 2009, Vol. 54, 6850

77. T. Okada, G. Xie, O. Gorseth, S. Kjelstrup, N. Nakamura, T. Arimura, *Electrochimica Acta*, 1998, Vol. 43, No. 24, 3741

78. G. Sasikumar, J. Ihm, H. Ryu, *Electrochimica Acta*, 2004, Vol. 50, 601

79. S. Lee, S. Mukerjee, J. McBreen, Y. Rho, Y. Kho, T. Lee,, *Electrochimica Acta*, 1998, Vol. 43, 3693

80. R. Silva, M. Francesco, A. Pozio, *Electrochimica Acta*, 2004, Vol. 49, 3211

81. A. Therdthianwong, P. Manomayidthikarn, S. Therdthianwong, *Energy*, 2007, Vol. 32, 2401

82. J. Amphlett, R. Barumert, R. Mann, B. Peppley, P. Roberge, *Journal of the Electrochemical Society*, 1995, Vol. 142, No. 1, 183

83. Q. Yan, H. Toghiani, J. Wu, *Journal of Power Sources*, 2006, Vol. 158, 316

84. D. Harris, *Análise Química Quantitativa*, LTC, 6ª Ed., 2005

85. G. Hinds, *Performance and Durability of PEM Fuel Cells: A Review*, NPL Report DEPC-MPE 002, National Physical Laboratory, Teddington, Middlesex, UK, 2004

86. P. Tipler, *Física*, LTC, Volume 1, 4ª Ed., 2000

87. G. Jeffery, J. Bassett, J. Mendham, R. Denney, *Vogel's – Textbook of quantitative chemical analysis*, Longman Group, 5th Ed., 1989

88. D. Lowde, J. Williams, B. McNicol, *Applications of Surface Science*, 1978, Vol. 1, 215

89. K. Mayrhofer, B. Blizanac, M. Arenz, V. Stamenkovic, P. Ross, N. Markovic, *Journal of Physical Chemistry B*, 2005, Vol. 109, 14433

90. E. Fox, H. Colon/Mercado, *International Journal of hydrogen energy*, 2010, Vol. I, 7

91. T. Schmidt, H. Gasteiger, G. Stab, P. Urban, D. Kolb, R. Behm, *Journal of the Electrochemical Society*, 1998, Vol. 145, No. 7, 2354

92. B. Blizanac, P. Ross, N. Markovic, *Journal of Physical Chemistry B*, 2006, Vol. 110, 4735

93. K. Mayrhofer, D. Strmcnik, B. Blizanac, V. Stamenkovic, M. Arenz, N. Markovic, *Electrochimica Acta,* 2008, Vol. 53, 3181

94. E. Higuchi, H. Uchida, M. Watanabe, *Journal of Electroanalytical Chemistry*, 2005, Vol. 583 69

95. T. Ralph, G. Hards, J. Keating, S. Campbell, D. Wilkinson, M. Davis, J. St-Pierre, M. Johnson, *Journal of the Electrochemical Society,* 1997, Vol. 144, No. 11, 3845

96. U. Paulus, A. Wokaun, G. Sherer, *Journal of Physical Chemistry B*, 2002, 106, 4181

97. E. Higuchi, H. Uchida, M. Watanabe, *Journal of Electroanalytical Chemistry*, 2005, Vol. 583, 69

98. D. Chu, *Electrochimica Acta*, 1998, Vol. 43, No. 24, 3711

99. R. Jiang, F. Anson, *Journal of Electroanalytical Chemistry*, 1991, Vol. 305, 171

100. K. Lee, L. Zhang, H. Lui, R. Hui, Z. Shi, J. Zhang, *Electrochimica Acta*, 2009, Vol. 54, 4704

101. A. Ayad, Y. Naimi, J. Bouet, J. Fauvarque, *Journal of Power Sources*, 2004, Vol. 130, 50

102. S. Gojkovic, S. Zecevic, R. Savinell, *Journal of the Electrochemical Society* 1998, Vol. 145, No. 11, 3713

103. D. Thompsett, Johnson Matthey Technology Centre, *Catalysts for the Proton Exchange Membrane Fuel Cell*, Fuel Cell Technology Handbook, CRC Press 2002

104. S. Srinivasan, *Fuel Cells – From fundamentals to applications*, Springer, 2006

105. H.-J. Zhang, X. Yuan, L. Sun, X. Zeng, Q.-Z. Jiang, Z. Shao, Z.-F. Ma, *International Journal of hydrogen energy*, 2010, Vol. 35, 2900

106. C. Wang, et al., *J. Phys. Chem. C,* 2009, Vol. 113, No. 45, 24

107. U. A. Paulus, A. Wokaun, G. Scherer, T. Schmidt, V. Stamenkovic, N. Markovic, P. Ross, *Electrochimica Acta*, 2002, Vol. 47, 3787

108. C. Paliteiro, N. Martins, *Electrochimica Acta*, 1998, Vol. 44, 1359

109. C. Coutanceau, M. Croissant, T. Napporn, C. Lamy, *Electrochimica Acta*, 2000, Vol. 46, 579

110. S. Zecevic, J. Wainright, M. Litt, S. Gojkovic, R. Savinell, *Journal of the Electrochemical Society,* 1997, Vol. 144, No. 9, 2973

111. A. Stassi, C. D'urso, V. Baglio, A. Di Blasi, V. Antonucci, A. Arico, A. Luna, A. Bonesi, W. Triaca,, *Journal of Applied Electrochemistry*, 2006, Vol. 36, No. 10, 1143

112. B. Merzougui, S. Swathirajan, *Journal of the Electrochemical Society* 2006, Vol. 153, No. 12, A2220

113. S. Gojkovic, S. Gupta, R. Savinell, *Electrochimica Acta*, 1999, Vol. 45, 889

114. T. Schmidt, U. Paulus, H. Gasteiger, R. Behm, *Journal of Electroanalytical Chemistry*, 2001, Vol. 508, 41

115. O. Contamin, E. Levart, *Journal of Electroanalytical Chemistry,* 1982, Vol. 136, 259

116. EG&G Services Parsons, Inc., *Fuel Cell Handbook*, U.S. Department of Energy, 5th Ed., 2000

117. C. Kunusch, P. Puleston, M. Mayosky, J. Moré, *International Journal of Hydrogen Energy*, 2010, 1 (article in press)

118. S. Srinivasan, E. Ticianelli, C. Derouin, A. Redondo, *Journal of Power Sources*, 1988, Vol. 22, 359

119. S. Srinivasan, O. Velev, A. Parthasarathy, D. Manko, A. Appleby, *Journal of Power Sources*, 1991, Vol. 36, 299

120. J. Zhang, Z. Xie, J. Zhang, Y. Tanga, C. Song, T. Navessin, Z. Shi, D. Song, H. Wang, D. Wilkinson, Z. Liu, S. Holdcroft, *Journal of Power Sources*, 2006, Vol. 160, 872

121. A. Bonakdarpour, M. Lefevre, R. Yang, F. Jaounen, T. Dahn, J. Dodelet, J. Dahn, *Electrochemical and Solid-State Letters*, 2008, Vol. 11 No. 6, B105

122. Y. Feng, T. He, N. Alonso-Vante, *Electrochimica Acta*, 2009, Vol. 46, 5252

123. T. Ralph, M. Hogarth, *Platinum Metals Review,* 2002, Vol. 46 No.3, 117